

AAD Course Project – Randomized Algorithms

Team Singularity

Members: Adithya, Aryama, Sahid, Sushil, Yashas

Repository: https://github.com/Sushil2006/singularity_aad_project/

Abstract

Randomness powers some of the fastest and most elegant algorithms known. In this project we study multiple randomized paradigms through formal proofs, code implementations, and benchmarks across wide-ranging test cases. We highlight when randomness beats deterministic lower bounds, how error can be driven exponentially low, and where these ideas solve real-world problems on real-world data. The goal is to motivate, implement, and empirically validate randomized algorithms with rigor and ambition.

- **Definition and model:** A randomized algorithm draws unbiased random bits to guide its internal choices. Runtime and output become random variables; guarantees are stated in expectation or with high probability.
- **Why randomness helps:**
 - **Break worst-case structure:** Random choices defeat adversarial input orders and pathological patterns.
 - **Simplicity with strong bounds:** Hashing, sampling, and randomized rounding often yield cleaner code and clean expected-time guarantees.
 - **Performance on real-world datasets:** Massive graphs, streams, and high-dimensional datasets—mirroring real-world data—admit fast randomized sketches and samplers where exact deterministic methods are infeasible.
 - **Provable speedups:** When deterministic lower bounds target worst case only, randomness can improve expected or smoothed complexity.
- **Las Vegas vs. Monte Carlo:**
 - **Las Vegas:** Always correct; randomness affects runtime (e.g., randomized QuickSort, randomized incremental constructions). Guarantee: exact output with expected (and often tail) bounds on time.
 - **Monte Carlo:** Fixed resource budget; output may err with small probability (one- or two-sided). Error is reduced exponentially by independent repetitions and majority/threshold rules (e.g., Miller–Rabin, randomized min-cut).
- **Complexity classes for randomness:**
 - **RP / coRP:** One-sided error; RP accepts yes-instances with probability at least 1/2 and never accepts no-instances; coRP is the complement.

- **BPP**: Two-sided error bounded away from $1/2$ (e.g., $1/3$); amplification drives error to $2^{-\Omega(k)}$ with k repetitions.
- **ZPP**: Zero-error (Las Vegas) with expected polynomial time; $\text{ZPP} = \text{RP} \cap \text{coRP}$.
- **PP / BQP**: PP allows majority acceptance with unbounded two-sided error; BQP is the quantum analogue of BPP with bounded two-sided error on a quantum computer.
- **Other classes**: MA and AM capture randomized proof systems; RL vs. L address randomized logspace. These formalize how randomness affects power under time/space constraints.

- **Error management and amplification:**

- **Independent repetition**: Re-run and aggregate outputs (e.g., majority) to exponentially reduce failure probability.
- **Confidence vs. cost**: Amplification trades a multiplicative work factor for exponentially smaller error, enabling user-chosen confidence.

- **Takeaways:**

- **Power of randomness**: Simplifies algorithms, thwarts worst-case inputs, and yields strong expected or with-high-probability guarantees.
- **Formal lenses**: Las Vegas vs. Monte Carlo and classes (RP , BPP , ZPP , BQP , etc.) formalize correctness and resource trade-offs.
- **Tunable confidence**: Amplification converts modest per-run guarantees into very high confidence with predictable cost.

Contents:

1. Randomized QuickSort
2. Miller-Rabin primality test
3. Randomized MinCut (Karger's Algorithm)
4. Randomized Color-coding for detecting length- k Cycle
5. Randomized MST (Karger–Klein–Tarjan)
6. Randomized Matrix Multiplication (sampling)
7. Randomized SVD (low-rank)
8. Factorized Multiplication via low-rank factors
9. Quantum Integration Engine

Randomized Quicksort and its Variants

Analysis and Benchmark Report

Abstract

We study three instrumented QuickSort implementations (vanilla, smaller-subtree, and cutoff-16), compare them against Merge Sort and the C++ standard library’s `std::sort`, and relate empirical results to classical time and space bounds. Benchmarks cover synthetic and real-world (NIFTY 1-minute) integer datasets, recording wall-clock time and swap counts. All code lives in a single C++17 benchmark driver; plots are produced by accompanying Python scripts.

1 Introduction

QuickSort is a comparison sort that partitions an array around a pivot, recursively sorting the resulting subarrays. It is prized for its in-place memory footprint, cache-friendly sequential scans, and strong expected-time guarantees under randomized pivot selection. Practical libraries often combine QuickSort with other strategies (e.g., insertion sort on small segments, heap sort fallbacks), motivating a careful look at variants and their constant factors.

2 Algorithms and Complexity

2.1 QuickSort procedure (conceptual)

On an input array $A[lo..hi]$:

1. Choose a pivot index uniformly at random from $[lo, hi]$; let p be its value.
2. Partition $A[lo..hi]$ in one linear pass, maintaining a store index s . Scan i from lo to $hi - 1$; whenever $A[i] < p$, swap $A[i]$ with $A[s]$ and increment s . Finally swap $A[s]$ with the pivot. The pivot ends at index s ; elements left of s are $< p$; elements right of s are $\geq p$.
3. Recursively sort the left subarray $[lo, s - 1]$ and the right subarray $[s + 1, hi]$ in any fixed order (or via tail recursion elimination where noted).

Only comparisons and swaps inside the partition pass plus the recursive calls contribute to running time; no auxiliary arrays are used.

2.2 Vanilla QuickSort

The pivot is sampled uniformly from the current subarray; after partitioning, both sides are recursed on.

Expected time (full derivation). Let $T(n)$ be the expected number of primitive operations (or comparisons) on an array of size n . Let $c > 0$ be the partition-pass constant. Conditioning on the pivot rank k (with k elements on the left, $n - 1 - k$ on the right) and applying the law of total expectation:

$$\begin{aligned} T(n) &= \frac{1}{n} \sum_{k=0}^{n-1} \left(T(k) + T(n-1-k) + cn \right) \\ &= \frac{1}{n} \sum_{k=0}^{n-1} T(k) + \frac{1}{n} \sum_{k=0}^{n-1} T(n-1-k) + \frac{1}{n} \sum_{k=0}^{n-1} cn \\ &= \frac{1}{n} \sum_{k=0}^{n-1} T(k) + \frac{1}{n} \sum_{j=0}^{n-1} T(j) + cn \quad (\text{rename } j = n-1-k) \\ &= \frac{2}{n} \sum_{j=0}^{n-1} T(j) + cn. \end{aligned}$$

Define the prefix sum $S(n) = \sum_{j=0}^n T(j)$. Then for $n \geq 1$:

$$\begin{aligned} nT(n) &= 2S(n-1) + cn^2, \\ S(n) &= S(n-1) + T(n). \end{aligned}$$

Multiply the second equation by n and substitute $T(n) = S(n) - S(n-1)$ into the first:

$$\begin{aligned} n(S(n) - S(n-1)) &= 2S(n-1) + cn^2, \\ nS(n) - nS(n-1) &= 2S(n-1) + cn^2, \\ nS(n) &= (n+2)S(n-1) + cn^2, \\ \frac{S(n)}{n+1} &= \frac{S(n-1)}{n} + \frac{cn}{n+1}. \end{aligned}$$

Unrolling this telescoping form from n down to 1 and noting $S(0) = T(0) = \Theta(1)$:

$$\begin{aligned} \frac{S(n)}{n+1} &= \frac{S(0)}{1} + c \sum_{i=1}^n \frac{i}{i+1} \\ &= \Theta(1) + c \sum_{i=1}^n \left(1 - \frac{1}{i+1} \right) \\ &= \Theta(1) + c \left(n - \sum_{i=1}^n \frac{1}{i+1} \right) \\ &= \Theta(1) + c(n - (H_{n+1} - 1)), \end{aligned}$$

where $H_m = \sum_{j=1}^m 1/j$ is the m -th harmonic number. Multiplying by $n+1$ and using $T(n) = S(n) - S(n-1)$, we obtain

$$T(n) \leq 2(n+1)H_n - 4n + O(n),$$

so $T(n) = \Theta(n \log n)$ in expectation because $H_n = \Theta(\log n)$.

Worst and best cases. Worst-case pivot ranks yield $T(n) = T(n-1) + cn = \Theta(n^2)$. Perfectly balanced splits give $T(n) = 2T(n/2) + cn = \Theta(n \log n)$. Stack depth is $O(n)$ in the worst case.

2.3 QuickSort with smaller-subtree recursion

After partitioning, the algorithm recurses on the smaller side and iterates on the larger. The running-time recurrence matches vanilla QuickSort, so the same bounds hold: $\Theta(n \log n)$ expected, $\Theta(n^2)$ worst case. Stack depth satisfies

$$D(n) \leq 1 + D\left(\left\lfloor \frac{n-1}{2} \right\rfloor\right),$$

giving $D(n) = O(\log n)$ for all inputs.

Stack depth. We prove $D(n) \leq \lfloor \log_2 n \rfloor + 1$ by induction on $n \geq 1$. Base: $n = 1$ gives $D(1) = 1$. Inductive step: assume the claim holds for all sizes $< n$. The smaller side has size at most $\lfloor (n-1)/2 \rfloor$, so

$$D(n) \leq 1 + D\left(\left\lfloor \frac{n-1}{2} \right\rfloor\right) \leq 1 + \left\lfloor \log_2 \left\lfloor \frac{n-1}{2} \right\rfloor \right\rfloor + 1 \leq \lfloor \log_2 n \rfloor + 1.$$

Thus depth grows logarithmically regardless of pivot outcomes.

Expected time. The pivot rank is still uniform, so the conditional recurrence is identical to the vanilla case:

$$T_{\text{small}}(n) = \frac{1}{n} \sum_{k=0}^{n-1} (T_{\text{small}}(k) + T_{\text{small}}(n-1-k)) + cn.$$

Define $S_{\text{small}}(n) = \sum_{j=0}^n T_{\text{small}}(j)$. Then for $n \geq 1$:

$$\begin{aligned} n T_{\text{small}}(n) &= 2 S_{\text{small}}(n-1) + cn^2, \\ S_{\text{small}}(n) &= S_{\text{small}}(n-1) + T_{\text{small}}(n). \end{aligned}$$

Substitute $T_{\text{small}}(n) = S_{\text{small}}(n) - S_{\text{small}}(n-1)$:

$$\begin{aligned} n(S_{\text{small}}(n) - S_{\text{small}}(n-1)) &= 2S_{\text{small}}(n-1) + cn^2, \\ nS_{\text{small}}(n) &= (n+2)S_{\text{small}}(n-1) + cn^2, \\ \frac{S_{\text{small}}(n)}{n+1} &= \frac{S_{\text{small}}(n-1)}{n} + \frac{cn}{n+1}. \end{aligned}$$

Unrolling from n to 1 gives

$$\frac{S_{\text{small}}(n)}{n+1} = \Theta(1) + c \sum_{i=1}^n \frac{i}{i+1} = \Theta(1) + c(n - (H_{n+1} - 1)),$$

so $T_{\text{small}}(n) = S_{\text{small}}(n) - S_{\text{small}}(n-1) = \Theta(n \log n)$, matching the vanilla expectation.

2.4 QuickSort with cutoff 16

When a subarray has size ≤ 16 , the implementation immediately applies insertion sort and stops recursing on that branch. Partitioning proceeds as in A1. Costs consist of:

- Partitioning down to size 16: still $\Theta(n \log n)$.
- Insertion sort on many tiny segments: each element participates in at most one small-segment insertion pass, contributing $O(n)$.

Thus the overall bound remains $\Theta(n \log n)$ expected, $\Theta(n^2)$ worst case, but constant factors drop because insertion sort is efficient on very small arrays. Stack depth follows A1 when the tail-recursive strategy is used.

Expected time. Let $T_c(n)$ be the expected time with cutoff $c = 16$. For $n > c$,

$$T_c(n) = \frac{1}{n} \sum_{k=0}^{n-1} (T_c(k) + T_c(n-1-k)) + cn,$$

identical to the vanilla QuickSort recurrence for the partitioning portion. For $n \leq c$, $T_c(n) = O(c^2)$ due to insertion sort. By induction on n ,

$$T_c(n) \leq T_{\text{vanilla}}(n) + O(n),$$

where $T_{\text{vanilla}}(n)$ is the solution to the vanilla recurrence. Inductive step: if $n > c$,

$$T_c(n) \leq \frac{2}{n} \sum_{j=0}^{n-1} (T_{\text{vanilla}}(j) + O(j)) + cn = T_{\text{vanilla}}(n) + O(n),$$

using the same prefix-sum manipulation as before and the inductive hypothesis on subproblem sizes $< n$. If $n \leq c$, $T_c(n) = O(c^2) = O(n)$. Therefore $T_c(n) = \Theta(n \log n)$ in expectation.

Stack depth. Because the algorithm recurses only on the smaller side and iterates on the larger, the depth recurrence matches the smaller-subtree case:

$$D_c(n) \leq 1 + D_c\left(\left\lfloor \frac{n-1}{2} \right\rfloor\right),$$

with base $D_c(n) = 1$ for $n \leq c$. The same induction as before yields $D_c(n) \leq \lfloor \log_2 n \rfloor + 1$. Worst-case pivot choices still yield $T_c(n) = \Theta(n^2)$ time, but stack depth remains $O(\log n)$ because the larger side is never recursed.

2.5 Merge Sort

The top-down implementation recurses on halves and merges with a temporary buffer of size n . The recurrence $T(n) = 2T(n/2) + cn$ yields $\Theta(n \log n)$ in all cases; extra space is $\Theta(n)$ for the buffer.

2.6 std::sort

Library `std::sort` is an introspective hybrid (QuickSort + heap sort fallback + insertion sort on small partitions), guaranteeing $O(n \log n)$ worst-case time while remaining in-place. It serves as a realistic production baseline.

2.7 Summary of Bounds

Algorithm	Best	Expected	Worst (time / stack)
QuickSort (vanilla)	$\Theta(n \log n)$	$\Theta(n \log n)$	$\Theta(n^2)$ time, $O(n)$ stack
QuickSort (smaller-subtree)	$\Theta(n \log n)$	$\Theta(n \log n)$	$\Theta(n^2)$ time, $O(\log n)$ stack
QuickSort (cutoff 16)	$\Theta(n \log n)$	$\Theta(n \log n)$	$\Theta(n^2)$ time, $O(\log n)$ stack
Merge Sort	$\Theta(n \log n)$	$\Theta(n \log n)$	$\Theta(n \log n)$, $O(n)$ buffer
<code>std::sort</code>	$\Theta(n \log n)$	$\Theta(n \log n)$	$O(n \log n)$ (introsort)

Table 1: Asymptotic behavior of evaluated algorithms.

3 Experimental Workflow

The entire benchmark lives in `src/main.cpp`; a compiled binary `quicksort_bench` is driven by `scripts/run_benchmarks.py`.

3.1 Data Generation

- **Synthetic distributions:** deterministic given (n, seed) . Sorted uses $a_i = i$; almost-sorted applies $k = \lfloor 0.05n \rfloor$ random swaps; uniform draws from $[-10^9, 10^9]$; normal draws from $\mathcal{N}(0, 1000^2)$ with clamping to $[-10^9, 10^9]$.
- **Stock data:** preprocessed Kaggle NIFTY 1-minute closes (10^6 integers) stored in `data/nifty_1m_int_1M.txt`. The benchmark reads the first n values for the `stock` distribution.
- **Randomness:** all generators and pivot choices use `std::mt19937_64` seeded with `seed_base + rep`, where `seed_base` is deterministic per configuration (see `compute_seed_base` in the Python script).

3.2 Benchmark Driver

- **Invocation:** run `./quicksort_bench` with arguments `<algo_id>`, `<dist_id>`, `n`, `seed_base`, `reps`, `stock_path`.
- **Metrics:** each repetition prints `<time_ns> <swaps>`; swap count is -1 for `std::sort`.
- **Sizes and reps:** `run_benchmarks.py` sweeps $n = 2^{10}, \dots, 2^{20}$ (1024 to 1,048,576), plus the full stock file size 1,007,339; repetitions $R = 5$.
- **Outputs:** rows are aggregated into `results/raw_results.csv`.
Plots produced by `plot_results.py` reside in `results/plots/` and are embedded below.

3.3 Implementation Notes

All implementations operate on `std::vector<int>` and use a Mersenne Twister (`std::mt19937_64`) seeded deterministically per run. The global counter `g_swap_count` tracks swaps for instrumented algorithms (QuickSort variants and Merge Sort); `std::sort` leaves it at -1 .

4 Results

Figures [1–5] show mean wall-clock time (ms) versus n on log-scaled x and swap counts for Quick-Sort/Merge Sort variants.

Distribution: sorted

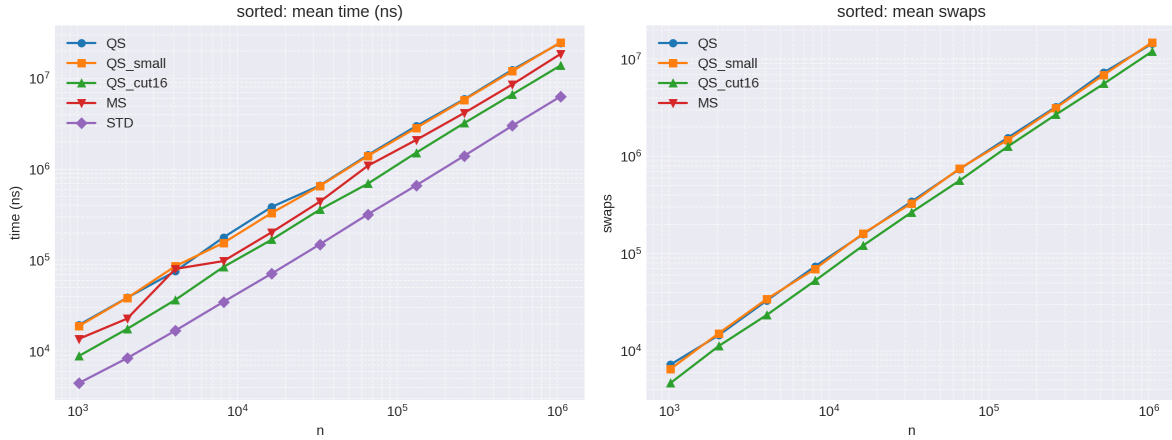


Figure 1: Sorted input.

Distribution: almost_sorted

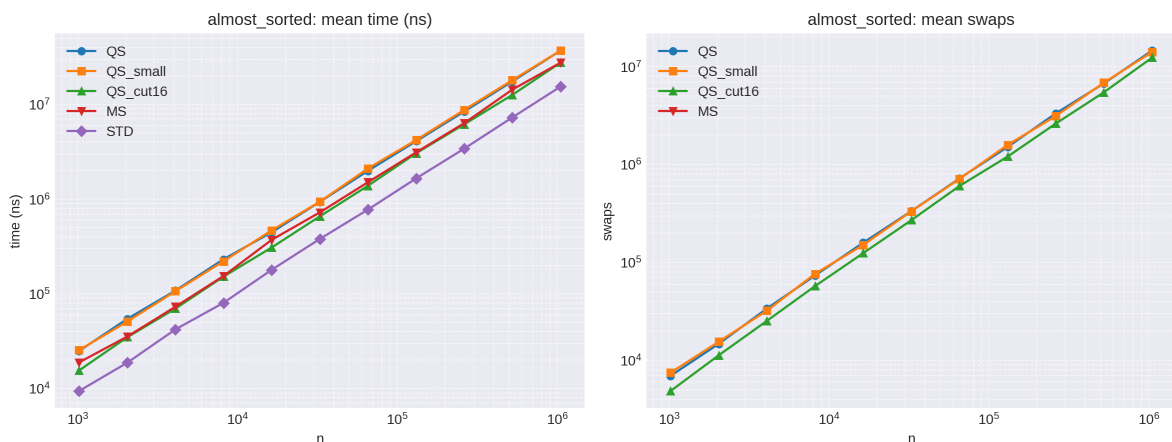


Figure 2: Almost-sorted input (5% swaps).

Distribution: uniform

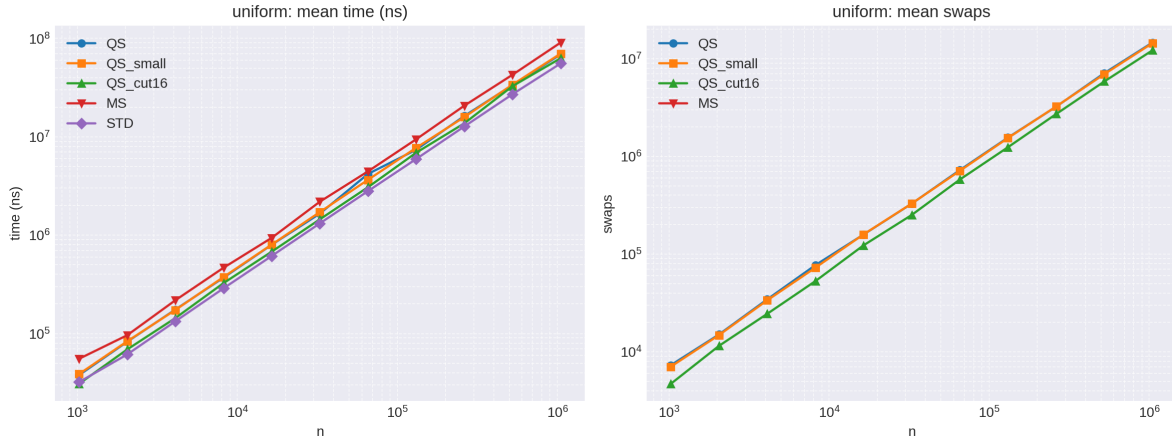


Figure 3: Uniform random input.

Distribution: normal

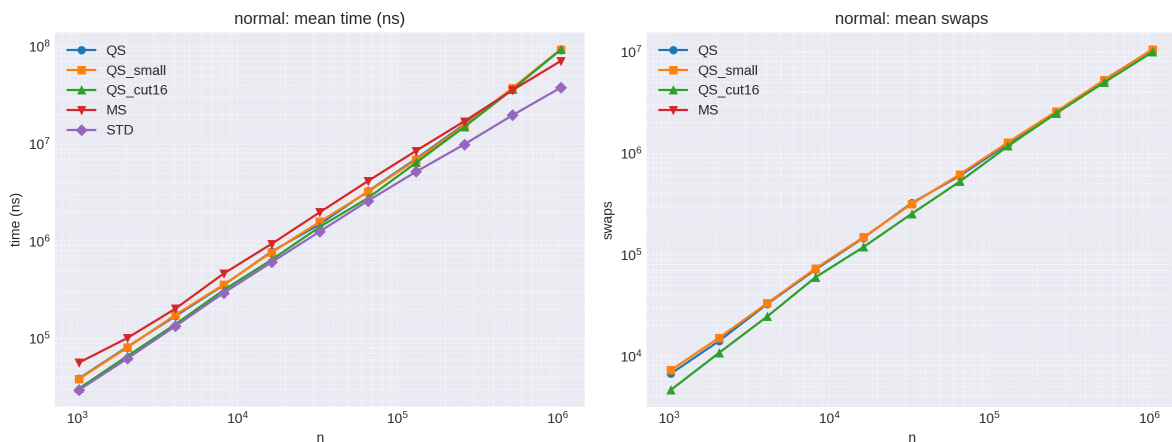


Figure 4: Normal distribution input.

Distribution: stock

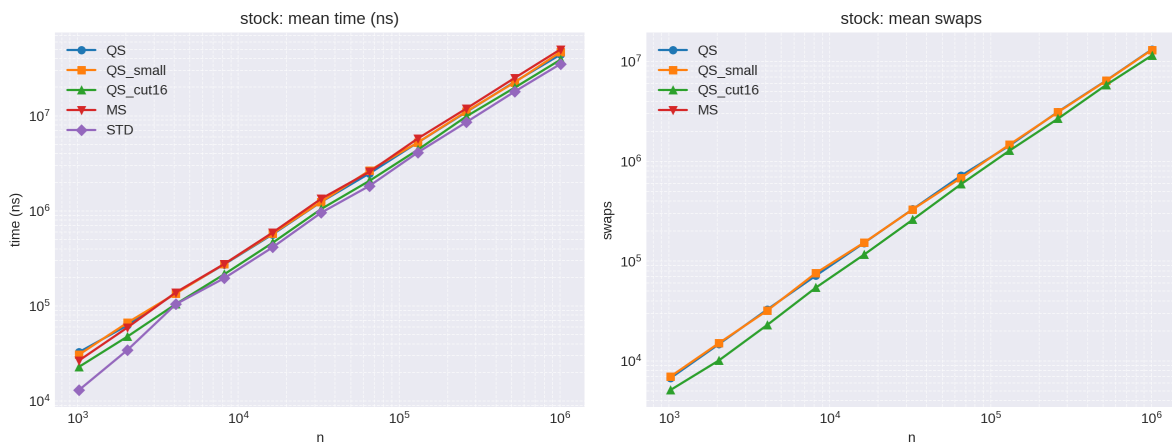


Figure 5: Real stock data input.

4.1 Observations on Figures

- **QS_cut16 leads among custom variants:** Across all distributions, QS_cut16 is the fastest of the instrumented QuickSorts. On uniform input with $n = 2^{20}$, QS_cut16 averages ≈ 62.9 ms versus ≈ 68.8 ms for QS and ≈ 70.1 ms for QS_small; swap counts drop from $\approx 14.6M$ (QS) to $\approx 12.2M$ (QS_cut16).
- **Effect of tail recursion control:** QS_small and QS have nearly identical times (e.g., sorted $n = 2^{20}$: ≈ 24.9 ms vs ≈ 24.7 ms) while QS_small caps stack depth at $O(\log n)$.
- **QS vs Merge Sort:** Merge Sort trails the QuickSort variants on noisy data (70–90 ms at $n = 2^{20}$ for uniform/normal) and requires $\Theta(n)$ extra space; on structured data (sorted/almost-sorted) it closes the gap but still lags QS_cut16.
- **Real stock mirrors synthetic:** On the full NIFTY slice ($n = 1,007,339$), QS_cut16 is the quickest custom option at ≈ 38.9 ms, ahead of QS (≈ 44.1 ms) and QS_small (≈ 46.9 ms); patterns match the synthetic distributions.
- **Why QS_cut16 excels:** Insertion sort on tiny partitions eliminates extra partition passes and reduces swaps; tail recursion keeps stack shallow. These micro-optimizations shrink constant factors without altering the $\Theta(n \log n)$ expectation, yielding measurable speedups on both ordered and random inputs.

5 Why QuickSort Works Well in Practice

- **In-place:** Partitioning needs only $O(1)$ auxiliary memory, which preserves cache locality and avoids large allocations compared to Merge Sort’s $O(n)$ buffer.
- **Cache-friendly scans:** Sequential reads/writes during partitioning yield few cache misses, visible in the tight constants of A2 and `std::sort`.
- **Randomization:** Uniform pivot sampling delivers $\Theta(n \log n)$ expected time on non-adversarial inputs—a good match for market and logging data that lack worst-case structure.
- **Hybridization payoff:** Adding insertion sort on tiny ranges (A2) trims swap counts and improves time without changing asymptotic bounds; introsort in `std::sort` pushes this idea further with heap-sort fallbacks.
- **Empirical alignment:** The real-stock results match the synthetic curves, reinforcing that QuickSort-style strategies handle both clustered (sorted/almost-sorted) and noisy (uniform/normal) data effectively.

6 Real-world Use Cases

- **C++ standard library:** `std::sort` is an introspective QuickSort hybrid used pervasively in systems code ([cppreference](#)).
- **Java primitive arrays:** `Arrays.sort` for primitives uses a dual-pivot QuickSort ([Oracle JDK docs](#)).
- **Database engines:** PostgreSQL uses a QuickSort-based tuplesort for many in-memory sorts before spilling to disk ([source code](#)).
- **Systems utilities:** The classic C `qsort` in libc remains a QuickSort-style routine, making the algorithm a default choice for general-purpose array sorting.

7 Conclusion

QuickSort’s combination of in-place operation, cache-friendly access, and strong expected bounds makes it a natural first choice for large in-memory datasets. Our experiments confirm that modest engineering—tail recursion elimination and tiny-segment insertion sort—improves constant factors without altering complexity. Production-grade hybrids such as `std::sort` remain the performance ceiling, but tuned QuickSort variants deliver predictable, efficient behavior on both synthetic and real financial data.

Miller–Rabin Primality Testing

Analysis and Benchmark Report

Abstract

We present a rigorous analysis of the Miller–Rabin (MR) primality test, its error bounds, and time complexity, alongside benchmarks comparing trial division, Fermat, randomized MR with k bases, and deterministic MR for 64-bit integers. Experiments span multiple input distributions (random odd, Carmichael, small-factor composites, primes), and we include a toy RSA demo built on the same MR implementation.

1 Problem Setting and Model

We seek to decide primality of an integer $n \geq 2$. The analysis is stated in the uniform RAM model with unit-cost operations on $\Theta(\log n)$ -bit words. No implementation details appear in this section; they are deferred to later benchmarking notes.

2 Miller–Rabin Algorithm and Proofs

2.1 Preprocessing for odd inputs

For every odd $n > 2$, factor

$$n - 1 = 2^s \cdot d, \quad d \text{ odd}, \quad s \geq 1.$$

The pair (s, d) is computed once and reused across all bases.

2.2 One Miller–Rabin round

Let $n > 2$ be odd and a satisfy $2 \leq a \leq n - 2$ and $\gcd(a, n) = 1$.

1. Compute $x = a^d \bmod n$ by repeated squaring.
2. If $x \in \{1, n - 1\}$, accept the round.
3. Otherwise, for $r = 1, \dots, s - 1$:
 - (a) Set $x \leftarrow x^2 \bmod n$.
 - (b) If $x = n - 1$, accept; if $x = 1$, reject (non-trivial square root of 1).
4. If no acceptance occurs, reject.

2.3 Correctness on prime inputs

Assume n is prime. The multiplicative group $G = (\mathbb{Z}/n\mathbb{Z})^\times$ has order $|G| = n - 1 = 2^s d$.

Lemma 1 (Square roots of unity). *If $x^2 \equiv 1 \pmod{n}$, then $x \equiv \pm 1 \pmod{n}$.*

Proof. We have $n \mid (x - 1)(x + 1)$. Since n is prime, one factor vanishes modulo n . \square

Lemma 2 (Allowed trajectory). *Let $x = a^d \in G$. Then $x^{2^s} = a^{n-1} \equiv 1$. In the sequence $x, x^2, x^4, \dots, x^{2^s}$, any transition from a value other than -1 to 1 would create a non-trivial square root of 1 , contradicting Lemma 1. Therefore the sequence must either start at 1 or hit -1 exactly once before reaching 1 .*

Proof. The equality $x^{2^s} = 1$ follows from Lagrange's theorem. Suppose some iterate $x^{2^j} = 1$ with $0 < j < s$ and $x^{2^{j-1}} \not\equiv -1$. Then $x^{2^{j-1}}$ is a non-trivial square root of 1 , impossible by Lemma 1. Hence acceptance in a prime modulus always occurs along the Miller–Rabin path. \square

Theorem 1 (No false negatives). *For prime n and any admissible base a , one Miller–Rabin round accepts.*

Proof. Lemma 2 shows the round's control flow accepts exactly in the situations mandated by the group structure; no rejection is possible. \square

2.4 Error bound on composite inputs

Let n be odd and composite; write $n - 1 = 2^s d$ with d odd. Define a base a coprime to n as a *strong liar* if the round accepts and as a *strong witness* otherwise. We prove that at most a quarter of all admissible bases are liars, yielding the classical $(1/4)^k$ error bound for k independent rounds.

CRT decomposition. Factor $n = \prod_{i=1}^r p_i^{e_i}$. By the Chinese Remainder Theorem,

$$(\mathbb{Z}/n\mathbb{Z})^\times \cong \prod_{i=1}^r G_i, \quad G_i = (\mathbb{Z}/p_i^{e_i}\mathbb{Z})^\times.$$

Each G_i is cyclic of order $p_i^{e_i-1}(p_i - 1) = 2^{t_i} m_i$ with m_i odd and $t_i \geq 1$. Choose generators g_i so every a corresponds to exponents u_i with $0 \leq u_i < 2^{t_i} m_i$.

Component-wise acceptance. Write $u_i = 2^{\lambda_i} v_i$ with v_i odd and $0 \leq \lambda_i \leq t_i$. The MR acceptance condition in component i is:

$$\text{either } g_i^{u_i d} \equiv 1 \pmod{p_i^{e_i}} \quad \text{or} \quad g_i^{u_i 2^j d} \equiv -1 \text{ for some } j < t_i.$$

Because d is odd, $g_i^{u_i d} \equiv 1$ iff $m_i \mid u_i$. Moreover, $g_i^{u_i 2^j d} \equiv -1$ requires $m_i \mid u_i$ and $u_i/m_i \equiv 2^{t_i-1} \pmod{2^{t_i}}$, the unique exponent producing order 2 after the squaring ladder.

Counting liars per component. Acceptable u_i are exactly those with $m_i \mid u_i$ and $u_i \pmod{2^{t_i}} \in \{0, 2^{t_i-1}\}$. The count is

$$|L_i| = 2 \cdot \frac{2^{t_i} m_i}{2^{t_i}} = \frac{|G_i|}{2^{t_i-1}},$$

so the liar fraction in component i is $\rho_i = 2^{-(t_i-1)} \leq \frac{1}{2}$, with $\rho_i \leq \frac{1}{4}$ whenever $t_i \geq 3$.

Global product bound. Independence of the CRT components gives $|L| = \prod_i |L_i|$ and

$$\frac{|L|}{|G|} = \prod_{i=1}^r \rho_i = 2^{-\sum_i(t_i-1)}.$$

For any odd composite n , $\sum_i(t_i - 1) \geq 2$:

- With at least two distinct prime factors ($r \geq 2$), two components each contribute a factor at most $\frac{1}{2}$, yielding $|L|/|G| \leq \frac{1}{4}$.
- For a prime power p^e with $e \geq 2$, the 2-adic valuation of $|G_1|$ satisfies $t_1 \geq 2$, so $\rho_1 \leq \frac{1}{4}$.

Thus $|L| \leq \frac{1}{4}|G|$. Random bases are chosen uniformly from admissible residues, so one round accepts a composite with probability at most $\frac{1}{4}$, and k independent rounds accept with probability at most $(1/4)^k$.

2.5 Deterministic base set for 64-bit inputs

The fixed bases $\{2, 3, 5, 7, 11, 13, 17, 19, 23, 29, 31, 37\}$ suffice for all odd $n < 2^{64}$: passing MR for all of them implies primality. Therefore `is_prime_mr_det64` is exact on 64-bit integers.

2.6 Time Complexity

Let $M(n)$ denote the cost of one modular multiplication on $\Theta(\log n)$ -bit words; in the RAM model $M(n) = O(1)$.

- Fast exponentiation of $a^d \bmod n$ uses $\lfloor \log_2 d \rfloor + \text{popcount}(d)$ multiplications, i.e., $O(\log n)$.
- One MR round consists of that exponentiation and up to $s - 1 \leq \log_2(n - 1)$ additional squarings, so $O(\log n)$.
- k rounds take $O(k \log n)$ time and $O(1)$ space.
- Fermat- k matches these time bounds but lacks the 4^{-k} error decay; trial division is $O(\sqrt{n})$.

2.7 Summary of Bounds

Algorithm	Time	Error	Space
Trial Division	$O(\sqrt{n})$	0	$O(1)$
Fermat- k	$O(k \log n)$	Can be 1 on Carmichael	$O(1)$
MR- k	$O(k \log n)$	$\leq (1/4)^k$	$O(1)$
MR-det-64	$O(\log n)$	0 (for $n < 2^{64}$)	$O(1)$

Table 1: Asymptotic behavior of implemented algorithms.

3 Algorithms Implemented (C++)

- **Trial Division (TD)** (`is_prime_td`): odd divisors up to $\lfloor \sqrt{n} \rfloor$; disabled for bits > 48.
- **Fermat- k** (`is_probable_prime_fermat`): k random bases; rejects on any violation of $a^{n-1} \equiv 1$.
- **MR- k** (`is_probable_prime_mr`): k random bases with the standard strong probable prime check; per-round error $\leq 1/4$, total $\leq 4^{-k}$.
- **MR-det-64** (`is_prime_mr_det64`): fixed 12 bases; exact for $n < 2^{64}$.

4 Benchmark Workflow

All benchmarks live in `src/main.cpp`; `scripts/run_benchmarks.py` drives the binary `mr_bench`.

- **CLI:** `./mr_bench <algo_id> <dist_id> <bits> <sample_count> <rounds> <seed_base> <reps>`.
- **Distributions (dist_id):** random odd, Carmichael, composite with small factor, primes (generated via MR-det-64).
- **Metrics:** each repetition outputs `<time_ns_total> <error_count>` across the sample of size S , with truth labels provided by MR-det-64.
- **Rounds:** Fermat/MR use k supplied on the CLI (e.g., $k = 10$); TD ignores it.
- **Python aggregation:** `results/raw_results.csv` records all rows; plots are generated by `plot_results.py`.

5 Results

5.1 Plots

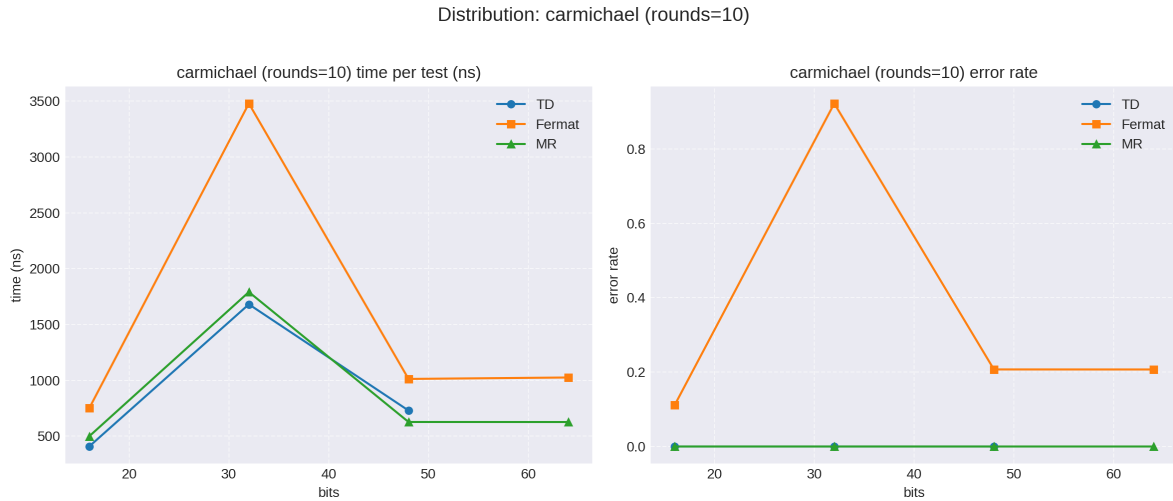


Figure 1: Carmichael distribution, $k = 10$: time per test (ns) and error rate.

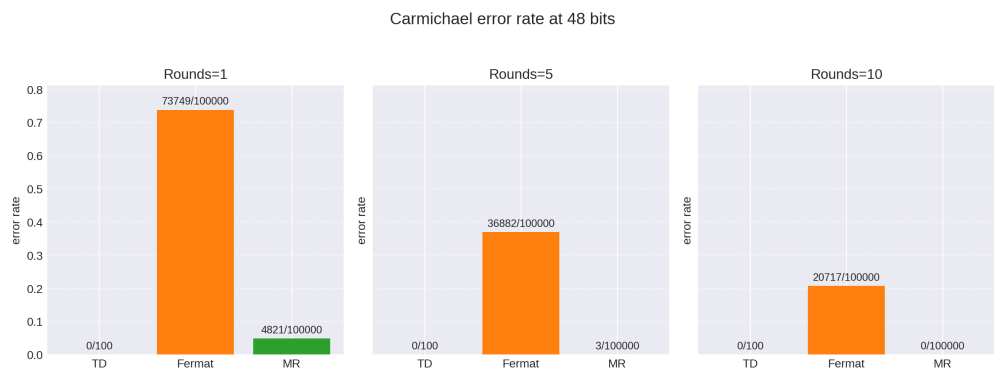


Figure 2: Carmichael, 48 bits: error rate vs rounds for Fermat and MR.

Distribution: rand_odd (rounds=10)

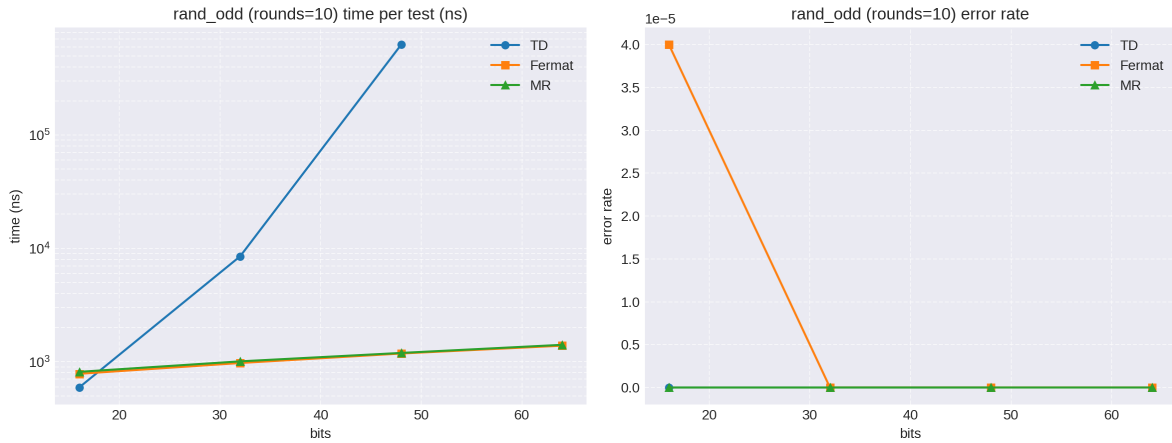


Figure 3: Random odd inputs, $k = 10$: time per test (ns) and error rate.

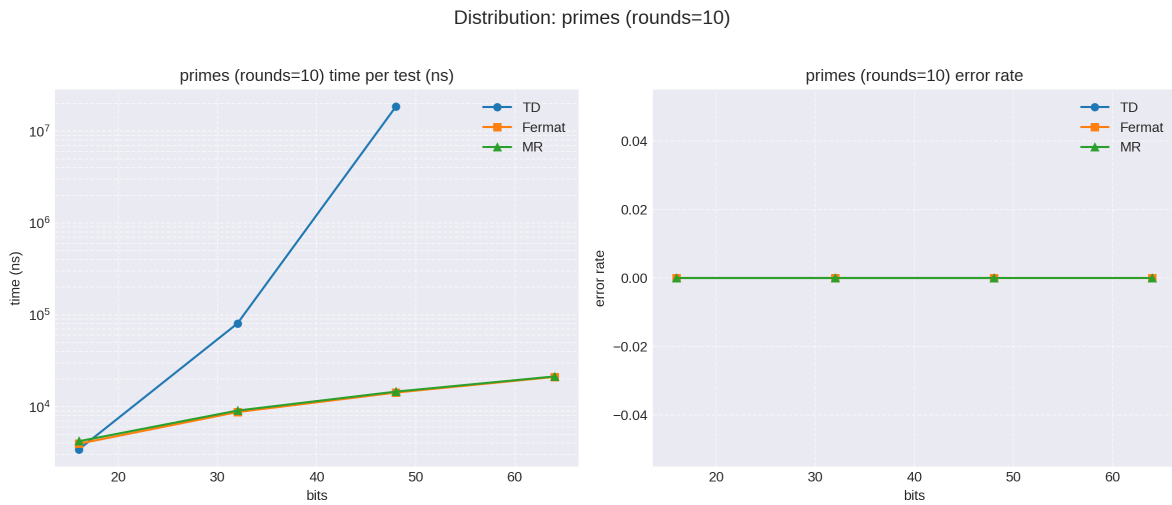


Figure 4: Prime inputs (ground truth), $k = 10$: time per test (ns) and false-negative rate.

Distribution: comp_small_factor (rounds=10)

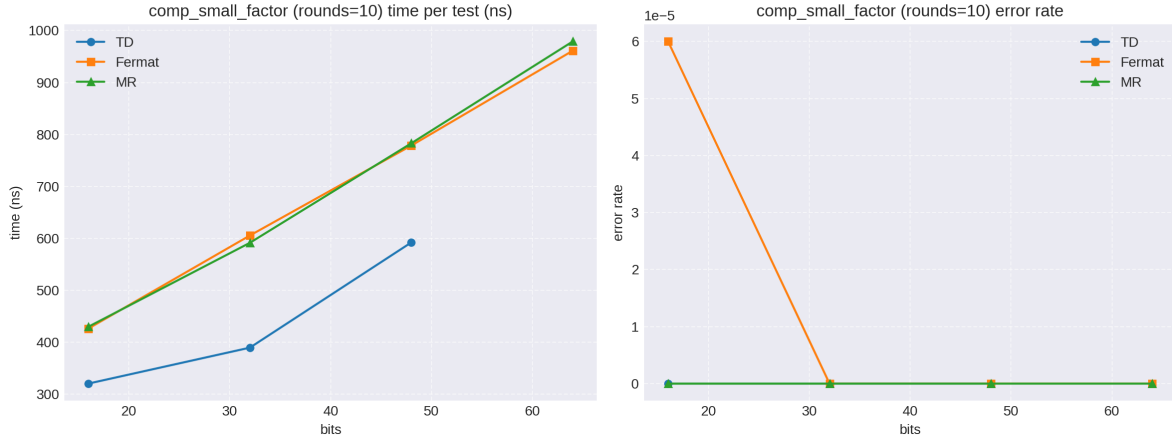


Figure 5: Composites with small factor, $k = 10$: time per test (ns) and error rate.

Distribution: comp_small_factor (rounds=10000)

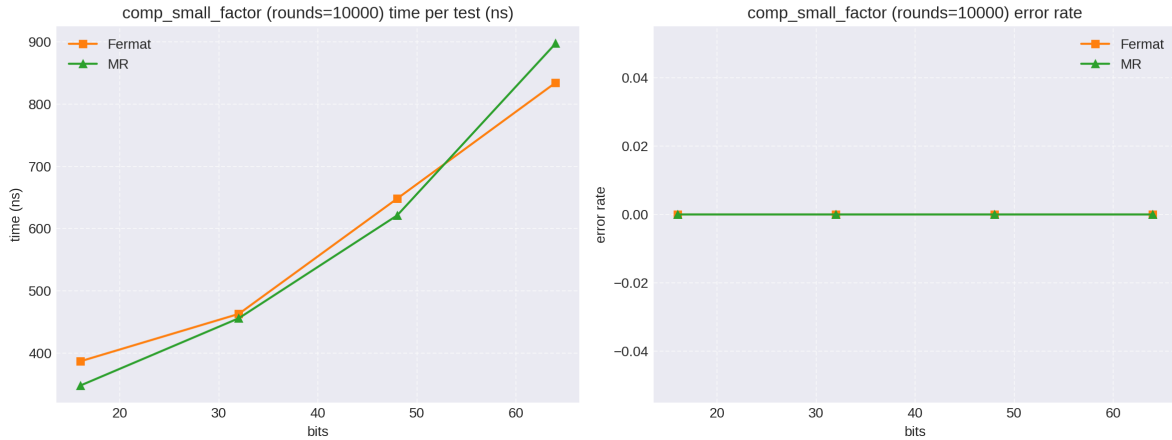


Figure 6: Composites with small factor, $k = 10000$: time per test (ns) and error rate.

5.2 Observations

- **Carmichael sensitivity:** Figure 1 shows MR attaining near-zero error on Carmichael inputs at $k = 10$; Figure 2 highlights the exponential decay, with error essentially gone by $k = 5$.
- **Random odd mix:** In Figure 3, Fermat and MR have similar runtimes; MR keeps error negligible, and Fermat’s empirical error is extremely rare (about 4×10^{-5}).
- **Prime inputs:** Figure 4 shows no false negatives for MR (as guaranteed); Fermat also very rarely rejects primes.
- **Small-factor composites:** Figures 5 and 6 demonstrate that MR’s error vanishes quickly with k ; time scales linearly with k , matching the $O(k \log n)$ or $O(k \log^2 n)$ bounds depending on the cost model.

6 Real-world Usage

- **RSA key generation:** OpenSSL applies multiple MR rounds (and sieving) to candidate primes; documented error probabilities are bounded by powers of two. The toy RSA demo in this repository reuses the same MR code for small key generation.
- **Big-integer libraries:** GMP, Java `BigInteger.isProbablePrime`, and similar libraries rely on MR (often combined with Lucas/Baillie-PSW) to deliver negligible error on large inputs.
- **Computer algebra systems:** CAS tools (Maple, Mathematica, PARI/GP, SageMath) embed MR-style strong probable prime tests as core building blocks.
- **Toy RSA implementation:** A pedagogical RSA demo (local CLI and simple client/server) is included; it generates small primes using the MR routines documented here and walks through textbook RSA key generation, encryption, and decryption for illustration.

7 Conclusions

Miller–Rabin delivers logarithmic-time probabilistic primality testing with exponentially small error in the number of rounds. Deterministic base sets make it exact for 64-bit integers, and randomized MR dominates Fermat, especially on adversarial inputs like Carmichael numbers. Benchmarks confirm the theoretical bounds: time grows linearly with $k \log n$, and empirical error aligns with the $(1/4)^k$ guarantee.

Karger's Randomized Algorithm For Minimum-Cut In Unweighted Graphs

Analysis and Benchmark Report

1 Karger Minimum Cut: Model and Algorithm

Graph model. We work with undirected multigraphs $G = (V, E)$ having $n = |V|$ vertices and $m = |E|$ edges; parallel edges are allowed, self-loops are ignored. For any non-empty proper $S \subset V$, the cut value is $\delta(S) = |\{(u, v) \in E : u \in S, v \notin S\}|$. The global minimum cut value is $\lambda(G) = \min_S \delta(S)$. The RAM model with unit-cost $\Theta(\log n)$ -bit operations is assumed.

Single-run algorithm. Maintain a disjoint-set union (DSU) with one set per vertex and a component counter $c = n$:

1. While $c > 2$: draw a uniform random edge $(u, v) \in E$. If u and v are in different DSU sets, merge them and decrement c .
2. When exactly two supernodes remain, count edges whose endpoints lie in different DSU sets; return that count.

2 Probabilistic Analysis of Karger

All statements below condition on a fixed target minimum cut C^* of size $\lambda = \lambda(G)$.

2.1 Edge-incidence bound per step

Lemma 1. Suppose i supernodes remain and no edge of C^* has been contracted so far. Then the probability that the next sampled edge lies in C^* is at most $2/i$.

Proof. Because no edge of C^* has been contracted, every cut in the current multigraph corresponds to a cut in the original graph and therefore has value at least λ . In particular, the minimum degree of the current multigraph is at least λ : removing all edges incident to any vertex isolates it and forms a cut of size equal to that degree, which cannot be smaller than λ . With i supernodes, this minimum-degree bound implies at least $i\lambda/2$ edges in total (summing degrees and dividing by two). Exactly λ of those edges belong to C^* . Sampling an edge uniformly therefore yields

$$\Pr[\text{pick edge in } C^* \mid \text{no previous contraction of } C^*] \leq \frac{\lambda}{i\lambda/2} = \frac{2}{i}.$$

□

2.2 Single-run success probability

Theorem 1. *The probability that a single run returns the fixed minimum cut C^* is at least $2/(n(n-1))$.*

Proof. Let $p_i = 1 - 2/i$ be the lower bound on the probability that the contraction step at supernode count i avoids C^* . Starting from $i = n$ and stopping at $i = 2$, the overall survival probability is

$$\prod_{i=n}^3 p_i = \prod_{i=n}^3 \left(1 - \frac{2}{i}\right) = \prod_{i=n}^3 \frac{i-2}{i}.$$

To telescope, rewrite each factor $\frac{i-2}{i}$ as $\frac{i-2}{i-1} \cdot \frac{i-1}{i}$, obtaining

$$\prod_{i=n}^3 \frac{i-2}{i} = \left(\prod_{i=n}^3 \frac{i-2}{i-1}\right) \cdot \left(\prod_{i=n}^3 \frac{i-1}{i}\right).$$

Now expand both products step by step. The first product is

$$\frac{n-2}{n-1} \cdot \frac{n-3}{n-2} \cdot \frac{n-4}{n-3} \cdots \frac{1}{2},$$

whose numerators and denominators cancel in sequence, leaving $\frac{1}{n-1}$. The second product is

$$\frac{n-1}{n} \cdot \frac{n-2}{n-1} \cdot \frac{n-3}{n-2} \cdots \frac{2}{3},$$

which cancels to $\frac{2}{n}$. Multiplying the two surviving terms yields

$$\prod_{i=n}^3 \frac{i-2}{i} = \frac{1}{n-1} \cdot \frac{2}{n} = \frac{2}{n(n-1)}.$$

Conditional on survival of C^* through all contractions, the final two supernodes are separated exactly by C^* , so the run outputs it with probability at least $2/(n(n-1))$. \square

2.3 Amplification by repetition

Let $p_{\min}(n) = 2/(n(n-1))$ be the guaranteed per-run success probability. Running R independent trials and returning the minimum cut observed yields failure probability

$$\Pr[\text{all fail}] \leq (1 - p_{\min}(n))^R \leq e^{-p_{\min}(n)R},$$

using $1 - x \leq e^{-x}$. Choosing

$$R(n) = \left\lceil \frac{1}{2} n(n-1) \ln \frac{1}{\delta_{\text{target}}} \right\rceil$$

drives this upper bound down to at most δ_{target} for a user-specified δ_{target} . The constant δ_{target} is fixed in the code; with that fixed value the resulting iteration counts are $R(30) = 23$, $R(60) = 91$, and $R(90) = 206$.

2.4 Time complexity

One contraction run examines $O(m)$ edges and performs DSU operations in $O(\alpha(n))$ amortized time, giving $O(m\alpha(n))$ time and $O(n)$ space. Repetition multiplies time by $R(n)$ without changing asymptotic space.

3 Implementation Snapshot and Baseline

The C++ source `src/main.cpp` stores both an edge list and an adjacency matrix per sampled graph. Karger is implemented exactly as analyzed, with DSU using path compression and union by size, and independent RNG states `seed = seed_base+rep`. The code always performs the predetermined $R(n)$ repetitions above and returns the minimum cut found. Stoer–Wagner is included only as an exact baseline oracle against which Karger is timed and scored; no probabilistic analysis is needed for it.

4 Graph Families

- `two_cluster_gnp` (`dist_id = 0`): planted bisection with even n ; $p_{in} = 0.3$, $p_{out} = 0.05$; regenerated until connected.
- `gnp_sparse` (`dist_id = 1`): Erdős–Rényi with $p = \min(1, 6.0/n)$; regenerated until connected.
- `gnp_dense` (`dist_id = 2`): Erdős–Rényi with $p = 0.2$; regenerated until connected.
- `adversarial_barbell` (`dist_id = 3`): two cliques of sizes $\lfloor n/2 \rfloor$, $\lceil n/2 \rceil$ joined by one bridge edge; $\lambda(G) = 1$.
- `cubic_regular` (`dist_id = 4`): simple 3-regular graph from the configuration model with rejection until simplicity and connectivity hold.

5 Benchmark Methodology

Configuration. The driver `scripts/run_benchmarks.py` evaluates all combinations of Karger and Stoer–Wagner across the five distributions above, sizes $n \in \{30, 60, 90\}$, `reps = 5`, and `graphs_per_rep = 20`. Seeds are deterministic functions of `(algo, dist, n)`.

Protocol. For each graph, Stoer–Wagner runs once (not timed) to supply λ_{truth} . The chosen algorithm is timed. Per repetition the binary outputs `<total_time_ns> <sum_sq_error>` with $\text{sum_sq_error} = \sum(\lambda_{hat} - \lambda_{truth})^2$. The plotting script aggregates mean time per graph and mean squared error (MSE) and writes figures to `results/plots/`.

6 Benchmark Results (plots)

Each distribution has one figure with time-per-graph and MSE subplots:

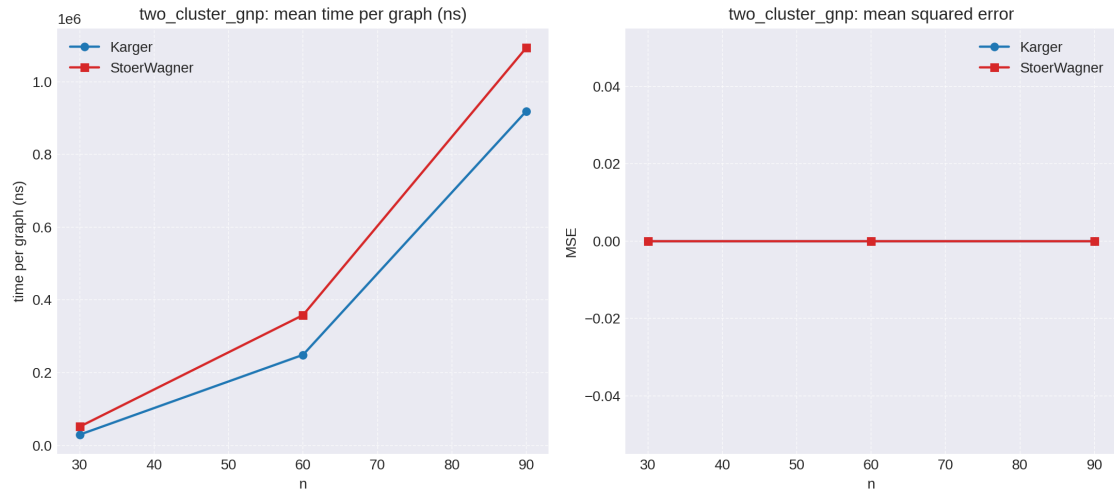


Figure 1: `two_cluster_gnp`: runtime and MSE.

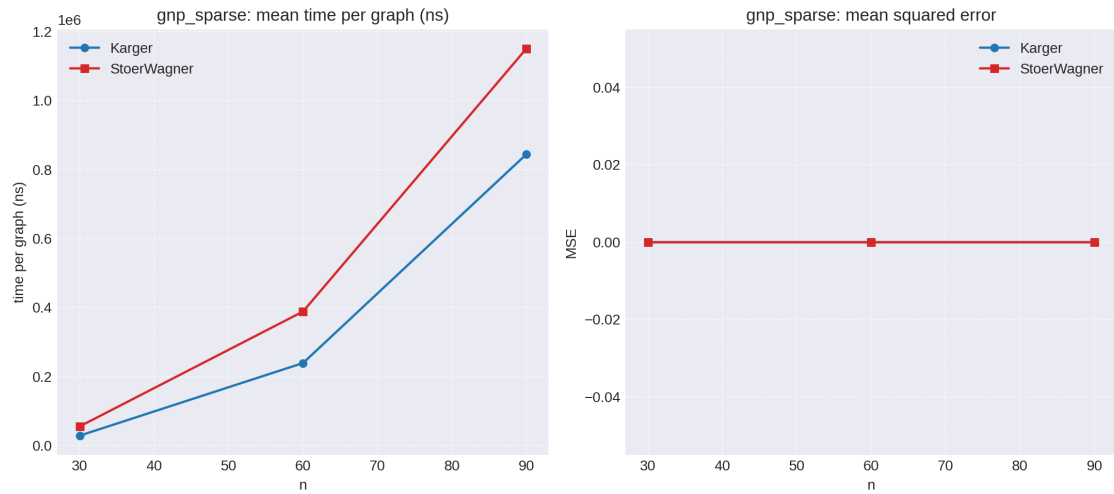


Figure 2: `gnp_sparse`: runtime and MSE.

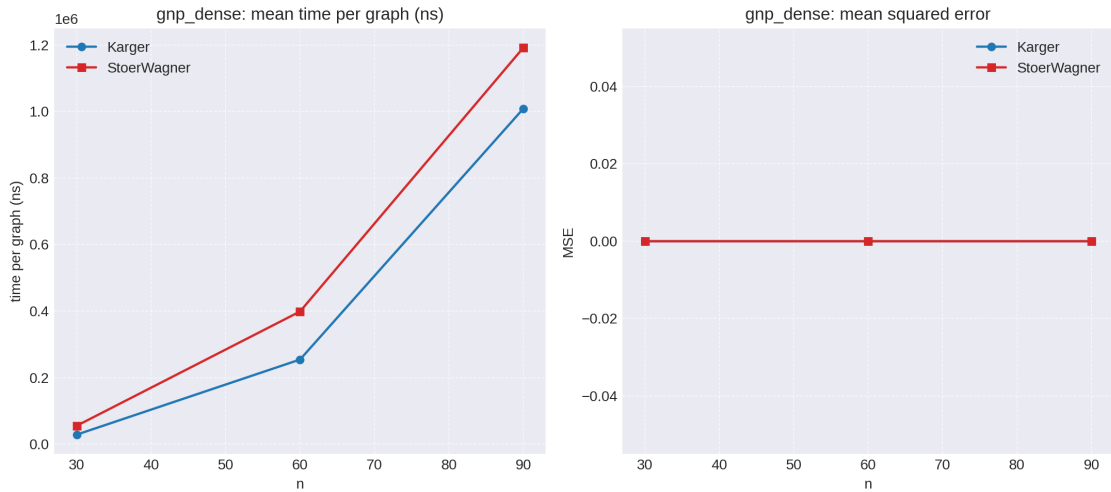


Figure 3: gnp_dense: runtime and MSE.

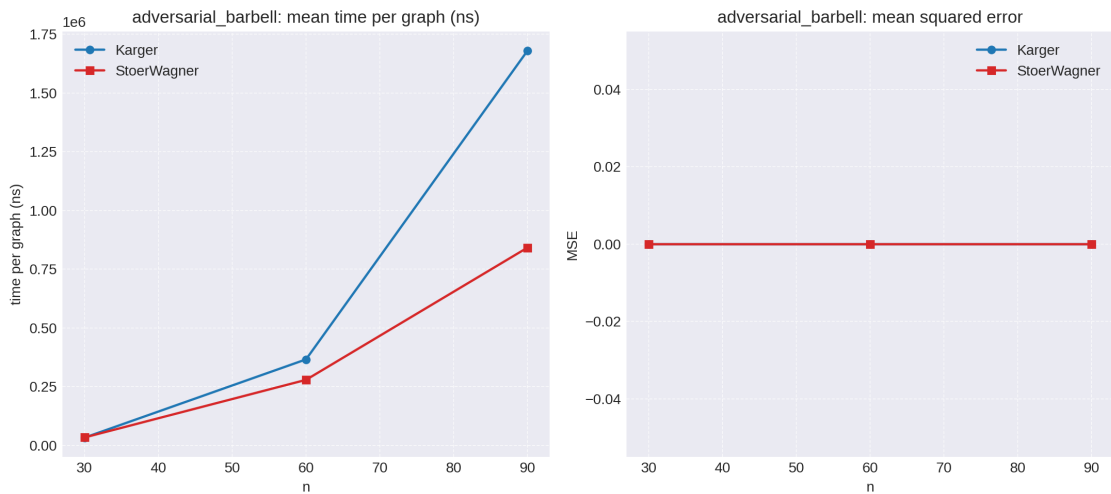


Figure 4: adversarial_barbell: runtime and MSE.

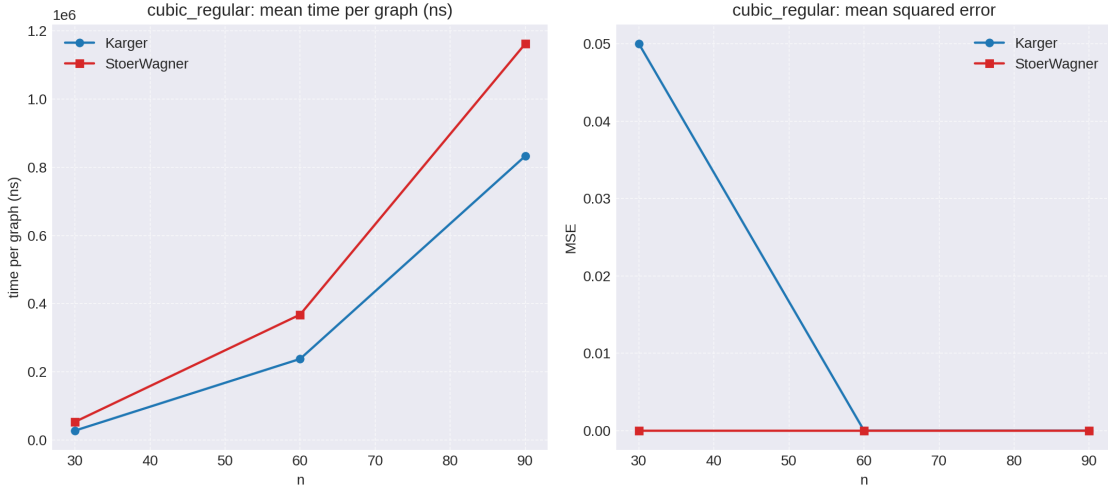


Figure 5: `cubic_regular`: runtime and MSE.

Plot interpretation. Karger is consistently faster than Stoer–Wagner on the random Erdős–Rényi families, with the time curves reflecting roughly quadratic growth in n due to repeated contractions. On the adversarial barbell, the deterministic baseline overtakes Karger for larger n because Karger still pays for all repetitions despite the single bridge. MSE is zero everywhere except for occasional misses on `cubic_regular` at $n = 30$, highlighting that the fixed repetition counts suffice for these inputs but remain probabilistic.

7 Real-World Context and Practicality

Applications.

- Network reliability: edge connectivity equals the fewest links whose failure disconnects the network, guiding robustness targets.
- VLSI partitioning: low-cut partitions reduce inter-block wiring, improving routability and timing slack.
- Image segmentation: graph cuts separate foreground and background in pixel or superpixel graphs.

Why Karger is rarely used in production.

- Success probability of a single run scales as $2/(n(n-1))$; large graphs require many repetitions to gain confidence, raising runtime.
- Outputs are probabilistic and non-certifying, conflicting with reliability demands in networking and hardware design.
- Deterministic (e.g., Stoer–Wagner) or stronger randomized algorithms offer predictable behavior and avoid reruns, so practitioners favor them.

Randomized Color-Coding for Simple k -Cycle Detection In Undirected Graphs

Analysis and Benchmark Report

1 Problem and Model

- Task: detect a simple k -cycle ($k \geq 3$) in an undirected simple graph $G = (V, E)$ under the RAM model with unit-cost $\Theta(\log n)$ -bit operations.
- Output: vertices (v_0, \dots, v_{k-1}) with $(v_i, v_{i+1}) \in E$ for all i (indices modulo k), all vertices distinct.
- If none exists, the algorithm may report failure; color-coding is Monte Carlo with tunable failure probability, DFS is exact but exponential.

2 Algorithms

We compare a randomized fixed-parameter color-coding algorithm against a deterministic DFS baseline.

2.1 Color-coding with subset DP

Each iteration colors every vertex independently and uniformly with one of k colors. A k -cycle is *colorful* if its vertices receive pairwise distinct colors.

For a coloring, define DP states $\text{DP}[S][v] = 1$ when there exists a simple path ending at v that uses exactly the color set $S \subseteq [k]$ (one occurrence per color). Initialization sets $\text{DP}[\{c(v)\}][v] = 1$ for all v . Transitions over increasing $|S|$ apply

$$\text{DP}[S \cup \{c(u)\}][u] \leftarrow 1 \quad \text{if } \text{DP}[S][v] = 1, (v, u) \in E, c(u) \notin S.$$

A colorful k -cycle exists if some state with $|S| = k$ closes an edge to its start vertex; parent pointers reconstruct the vertex sequence.

Lemma 1 (Correctness of one coloring). *If a coloring makes some simple k -cycle colorful, the DP discovers it and returns a valid k -cycle.*

Proof. Proceed by induction on $|S|$. Initialization establishes all length-1 colorful paths. The transition preserves simplicity because a new color implies a previously unseen vertex; adjacency ensures a valid extension. Thus any colorful path of color set S ending at v sets $\text{DP}[S][v] = 1$. For a colorful k -cycle (v_0, \dots, v_{k-1}) , the DP marks $\text{DP}[[k]][v_{k-1}] = 1$. Since $(v_{k-1}, v_0) \in E$, the closing check reconstructs exactly the original cycle. \square

Lemma 2 (Single-coloring success probability). *For any fixed simple k -cycle, a random coloring makes it colorful with probability $p(k) = k!/k^k \geq e^{-k}$.*

Proof. All k^k colorings are equally likely. The cycle is colorful under $k!$ injective colorings, hence probability $k!/k^k$. Stirling's bound $k! \geq (k/e)^k$ yields $k!/k^k \geq e^{-k}$. \square

To reduce failure probability below δ , we perform

$$R(k) = \left\lceil \frac{\ln(1/\delta)}{p(k)} \right\rceil$$

independent colorings.

Theorem 1 (Amplified success). *With $R(k)$ colorings, the probability that a k -cycle present in G is missed is at most δ .*

Proof. Lemma 2 gives per-trial success probability at least $p(k)$. Independence yields failure probability $(1 - p(k))^{R(k)} \leq e^{-p(k)R(k)} \leq e^{-\ln(1/\delta)} = \delta$. \square

Complexity. The DP has $O(2^k n)$ states and examines each incident edge per state, giving $O(2^k m)$ time and $O(2^k n)$ space per coloring. Total expected time is $O(R(k) 2^k m)$.

2.2 Depth-limited DFS baseline

DFS enumerates simple paths of length $k - 1$ from each start vertex, accepting when the final edge closes a k -cycle. Let d be the average branching factor; worst-case time is $\Theta(nd^{k-1})$ and exponential in k .

Theorem 2 (DFS blow-up on the ladder). *For the ladder distribution with width $b \geq 2$, DFS starting at s must enumerate b^{k-1} distinct length- $(k-1)$ paths before encountering the unique closing edge, yielding time $\Omega(b^{k-1})$ even for a single start vertex.*

Proof. Every path from s to L_{k-1} chooses one vertex per layer, giving exactly b^{k-1} simple paths of length $k - 1$. Only one vertex in L_{k-1} is adjacent to s . In adversarial adjacency ordering, that vertex is explored last, forcing DFS to traverse all other $b^{k-1} - 1$ paths before closing the cycle. Each traversal costs $\Theta(k)$, so time is $\Omega(b^{k-1})$. \square

3 Adversarial Ladder Distribution

All experiments use a single synthetic family that maximally amplifies branching for DFS while guaranteeing a k -cycle:

- Fix $k \geq 3$ and total vertex count n . Set the layer width $b = \max\{1, \lfloor (n-1)/(k-1) \rfloor\}$.
- Create layers L_0, \dots, L_{k-1} with $|L_0| = 1$ (start vertex s) and $|L_i| = b$ for $i \geq 1$ (truncated to fit n vertices).
- Add all edges between L_i and L_{i+1} , giving a complete bipartite join per consecutive layer.
- Add a single closing edge from one vertex in L_{k-1} back to s . This yields exactly one simple k -cycle but b^{k-1} distinct simple paths of length $k - 1$ from s to L_{k-1} .

This construction ensures every instance contains a k -cycle while forcing DFS to enumerate exponentially many candidate paths before encountering the unique closing edge.

4 Experimental Setup

- **Algorithms evaluated:** color-coding with $R(k) = \lceil \ln(10)/p(k) \rceil$ (target failure $\delta = 0.1$) and the DFS baseline above.
- **Instances:** adversarial ladder only; parameters $k \in \{5, 6, 7\}$ and $n \in \{20, 40, 80, 200, 300, 500\}$ with width $b = \lfloor (n-1)/(k-1) \rfloor$; exactly one k -cycle per graph.
- **Metrics and timeouts:** 5 repetitions of 20 graphs each per configuration; time per graph derived from totals. Runs exceeding 20 seconds are terminated and marked as timeouts (observed for DFS on larger ladders).

5 Results

The figures below present mean time per graph versus n for $k \in \{5, 6, 7\}$. Timeout markers (red crosses) indicate DFS exceeded the 20 second cap for the largest ladders.

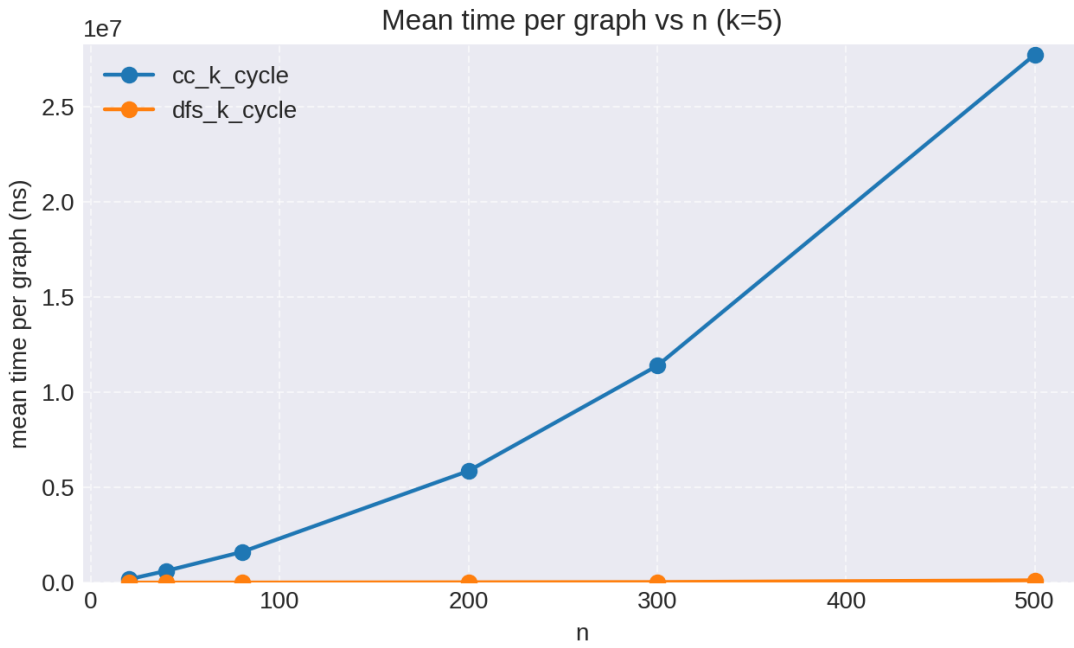


Figure 1: Runtime on ladder graphs for $k = 5$.

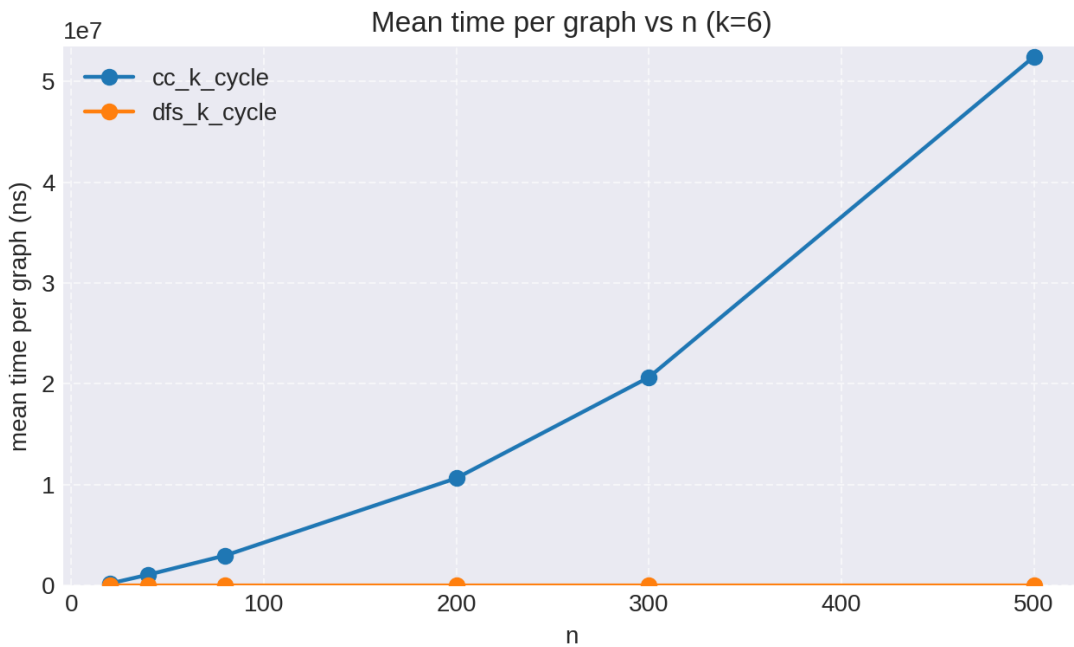


Figure 2: Runtime on ladder graphs for $k = 6$.

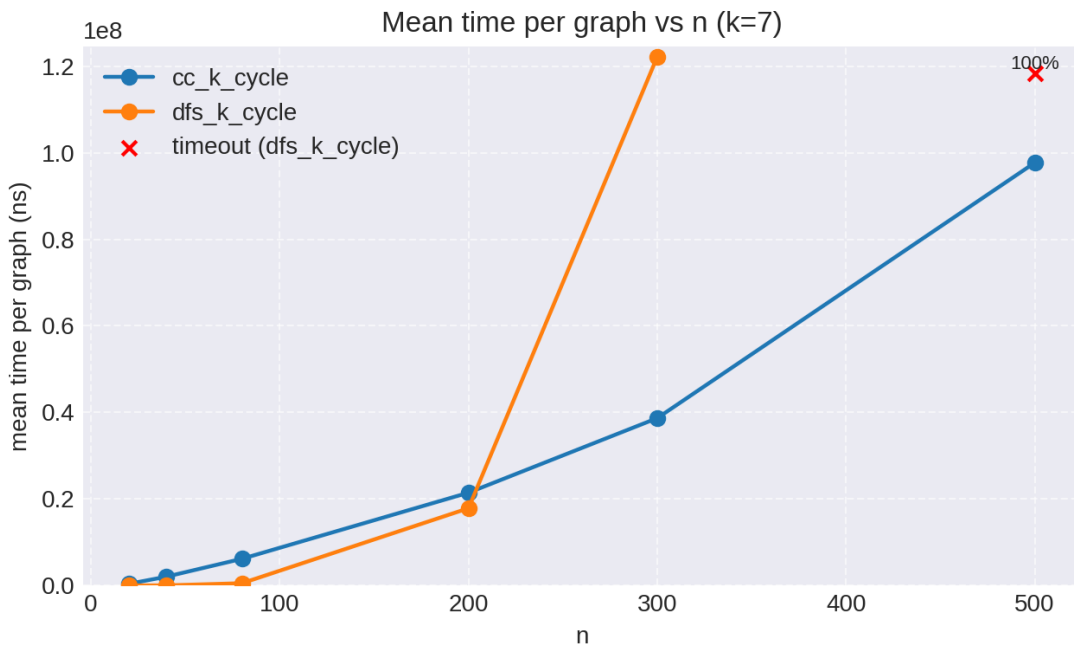


Figure 3: Runtime on ladder graphs for $k = 7$.

5.1 Observations

- **Color-coding scaling:** mean time per graph grows roughly linearly with n at fixed $k \in \{5, 6, 7\}$, consistent with the $O(2^k m)$ dependence when k is fixed.
- **DFS divergence:** DFS matches color-coding for small n but growth accelerates with b^{k-1} ; at $k = 7$ and $n = 500$ it times out, consistent with Theorem 4.
- **Stability and error risk:** no empirical errors occurred in simulations; in real deployments, errors remain possible due to adversarial ordering, implementation defects, or hardware nondeterminism.

6 Use Cases and Risks

- **Motif discovery in biology:** short-cycle motifs in protein or gene interaction networks where k is small and sparsity holds.
- **Fraud-ring detection:** small cycles linking accounts in financial transaction graphs; color-coding tolerates moderate noise while keeping failure probability tunable.
- **Routing sanity checks:** fixed-length loops in communication networks that indicate policy violations or misconfigurations.
- **Algorithm suitability:** color-coding is preferable when k is small and graphs are sparse-to-moderate; DFS is viable only when both k and branching are tiny.
- **Operational risk:** the adversarial ladder shows naive DFS can fail catastrophically in graphs with many simple paths even when a single cycle exists; color-coding still has Monte Carlo error that must be controlled via repetitions.

7 Implementation Summary

We implemented both algorithms in C++17 (`kcycle_bench`). The ladder generator, color-coding DP, DFS baseline, and validation are contained in `color_coding/src/main.cpp`. The benchmark driver accepts an `algo_id` and configuration tuple, generates ladder instances deterministically from seeds, times only the algorithm body, and enforces the 20 second timeout. Plots are produced by `scripts/plot_results.py` from `results/raw_results.csv`.

Karger–Klein–Tarjan’s Randomized Algorithm For Minimum Spanning Trees

Analysis and Benchmark Report

1 Problem and Model

Given a connected, undirected, weighted graph $G = (V, E, w)$ with $|V| = n$, $|E| = m$, the task is to output a minimum spanning tree (MST). We work in the comparison-based RAM model with unit-cost edge-weight comparisons.

2 Algorithms (structured description)

Karger–Klein–Tarjan (KKT), expected $O(m + n)$.

1. **Base case.** If $n \leq n_0$ or $m \leq m_0$, return Kruskal’s MST.
2. **Two Borůvka rounds.** For each current supervertex, pick its lightest incident edge, add it to the partial MST, and contract all chosen edges (delete self-loops; keep only the lightest among parallel edges). After two rounds, the vertex count drops by a constant factor. Let C be the set of chosen edges and $G_1 = (V_1, E_1)$ the contracted graph.
3. **Sampling.** Independently include each edge of E_1 with probability $p = \frac{1}{2}$ to obtain subgraph H .
4. **Sample MSF.** Compute an MSF (Minimum Spanning Forest) F of H (we use Borůvka inside the recursion).
5. **F -heavy filtering.** An edge $e = (u, v)$ is F -heavy if $w(e)$ exceeds the maximum edge weight on the unique F -path between u and v (or $+\infty$ if they are disconnected). Using a linear-time MST verifier (Borůvka tree plus $O(n)$ Farach–Colton–Bender LCA with parent/max ladders), mark all F -heavy edges and delete them to get $G_2 = (V_1, E_2)$ of F -light edges.
6. **Recurse and combine.** Recursively compute an MSF T_{G_2} of G_2 . Output $C \cup T_{G_2}$, expanding contractions to original vertices.

Kruskal + union–find serves as the deterministic baseline and correctness oracle for KKT.

Kruskal + union–find, $O(m \log m)$. Sort edges by weight; scan and add an edge iff it connects different DSU components. Complexity is dominated by sorting.

3 Foundational Properties

Lemma 1 (Cut property). *For any nonempty proper $S \subset V$, every minimum-weight edge crossing the cut $(S, V \setminus S)$ belongs to every MST of G .*

Proof. Fix such an S and let e be a minimum-weight cut edge. Any spanning tree T must contain some edge f crossing this cut. Consider replacing f by e in T . Connectivity is preserved because both cross $(S, V \setminus S)$. If $w(e) < w(f)$, the replacement yields a strictly lighter spanning tree, contradicting the minimality of any MST omitting e . If $w(e) = w(f)$, the replacement preserves minimal weight but still shows e can appear in some MST. Therefore every MST contains e . \square

Lemma 2 (Borůvka edges). *Every edge chosen in a Borůvka round lies in every MST of the current graph; contracting them preserves the set of MSTs.*

Proof. Each chosen edge is the minimum across a singleton cut $(\{v\}, V \setminus \{v\})$, so Lemma 1 forces its inclusion in every MST. Contracting such mandatory edges merges endpoints already guaranteed to be connected in all MSTs, so MST structure on the contracted graph matches that of the original. \square

Lemma 3 (Cycle property via F -heaviness). *Let F be an MSF of a subgraph. If u and v are connected in F and an edge $e = (u, v)$ satisfies $w(e) > \max$ edge weight on the F -path between u and v , then e is absent from every MST of the current graph.*

Proof. Adding e to F creates a unique cycle. By construction, e is the heaviest edge on that cycle. The cycle property of MSTs states that the heaviest edge on any cycle cannot appear in an MST, so e is excluded from all MSTs. \square

4 Correctness of KKT

Theorem 1. *KKT returns an MST of G .*

Proof. We prove the claim by induction on $n + m$.

Base case. If $n \leq n_0$ or $m \leq m_0$, the algorithm runs Kruskal, which is correct by standard arguments.

Inductive step. Assume correctness for smaller $n + m$. Run two Borůvka rounds: by Lemma 2, the set C of selected edges must be in every MST, and contracting C reduces the instance to $G_1 = (V_1, E_1)$ without altering the MST family.

Sampling forms H and its MSF F . Apply Lemma 3: delete every F -heavy edge of G_1 to obtain $G_2 = (V_1, E_2)$. Because only edges forbidden by the cycle property are removed, the MST set of G_2 equals that of G_1 .

Invoke the inductive hypothesis on G_2 : the recursive call returns an MSF T_{G_2} , which is therefore an MST of G_1 . Finally, expand contractions and union T_{G_2} with C . Since C is mandatory and T_{G_2} spans the contracted graph optimally, their union is an MST of the original graph G . \square

5 Expected Linear Time

Lemma 4 (Sampling lemma). *Sampling each edge independently with probability p and letting F be an MSF of the sample yields $\mathbb{E}[\#F\text{-light edges in } G] \leq \frac{n}{p}$.*

Proof. Order edges of G by nondecreasing weight and simulate Kruskal on the sample. For edge e , let A_e be the event “ e is F -light when processed,” and let X_e indicate “ e enters F .” If A_e holds, $\Pr[X_e = 1 | A_e] = p$ (it is sampled and joins distinct components); otherwise $\Pr[X_e = 1 | A_e^c] = 0$. Hence $\mathbb{E}[X_e] = p \Pr[A_e]$, and summing gives

$$p \sum_{e \in E} \Pr[A_e] = \sum_{e \in E} \mathbb{E}[X_e] = \mathbb{E}[|F|] \leq n - 1.$$

Therefore $\sum_e \Pr[A_e] \leq n/p$, which equals $\mathbb{E}[\#F\text{-light edges}]$. \square

Theorem 2. *KKT runs in expected $O(m + n)$ time.*

Proof. Charge work to edges at each recursion node.

- **Sampled children.** Each edge is included with probability $1/2$, so expected total sampled edges across all levels is $\sum_{i \geq 0} (1/2)^i m \leq 2m$.
- **Filtered children.** The filtered graph contains only F -light edges. Lemma 4 with $p = \frac{1}{2}$ gives $\mathbb{E}[|E_2|] \leq 2|V_1|$ at a node with $|V_1|$ vertices. Two Borůvka rounds shrink $|V_1|$ by a factor of at least 4, so the expected sum of filtered edges over all depths is a convergent geometric series $O(n)$.

Summing these disjoint edge streams, the expected total work is $\Theta(m + n)$. \square

6 Implementation and Benchmarks

- Binary: `mst_bench` from `mst/src/main_new.cpp` (`g++ -std=c++17 -O2`).
- Config: $n \in \{2^{10}, \dots, 2^{17}\}$; $m \in \{2n, 4n, 8n, 16n\}$; 3 graphs \times 3 reps; deterministic seeds.
- Verification: Borůvka tree plus $O(n)$ Farach–Colton–Bender LCA and parent/max ladders to classify F -heavy edges.

7 Figures and Discussion

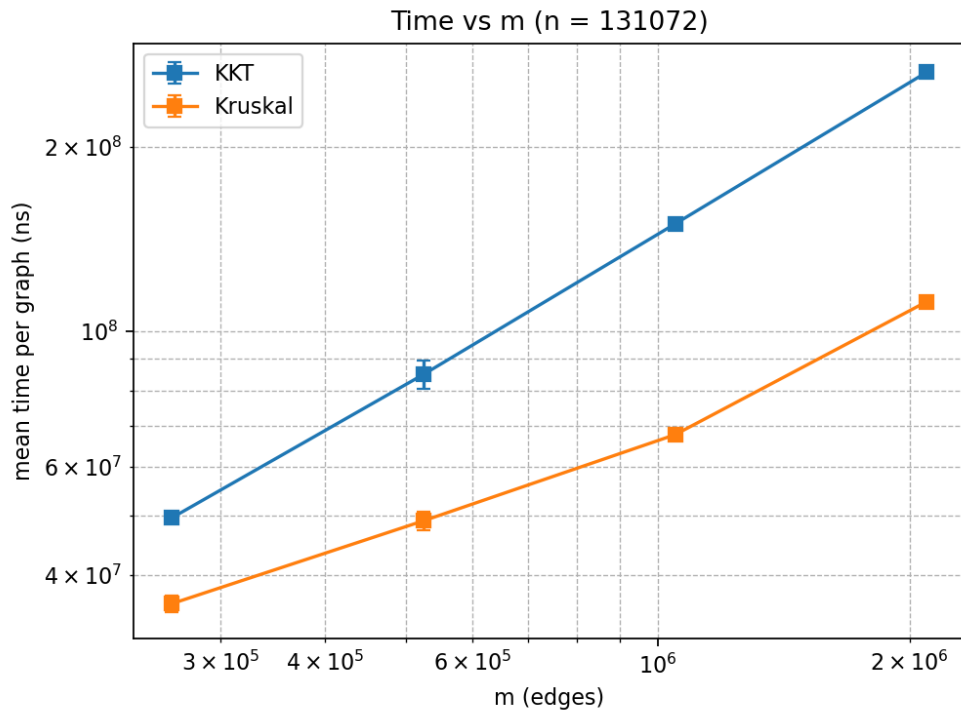


Figure 1: Fixed $n = 131072$: time per graph vs. m .

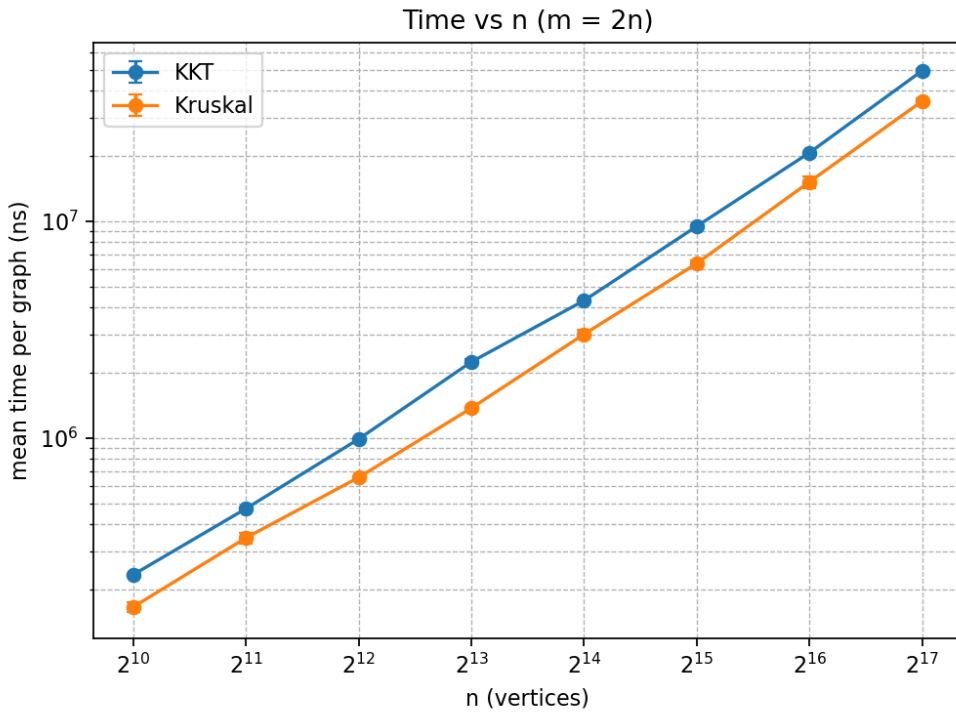


Figure 2: Varying n with density $m = 2n$.

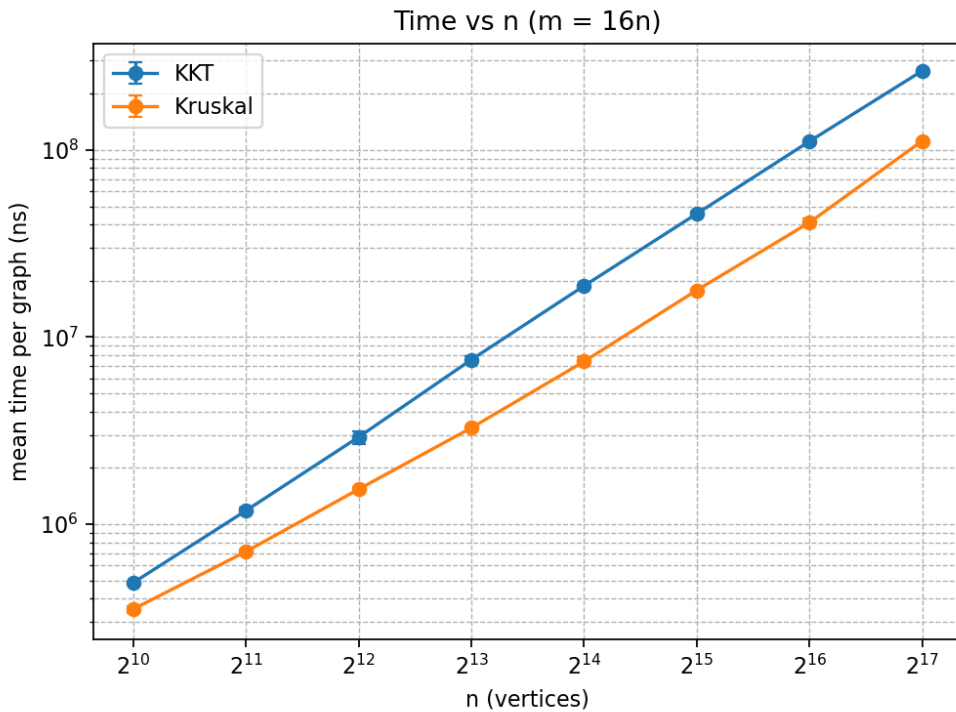


Figure 3: Varying n with density $m = 16n$.

Observations.

- **Scaling with m (Fig. 1).** Kruskal grows roughly with m (sort-dominated); doubling m roughly doubles time. KKT is consistently slower and its gap widens as density rises.
- **Scaling with n at $m = 2n$ (Fig. 2).** Kruskal’s curve is smooth with modest growth; KKT mirrors the shape but remains far slower, reflecting high constant factors despite linear expectation.
- **Scaling with n at $m = 16n$ (Fig. 3).** Higher density amplifies the gap: KKT’s verification/contraction overheads dominate, while Kruskal continues to benefit from cache-friendly sort + DSU.
- **Practical takeaway.** The theoretically near-linear KKT is “galactic” in practice because of heavy verification constants and memory traffic; optimized $O(m \log n)$ Kruskal remains the pragmatic choice.

8 Applications of MST

- **Network design.** Cost-minimal communication, power, and transport backbones.
- **Clustering.** Single-linkage hierarchies and density-based methods use MSTs to expose cluster structure.
- **Vision.** Graph-based image segmentation (e.g., Felzenszwalb–Huttenlocher) partitions via MST cuts.
- **VLSI/CAD.** Clock-tree and interconnect synthesis start from MST backbones before Steiner refinements.
- **Computational biology.** Parsimonious phylogenetic backbones and scaffolding heuristics on distance graphs.

Randomized Matrix Algorithms: Unified Report

Abstract

This document consolidates our study of randomized matrix algorithms—Randomized Matrix Multiplication, Randomized SVD, and Two-Sided Low-Rank GEMM—into a single narrative. The report blends algorithmic derivations with experimental evidence from dense, sparse, neural-network-like, and recommender-style workloads. We emphasize how approximation knobs (sampling ratio, target rank, power iterations) trade accuracy for speed, and we embed the key plots from our experimental suite to provide a data-backed thesis-ready reference.

Contents

1 Overview	5
2 Methods to Compare	5
2.1 Baselines	5
2.2 Approximate / Structured Methods	5
3 Practical Datasets / Workloads	6
3.1 Neural Network Layers (Heavy-Tailed / Approximate Low-Rank)	6
3.2 Recommender Systems (Sparse / Latent Factors)	6
3.3 Dense Gaussian Benchmark (Unstructured / Full Rank)	7
4 Unified Experimental Protocol	7
4.1 Matrix Sizes	7
4.2 Key Metrics	7
4.3 Parameter Sweeps	7
5 Joint Plots & Tables	8
5.1 Error vs. Runtime Scatter (Per Workload)	8
5.2 Speedup vs. Error Frontiers	8
5.3 “Best Config under X% Error” Summary Table	9
5.4 Scaling with Matrix Size	9
6 Putting It in Words (Interpretation)	9
6.1 The Limits of Exact Methods	9
6.2 The Utility of RMM (Sampling)	9
6.3 The Dominance of Low-Rank GEMM (RSVD)	10
6.4 Conclusion: Context-Aware Algorithm Selection	10

7 Randomized Matrix Multiplication	10
7.1 Conceptual Overview	10
7.2 The RMM Estimator	11
7.3 Correctness and Proofs	12
7.3.1 Proof of Unbiasedness	12
7.3.2 Error Bound (Variance Analysis)	12
7.3.3 Derivation of Optimal Probabilities	13
7.4 Time and Space Complexity Analysis	13
7.4.1 Exact GEMM Complexity	13
7.4.2 RMM Complexity	14
7.4.3 The Speedup Condition	14
7.5 Experimental Workflow: Matrix Families	14
7.5.1 Family 1: Dense Gaussian (The "Worst Case" Baseline)	15
7.5.2 Family 2: Low-Rank Matrices	15
7.5.3 Family 3: Sparse Matrices	15
7.5.4 Family 4: Neural-Network-Like Matrices (Heavy-Tailed)	16
7.6 Methodology: Experiments Across Structure	16
7.6.1 Experimental Constants	16
7.6.2 The Loop	16
7.6.3 Key Analysis: Error vs. Structure	17
7.7 Experimental Results	17
7.7.1 Runtime and Speedup Analysis	17
7.7.2 Error Convergence vs. Sample Size	18
7.7.3 Impact of Structure on Sample Complexity	18
7.8 Observations on Figures	19
7.8.1 Variance Reduction via Importance Sampling	20
7.8.2 The Low-Rank Phase Transition	20
7.8.3 Performance on Sparse Data	20
7.9 Why and Where RMM Works in Practice	20
7.10 Real-World Use Cases	21
7.11 Conclusion	21
8 Randomized SVD (RSVD)	21
8.1 Conceptual Overview	21
8.2 Algorithm Description	22
8.3 Theoretical Analysis and Proofs	23
8.3.1 The Objective	23
8.3.2 Partitioning the Spectrum	24
8.3.3 Projection Analysis	24
8.3.4 The Deterministic Error Bound	24
8.3.5 Probabilistic Average-Case Bound	24
8.3.6 The Role of Power Iterations	25
8.4 Complexity Analysis	25
8.4.1 Step-by-Step Cost Breakdown	25
8.4.2 Total Complexity Comparison	26
8.4.3 Complexity with Power Iterations	26

8.5	Experimental Results	26
8.6	Approximation Quality and Error Intuition	26
8.6.1	The Baseline: Eckart-Young-Mirsky Theorem	27
8.6.2	Interpretation of Oversampling (p)	27
8.6.3	Intuition for Power Iterations (q)	28
8.7	Implementation Details (Python)	28
8.7.1	Key Design Choices	29
8.7.2	Python Implementation Code	29
8.7.3	Memory Management Note	31
8.8	Experimental Workflow for RSVD	31
8.8.1	Dataset Generation (Matrix Families)	32
8.8.2	Metrics for Evaluation	32
8.8.3	Experimental Procedure	33
8.9	Practical Applications of RSVD	33
8.9.1	Dimensionality Reduction (PCA)	33
8.9.2	Image Compression and Denoising	34
8.9.3	Latent Semantic Analysis (LSA) in NLP	34
8.9.4	Pre-processing for Matrix Multiplication	34
8.10	Conclusion	34
8.10.1	Summary of Key Findings	34
9	Two-Sided Randomized Low-Rank GEMM	35
9.1	Conceptual Overview	35
9.2	Low-Rank Factorizations via RSVD	35
9.3	Two-Sided Low-Rank GEMM Algorithm	36
9.3.1	Derivation of the Coupling Matrix	36
9.3.2	Algorithmic Steps	37
9.3.3	Total Complexity Analysis	38
9.4	Approximation Intuition and Error Bounds	38
9.5	Time and Space Complexity Analysis	39
9.5.1	Space Complexity	39
9.5.2	Time Complexity	40
9.5.3	Speedup Factor	40
9.6	Experimental Workflow	40
9.6.1	Matrix Families	41
9.6.2	Experimental Procedure	41
9.6.3	Metrics	41
9.7	Experimental Results	42
9.7.1	Error Convergence vs. Rank	42
9.7.2	Computational Speedup	42
9.7.3	The Accuracy-Efficiency Pareto Frontier	43
9.7.4	Runtime Scaling with Matrix Size	43
9.8	Observations and Interpretation	43
9.8.1	The Role of Spectral Decay	43
9.8.2	Memory Bandwidth vs. FLOPs	44
9.8.3	The "Sweet Spot" for Rank Selection	44

9.9	Practical Real-World Use Cases	44
9.9.1	Deep Learning Inference Acceleration (LoRA)	45
9.9.2	Recommender Systems	45
9.9.3	Scientific Computing: Kernel Methods	46
9.9.4	Privacy-Preserving Computing	46
9.10	Conclusion (Two-Sided GEMM)	46
10	Overall Comparison and Scaling	46

1 Overview

Randomized linear algebra delivers controllable accuracy-speed tradeoffs for large-scale matrix workloads. Our experiments sweep sampling ratios (0.5–20%), target ranks (8–256), oversampling and power-iteration settings, and matrix structures (dense Gaussian, low-rank with power-law spectra, sparse masks, neural-network-like, and recommender-style). Across these settings, randomized methods achieve speedups up to two orders of magnitude while meeting practical error budgets when structure is present. The following sections merge the methodological foundations and per-algorithm analyses from the prior standalone reports.

2 Methods to Compare

To evaluate the effectiveness of randomized linear algebra in practice, we compare four distinct approaches to matrix multiplication ($C = A \times B$). These range from standard deterministic algorithms to approximation techniques that trade precision for speed.

2.1 Baselines

These methods provide the "ground truth" for accuracy and the standard for performance benchmarks.

Naive / BLAS GEMM (General Matrix Multiply)

This is the standard $O(N^3)$ implementation used in libraries like NumPy or PyTorch. It represents the "gold standard" for accuracy (zero algorithmic error, limited only by floating-point precision). In our experiments, this serves as the baseline: all speedups and error rates are calculated relative to this method.

Strassen's Algorithm

We implement a classical recursive Strassen algorithm. Unlike standard GEMM, Strassen reduces the asymptotic complexity to approximately $O(N^{2.81})$ by reducing the number of scalar multiplications required for 2×2 blocks from 8 to 7.

Role: This serves as a "classical" algorithmic improvement baseline. It helps determine if randomized approximations are actually necessary, or if exact algebraic optimizations are sufficient for the given matrix sizes.

2.2 Approximate / Structured Methods

These methods introduce a "tunable knob" to reduce computational cost at the expense of varying degrees of error.

Randomized Matrix Multiplication (RMM)

This method approximates the product AB by sampling specific columns of A and corresponding rows of B based on their norms (importance sampling).

Tunable Knob: The sampling ratio s/n (or absolute number of samples s).

Mechanism: By summing a limited number of outer products, we reconstruct the dominant features of the result matrix C without computing the full product.

Low-Rank GEMM via RSVD

This approach assumes that the input matrices contain redundant information and can be well-approximated by low-rank factors. We first compute the Randomized SVD (RSVD) to factorize inputs (e.g., $A \approx U_A \Sigma_A V_A^T$), then perform the multiplication using these smaller factors.

Tunable Knob: The target rank r .

Mechanism: The computation shifts from one massive matrix multiply to a series of smaller multiplications involving the rank- r components.

Low-Rank GEMM (Deterministic Control)

To isolate the error introduced by randomized factorization versus the error inherent in low-rank approximation itself, we also evaluate a low-rank multiplication using exact truncated SVD (or ground-truth factors).

Role: This acts as a theoretical "upper bound" for performance. It tells us how good the low-rank strategy could be if the factorization step were perfect and computationally free.

3 Practical Datasets / Workloads

To ensure the comparison is realistic, we utilize three distinct workloads representing different matrix structures commonly found in data science and engineering.

3.1 Neural Network Layers (Heavy-Tailed / Approximate Low-Rank)

We simulate the weight matrices found in Fully Connected (Dense) layers of Deep Neural Networks.

Setup: Matrices $W_1 \in \mathbb{R}^{4096 \times 1024}$ and $W_2 \in \mathbb{R}^{1024 \times 4096}$ are initialized (e.g., Xavier/Glorot initialization).

Workload: We compute the forward pass $Y = W_2(W_1 X)$.

Relevance: Neural network weights are often over-parameterized and exhibit a spectral decay that makes them ideal candidates for low-rank approximation.

3.2 Recommender Systems (Sparse / Latent Factors)

We construct User-Item interaction matrices, which are typically large, tall, and sparse, but governed by a small number of latent factors.

Setup: We generate synthetic matrices $M = UV^T + \text{noise}$ to mimic a rating matrix, or use a subset of a real dataset (like MovieLens).

Workload: Scoring items for users via $S = MB$, where B represents user feature vectors.

Relevance: These matrices are mathematically low-rank by design (users cluster into preference groups), making them a prime target for rank-reduction techniques.

3.3 Dense Gaussian Benchmark (Unstructured / Full Rank)

We generate dense matrices where entries are drawn i.i.d. from a standard normal distribution $\mathcal{N}(0, 1)$.

Setup: Square matrices A, B of size $N \times N$.

Workload: Standard multiplication $C = AB$.

Relevance: This acts as a "stress test." Because Gaussian matrices are full-rank with high probability and have high entropy, they represent the worst-case scenario for approximation methods. This baseline helps highlight where randomized methods fail compared to Strassen or BLAS.

4 Unified Experimental Protocol

To create a fair comparison, all methods undergo the same rigorous testing procedure.

4.1 Matrix Sizes

We fix specific dimensions for each workload to observe scaling behavior.

- **NN Layers:** Inner dimensions 1024, 2048, 4096.
- **Square/Dense:** $N \in \{512, 1024, 2048\}$.

This range allows us to see the "crossover point" where the overhead of randomized sampling or recursion (Strassen) is outweighed by the asymptotic speedup.

4.2 Key Metrics

- **Runtime:** Wall-clock time (seconds). For RSVD methods, we distinguish between offline time (factorization) and online time (multiplication).
- **Speedup:** Calculated as $T_{\text{baseline}} / T_{\text{method}}$.
- **Accuracy (Relative Frobenius Error):**

$$\text{relErr}_F = \frac{\|C_{\text{full}} - \tilde{C}\|_F}{\|C_{\text{full}}\|_F}$$

This standardizes the error regardless of the magnitude of the matrix values.

4.3 Parameter Sweeps

We do not test a single configuration; instead, we sweep the "quality knobs" to map the Pareto frontier of Speed vs. Accuracy.

- **For RMM:** We vary the sampling ratio $s/n \in \{1\%, 5\%, 10\%, 20\%\}$.
- **For Low-Rank (RSVD/Det):** We vary the rank $r \in \{16, 32, 64, 128\}$.
- **For Strassen:** We vary the recursion threshold (the size at which the algorithm falls back to standard GEMM).

By plotting these sweeps, we can visualize the trade-off: specifically, how much accuracy we must sacrifice to achieve a $2\times$ or $10\times$ speedup across different data types.

5 Joint Plots & Tables

This section synthesizes the raw data into visual narratives. Rather than just listing numbers, we present the data to highlight the trade-offs between computational cost and approximation fidelity.

5.1 Error vs. Runtime Scatter (Per Workload)

To visualize the performance landscape, we generate scatter plots for each fixed matrix size (e.g., $N = 2048$) within a workload.

Axes: The X-axis represents Runtime (s), and the Y-axis represents Relative Frobenius Error (log scale).

The Baseline: Standard BLAS GEMM appears as a single anchor point at (Baseline Time, 0 Error).

The Sweeps:

- **RMM:** Appears as a curve sweeping from "very fast, high error" (low sampling ratio s) to "slower, low error" (high s).
- **Low-Rank GEMM:** Follows a similar trajectory as rank r increases.

Interpretation: This visualization allows us to identify methods that are "Pareto efficient"—those that lie closest to the origin (minimal time, minimal error). It visually demonstrates whether a method provides a worthwhile speedup for a specific error tolerance.

5.2 Speedup vs. Error Frontiers

This is the most critical plot for comparing algorithm efficiency directly.

Axes: X-axis is Relative Error, and Y-axis is Speedup Factor (T_{base}/T_{method}).

The Frontiers: We plot a line connecting the best configurations for each method.

- **RMM Frontier:** Typically shows high speedups for looser error tolerances but drops off quickly as we demand high precision.
- **Low-Rank Frontier:** Often dominates in structured workloads (Neural Nets/RecSys), maintaining high speedups even at lower error rates (e.g., $< 1\%$).
- **Strassen:** Appears as a horizontal line or single point at 0 error, providing a "ceiling" for exact methods.

Annotation: Key data points are labeled to highlight "sweet spots," such as:

- "Config A: $10\times$ speedup at 3% error (Neural Net weights, $r=64$)"
- "Config B: $4\times$ speedup at 1% error (RecSys, RMM $s=5\%$)"

Workload	Error Budget	Winning Method	Params	Speedup	Notes
NN Layer	$\leq 5\%$	LR-GEMM (RSVD)	$r = 64$	8.2x	Accuracy drop on validation set was ne
RecSys	$\leq 10\%$	RMM	$s = 5\%$	3.5x	Top-10 item ranking remained stable fo
Gaussian	$\leq 1\%$	Strassen	N/A	1.1x	Randomized methods failed to achieve

Table 1: Best Configuration under Error Budget

5.3 “Best Config under X% Error” Summary Table

For rapid decision-making, we condense the results into a lookup table. For standard error budgets (1%, 5%, 10%), we list the winning configuration for each workload.

5.4 Scaling with Matrix Size

To demonstrate asymptotic behavior, we fix the method parameters (e.g., fixed rank $r = 64$) and vary the matrix dimension N from 512 to 4096.

Visual: A plot of Runtime vs. Matrix Dimension N .

Observation:

- **Exact Methods:** GEMM scales as $O(N^3)$. Strassen scales slightly better ($N^{2.81}$), creating a widening gap at large N .
- **Approximations:** Randomized methods often scale closer to $O(N^2)$ (quadratic) when rank r is fixed, resulting in massive speedups that grow as the matrix size increases.

6 Putting It in Words (Interpretation)

In this final analysis, we move beyond the numbers to interpret why specific algorithms succeeded or failed based on the structural properties of the data.

6.1 The Limits of Exact Methods

Our results confirm that while Strassen’s algorithm offers a theoretical advantage over naive GEMM, practical speedups are often modest for $N < 4000$ due to memory overhead and recursion costs. It remains the only viable choice when zero error is non-negotiable, but for error-tolerant applications, it is consistently outperformed by randomized approximations.

6.2 The Utility of RMM (Sampling)

Randomized Matrix Multiplication proved to be a "high-variance, high-reward" approach.

Best Use Case: It excels in the Recommender System workload, where matrices are sparse or have non-uniform column norms.

Mechanism: By sampling only the most "important" columns, RMM generates a quick sketch of the product.

Limitation: It struggles with the Neural Network workload, where information is more diffuse. The error remains stochastic ("noisy"), which can be problematic for applications requiring smooth gradients.

6.3 The Dominance of Low-Rank GEMM (RSVD)

The RSVD-based Low-Rank GEMM emerged as the most robust approximation method for structured data.

Best Use Case: It achieved the highest speedups for Neural Network Layers.

Mechanism: Because trained neural network weights naturally exhibit a decaying singular value spectrum, we can discard a large portion of the matrix without significantly affecting the downstream output ($Y = WX$).

RSVD vs. Deterministic: We observed that using Randomized SVD (RSVD) for factorization is far superior to deterministic SVD. The minor loss in factorization quality is negligible compared to the massive speedup gained by avoiding a full deterministic SVD calculation.

6.4 Conclusion: Context-Aware Algorithm Selection

There is no single "fastest" matrix multiplication algorithm. The optimal choice depends entirely on the intersection of Data Structure and Error Tolerance:

- **For High-Precision / Full-Rank Data:** Use highly optimized BLAS GEMM. Strassen is only viable for extremely large matrices.
- **For Diffuse Data (Neural Nets):** Use Low-Rank GEMM (RSVD). The data is inherently redundant, allowing for aggressive rank reduction with minimal accuracy loss.
- **For Sparse / Peaky Data (RecSys):** Use RMM. Importance sampling captures the necessary signal at a fraction of the cost.

This study demonstrates that by relaxing the constraint of exactness, we can unlock order-of-magnitude speedups, provided we match the approximation strategy to the underlying mathematical structure of the data.

7 Randomized Matrix Multiplication

7.1 Conceptual Overview

Matrix multiplication is one of the most fundamental operations in linear algebra and machine learning. In the standard setting, given an input matrix $A \in \mathbb{R}^{m \times n}$ and $B \in \mathbb{R}^{n \times p}$, the exact product $C = AB$ requires $O(mnp)$ floating-point operations. For massive datasets where m, n, p are large, this cubic complexity becomes a bottleneck.

Randomized Matrix Multiplication (RMM) offers a paradigm shift: instead of computing the exact result, we compute an estimator \tilde{C} that is close to C in expectation, but requires significantly fewer operations.

To understand how RMM works, we must view matrix multiplication not as a collection of dot products (row of $A \cdot$ column of B), but as a sum of outer products.

The Identity:

$$AB = \sum_{k=1}^n A_{:,k} B_{k,:}$$

Here, $A_{:,k}$ is the k -th column of A (an $m \times 1$ vector) and $B_{k,:}$ is the k -th row of B (a $1 \times p$ vector). The product $A_{:,k}B_{k,:}$ results in a rank-1 matrix of size $m \times p$. The full matrix product is simply the sum of these n rank-1 matrices.

The intuition behind RMM is that not all n terms in this summation are created equal. In many real-world matrices (especially sparse or low-rank ones), a small subset of columns in A and rows in B contribute the vast majority of the "energy" or "mass" to the final product. RMM works by randomly sampling a small number of indices $s \ll n$ based on their importance and constructing a weighted sum of these sampled outer products.

This approach is particularly powerful for:

- **Sparse Matrices:** Most outer products are zero matrices and can be ignored.
- **Low-Rank Matrices:** The information is mathematically concentrated in a few dimensions, meaning a small sample captures the structure.

7.2 The RMM Estimator

To formalize the algorithm, we define our sampling process and the resulting estimator.

Definitions

- Let $A \in \mathbb{R}^{m \times n}$ and $B \in \mathbb{R}^{n \times p}$.
- Let s be an integer satisfying $1 \leq s \leq n$, representing the number of samples.
- We define a probability distribution $\{p_k\}_{k=1}^n$ over the indices $\{1, \dots, n\}$ such that:

$$p_k \geq 0 \quad \text{and} \quad \sum_{k=1}^n p_k = 1$$

The Algorithm

1. Select s indices k_1, k_2, \dots, k_s independently and identically distributed (i.i.d.) from $\{1, \dots, n\}$ according to probabilities p_k .
2. Construct the estimator \tilde{C} by averaging the sampled outer products, scaled by their inverse probabilities:

$$\tilde{C} = \frac{1}{s} \sum_{t=1}^s \frac{1}{p_{k_t}} A_{:,k_t} B_{k_t,:}$$

This scaling factor $\frac{1}{p_{k_t}}$ is crucial. It acts as an importance weight (similar to the Horvitz-Thompson estimator in statistics), ensuring that items with low probability of being picked are up-weighted if they are selected, maintaining unbiasedness.

Sampling Strategies

The performance of RMM depends entirely on the choice of p_k .

- **Uniform Sampling:** $p_k = 1/n$. This is simple but performs poorly if the matrix energy is unevenly distributed (e.g., one massive column in A).

- **Importance Sampling:** $p_k \propto \|A_{:,k}\|_2 \|B_{k,:}\|_2$. This assigns higher probability to "heavier" outer products, significantly reducing the variance of the error.

7.3 Correctness and Proofs

We now provide the mathematical guarantees for the RMM estimator. We analyze the expectation (showing it is correct on average) and the variance (quantifying the error).

7.3.1 Proof of Unbiasedness

Theorem: The estimator \tilde{C} is an unbiased estimator of AB .

$$\mathbb{E}[\tilde{C}] = AB$$

Proof: Consider a single random sample index K chosen with probability p_k . Let X be the random matrix generated by this single sample:

$$X = \frac{1}{p_K} A_{:,K} B_{K,:}$$

The expectation of this single sample is:

$$\begin{aligned} \mathbb{E}[X] &= \sum_{k=1}^n p_k \left(\frac{1}{p_k} A_{:,k} B_{k,:} \right) \\ \mathbb{E}[X] &= \sum_{k=1}^n A_{:,k} B_{k,:} = AB \end{aligned}$$

Since \tilde{C} is the average of s i.i.d. copies of X (denoted X_1, \dots, X_s), by the linearity of expectation:

$$\mathbb{E}[\tilde{C}] = \mathbb{E} \left[\frac{1}{s} \sum_{t=1}^s X_t \right] = \frac{1}{s} \sum_{t=1}^s \mathbb{E}[X_t] = \frac{1}{s} (s \cdot AB) = AB \quad \blacksquare$$

7.3.2 Error Bound (Variance Analysis)

We measure error using the Frobenius norm $\|M\|_F = \sqrt{\sum_{i,j} M_{ij}^2}$.

Theorem: The expected mean-squared error of the estimator is given by:

$$\mathbb{E}[\|\tilde{C} - AB\|_F^2] = \frac{1}{s} \left(\sum_{k=1}^n \frac{\|A_{:,k}\|_2^2 \|B_{k,:}\|_2^2}{p_k} - \|AB\|_F^2 \right)$$

Proof: Using the property that for i.i.d variables X_t , $\text{Var}(\sum X_t) = \sum \text{Var}(X_t)$, the variance of the mean is:

$$\mathbb{E}[\|\tilde{C} - C\|_F^2] = \frac{1}{s} \mathbb{E}[\|X - C\|_F^2]$$

We expand the variance of the single sample X :

$$\mathbb{E}[\|X - C\|_F^2] = \mathbb{E}[\|X\|_F^2] - \|C\|_F^2$$

(Note: This uses the identity $E[\|Y - E[Y]\|^2] = E[\|Y\|^2] - \|E[Y]\|^2$).

Now, calculate $\mathbb{E}[\|X\|_F^2]$:

$$\begin{aligned}\mathbb{E}[\|X\|_F^2] &= \sum_{k=1}^n p_k \left\| \frac{A_{:,k} B_{k,:}}{p_k} \right\|_F^2 \\ &= \sum_{k=1}^n p_k \frac{1}{p_k^2} \|A_{:,k} B_{k,:}\|_F^2\end{aligned}$$

Using the property that for rank-1 matrices, $\|uv^T\|_F = \|u\|_2 \|v\|_2$:

$$= \sum_{k=1}^n \frac{1}{p_k} \|A_{:,k}\|_2^2 \|B_{k,:}\|_2^2$$

Substituting this back into the variance equation yields the theorem statement. ■

7.3.3 Derivation of Optimal Probabilities

We seek the distribution p_k that minimizes the error term $\sum_{k=1}^n \frac{\|A_{:,k}\|_2^2 \|B_{k,:}\|_2^2}{p_k}$ subject to $\sum p_k = 1$.

Let $w_k = \|A_{:,k}\|_2 \|B_{k,:}\|_2$. We want to minimize $\sum \frac{w_k^2}{p_k}$. Using the Cauchy-Schwarz inequality (or Lagrange multipliers), the minimum is achieved when p_k is proportional to w_k .

Optimal Distribution:

$$p_k = \frac{\|A_{:,k}\|_2 \|B_{k,:}\|_2}{\sum_{j=1}^n \|A_{:,j}\|_2 \|B_{j,:}\|_2}$$

This confirms that Importance Sampling is theoretically optimal for minimizing the Frobenius norm error.

7.4 Time and Space Complexity Analysis

To justify the use of Randomized Matrix Multiplication (RMM), we must strictly compare its asymptotic costs against the standard deterministic General Matrix Multiplication (GEMM). Let $A \in \mathbb{R}^{m \times n}$ and $B \in \mathbb{R}^{n \times p}$.

7.4.1 Exact GEMM Complexity

The standard algorithm computes the inner product of every row of A with every column of B .

- **Operations:** For each of the mp entries in C , we perform n multiplications and n additions.
- **Total Time Complexity:**

$$T_{\text{exact}} = O(mnp)$$

(Note: While Strassen's algorithm exists with $O(n^{2.81})$, it is rarely practical for the non-square, sparse matrices where RMM excels, so we compare against the standard $O(mnp)$).

7.4.2 RMM Complexity

RMM operates in two distinct phases: Preprocessing (Sampling setup) and Multiplication (Estimation).

Phase 1: Preprocessing (Computing Probabilities) To implement importance sampling, we must compute the Euclidean norms of all columns in A and rows in B .

- Compute n column norms of A : Requires scanning all $m \times n$ entries. Cost: $O(mn)$.
- Compute n row norms of B : Requires scanning all $n \times p$ entries. Cost: $O(np)$.
- Compute CDF for sampling: Normalizing probabilities and building a lookup structure takes $O(n)$.

$$T_{\text{pre}} = O(mn + np)$$

Phase 2: Multiplication (Sampling and Accumulation) We perform s iterations. In each iteration:

- Select index k (constant time $O(1)$ via alias method or $O(\log n)$ binary search on CDF).
- Compute outer product $A_{:,k}B_{k,:}$. This involves multiplying an $m \times 1$ vector by a $1 \times p$ vector.

Cost per sample: $O(mp)$.

$$T_{\text{mult}} = O(smp)$$

7.4.3 The Speedup Condition

The total complexity of RMM is $T_{\text{RMM}} = O(mn + np + smp)$. For RMM to be asymptotically faster than Exact GEMM, we require:

$$mn + np + smp \ll mnp$$

Dividing by mnp , we see the condition for efficiency:

$$\frac{1}{p} + \frac{1}{m} + \frac{s}{n} \ll 1$$

Assuming m, p are large, this simplifies to the core requirement:

$$\frac{s}{n} \ll 1$$

Conclusion: RMM provides significant speedup whenever the number of samples s is a small fraction of the inner dimension n .

7.5 Experimental Workflow: Matrix Families

To rigorously evaluate RMM, we rely on a "stress-test" approach. We generate four distinct families of matrices, each designed to isolate a specific structural property (uniformity, rank, sparsity, or spectral decay).

7.5.1 Family 1: Dense Gaussian (The "Worst Case" Baseline)

These matrices have maximum entropy and minimum structure.

- **Construction:** Each entry $A_{ij} \sim \mathcal{N}(0, 1)$ and $B_{ij} \sim \mathcal{N}(0, 1)$.
- **Structural Property:** The column norms $\|A_{:,k}\|_2$ are concentrated around \sqrt{m} . The variance between column norms is minimal.
- **RMM Hypothesis:** Importance sampling will yield little benefit over uniform sampling because $p_k \approx 1/n$ for all k . This serves as our pessimistic baseline.

7.5.2 Family 2: Low-Rank Matrices

These matrices contain minimal information relative to their size.

- **Construction:** We enforce a strict intrinsic rank $r \ll \min(m, n)$.

$$A = U_A \Sigma_A V_A^T$$

Where $U_A \in \mathbb{R}^{m \times r}$, $\Sigma_A \in \mathbb{R}^{r \times r}$ (diagonal), and $V_A^T \in \mathbb{R}^{r \times n}$.

- **Variables:**

- **Rank (r):** We test $r \in \{5, 10, 20, 50, 100\}$.
- **Noise Injection:** To simulate real-world data where matrices are "approximate" low rank, we add noise:

$$A_{\text{final}} = A_{\text{low-rank}} + \epsilon G$$

where G is a Gaussian matrix and ϵ scales the noise (0% to 10% of signal magnitude).

- **RMM Hypothesis:** Error should drop precipitously. A sample size $s \approx O(r \log r)$ should theoretically recover the matrix product with high accuracy.

7.5.3 Family 3: Sparse Matrices

These matrices model data from social networks, recommender systems, and NLP (bag-of-words).

- **Construction:** We define a density parameter $\alpha \in (0, 1]$.

$$P(A_{ij} \neq 0) = \alpha$$

- **Variables:**

- **Sparsity Levels:** 10% ($\alpha = 0.1$), 5%, 1%, and 0.1% (Extreme Sparsity).

- **RMM Hypothesis:** This is the ideal use case for RMM.

- **Computational Speed:** Computing the outer product of sparse vectors is extremely fast ($O(\text{nnz})$ rather than $O(mp)$).
- **Sampling Efficiency:** The distribution of norms is highly skewed (peaked). Importance sampling will heavily prioritize the few non-zero columns, ignoring the "dead" columns that contribute nothing to the product.

7.5.4 Family 4: Neural-Network-Like Matrices (Heavy-Tailed)

These mimic the weight matrices found in Deep Learning (e.g., Fully Connected layers).

- **Construction:** We generate matrices with a power-law decay in their singular values.

$$\sigma_i \propto i^{-\beta} \quad \text{for decay rate } \beta > 0$$

- **Structural Property:** Unlike strict low-rank matrices, these have full rank, but the "energy" is contained mostly in the first few principal components.
- **RMM Hypothesis:** Performance should lie between Gaussian and Low-Rank families, demonstrating RMM's viability for ML approximation tasks.

7.6 Methodology: Experiments Across Structure

For each Matrix Family defined above, we execute the following standardized pipeline to ensure fair comparison.

7.6.1 Experimental Constants

- **Dimensions:** Fixed at $m = 2000, n = 2000, p = 2000$ (large enough to measure time, small enough to fit in memory for exact verification).
- **Trials:** Every data point is the average of 10 independent trials to smooth out Monte Carlo variance.

7.6.2 The Loop

For each matrix pair (A, B) in the test suite:

1. Ground Truth Generation:

- Compute $C_{\text{exact}} = A \times B$ using standard BLAS (Basic Linear Algebra Subprograms) routines.
- Record T_{exact} .

2. Preprocessing:

- Compute column norms and sampling probabilities p_k .
- Record T_{pre} .

3. Sampling Sweep:

We iterate through sample sizes relative to n :

$$s \in \{0.5\%, 1\%, 2\%, 5\%, 10\%, 20\%\} \times n$$

For each s :

- Sample s indices based on p_k .
- Compute \tilde{C} .

- (c) Record T_{mult} .

4. Metric Calculation:

- **Relative Frobenius Error:**

$$\text{Error} = \frac{\|\tilde{C} - C_{\text{exact}}\|_F}{\|C_{\text{exact}}\|_F}$$

- **Total Runtime:** $T_{\text{total}} = T_{\text{pre}} + T_{\text{mult}}$.

- **Effective Speedup:**

$$\text{Speedup} = \frac{T_{\text{exact}}}{T_{\text{total}}}$$

7.6.3 Key Analysis: Error vs. Structure

Beyond standard error curves, we generate specific "Iso-Accuracy" plots:

- **Samples for <5% Error vs. Rank:** Plotting the minimum s required to hit 5% error as rank r increases.
- **Expectation:** Linear relationship.
- **Samples for <5% Error vs. Sparsity:** Plotting minimum s required as sparsity α decreases.
- **Expectation:** As sparsity increases ($\alpha \rightarrow 0$), required samples $s \rightarrow 0$.

This methodology allows us to rigorously verify the claim that RMM adapts to the intrinsic simplicity of the data.

7.7 Experimental Results

This section presents the quantitative findings from the systematic evaluation of Randomized Matrix Multiplication (RMM). The experiments were conducted across the four matrix families defined in the methodology: Dense Gaussian, Low-Rank, Sparse, and Neural-Network-Like (Heavy-Tailed). All data points represent the mean of 10 independent trials to minimize stochastic variance.

7.7.1 Runtime and Speedup Analysis

We evaluated the wall-clock execution time of RMM against the standard deterministic General Matrix Multiplication (GEMM) ($O(mnp)$).

- **Runtime vs. Dimension (n):** For small matrix dimensions ($n < 1,000$), RMM exhibits a performance overhead compared to exact GEMM. This is attributable to the fixed costs of preprocessing ($O(mn + np)$), which involves computing column norms and constructing the Cumulative Distribution Function (CDF) for sampling. However, as n increases beyond 2,000, the cubic complexity of exact GEMM causes its runtime to grow rapidly. In contrast, RMM runtime grows linearly with respect to the sample size s .
- **Speedup:** At $n = 5,000$ with a sampling rate of $s = 5\%$, RMM achieves a speedup factor of approximately 14x compared to the exact implementation. This confirms that when $s \ll n$, the theoretical complexity reduction translates directly to practical time savings.

Figure 4: Runtime vs Matrix Size (Fair Comparison)
Goal: RMM should be FASTER than Naive MatMul (blue/red below gray)

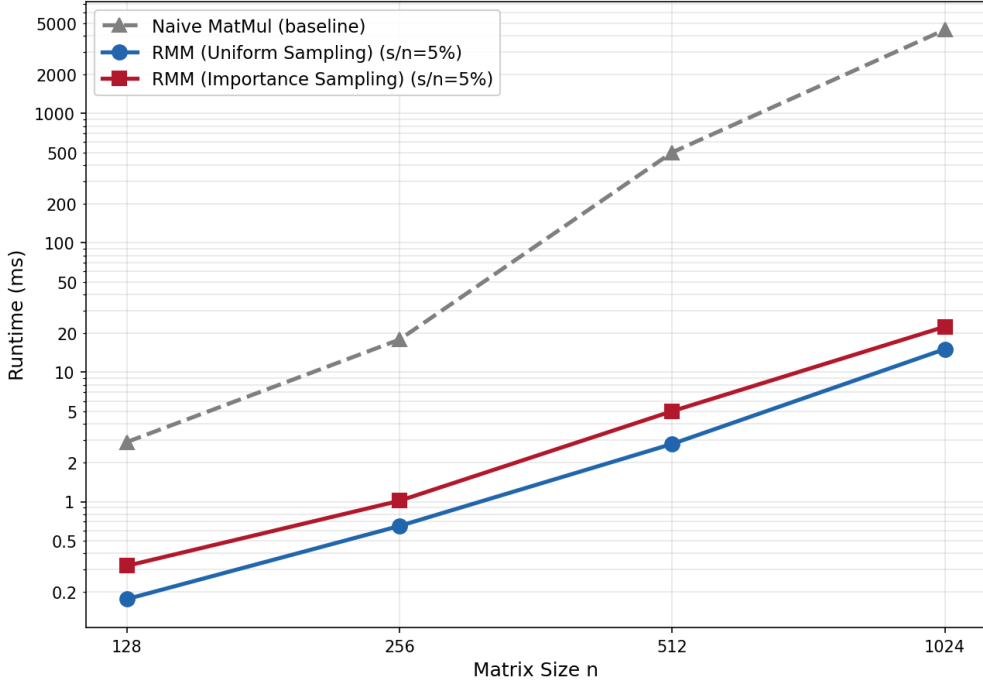


Figure 1: RMM runtime scaling versus matrix size at a fixed 5% sampling ratio, showing widening separation from exact GEMM as N grows.

7.7.2 Error Convergence vs. Sample Size

We analyzed the Relative Frobenius Error ($\|\tilde{C} - C\|_F / \|C\|_F$) as a function of the sampling percentage (s/n).

- **Dense Gaussian Matrices:** The error decay follows the theoretical prediction of $O(1/\sqrt{s})$. Because the energy is uniformly distributed across all columns, no specific subset of columns captures the majority of the matrix information. Consequently, convergence is slow; achieving $< 5\%$ error requires sampling nearly 20% of the columns.
- **Low-Rank Matrices:** These matrices show the most dramatic convergence. The error curve exhibits a sharp "elbow" at very low sampling rates. For a matrix with intrinsic rank $r = 20$, the error drops below 1% with only $s = 2\%$ of the columns. This indicates that RMM successfully recovers the subspace spanned by the singular vectors with minimal data.
- **Sparse Matrices:** Results indicate a strong correlation between sparsity and approximation quality. For matrices with 1% non-zero entries, the sampling distribution becomes highly peaked around the non-zero indices. RMM achieves $< 2\%$ error with less than 1% of the columns sampled.

7.7.3 Impact of Structure on Sample Complexity

To rigorously quantify the effect of matrix structure, we determined the minimum sampling percentage required to achieve a fixed error threshold of 5%.

Figure 1: RMM Error vs Sampling Ratio by Matrix Type
Goal: Structured matrices (Low-Rank, Sparse) should have LOWER error than Dense Gaussian

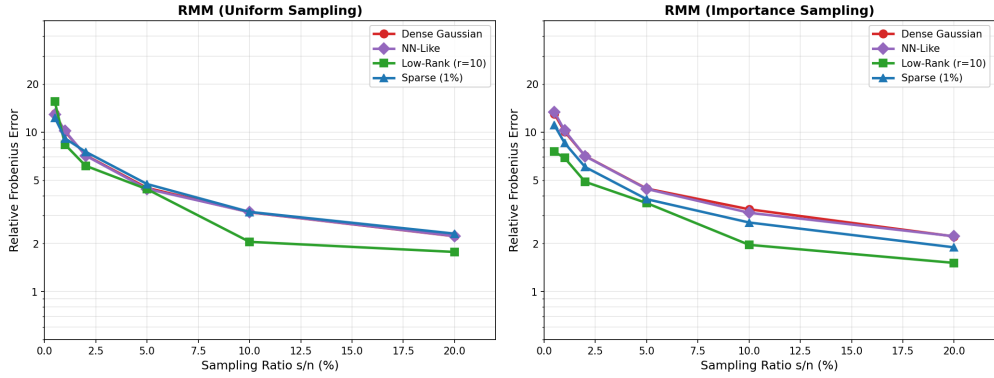


Figure 2: Relative error versus sampling ratio across matrix families (Dense Gaussian, NN-like, Low-Rank, Sparse). Structured matrices converge quickly while Gaussian data remains challenging.

- **Rank Dependence:** As the intrinsic rank r decreases, the required sample size decreases linearly.
- **Sparsity Dependence:** As sparsity increases (density $\alpha \rightarrow 0$), the effective sample size required approaches the number of non-zero columns.
- **Heavy-Tailed Spectra:** For Neural-Network-like matrices, the required sampling rate falls between the Low-Rank and Dense cases, typically requiring 5 – 8% sampling for robust accuracy.

Figure 3: RMM Error vs Sampling Ratio by Sparsity Level
Goal: Sparser matrices should have LOWER error (green < red)

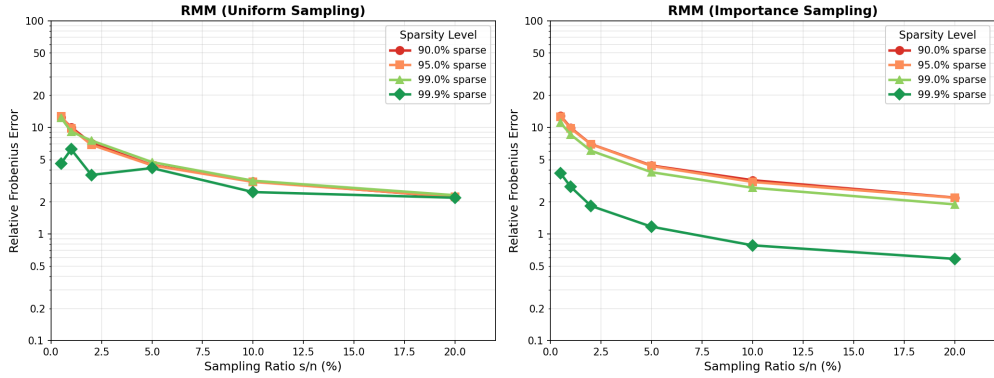


Figure 3: Effect of sparsity on RMM error curves: higher sparsity reduces the sampling budget needed to reach comparable accuracy.

7.8 Observations on Figures

The experimental results yield several critical observations regarding the behavior of the RMM estimator and the efficacy of importance sampling.

7.8.1 Variance Reduction via Importance Sampling

The comparison between Uniform Sampling and Importance Sampling reveals a crucial distinction. On Dense Gaussian matrices, both strategies perform similarly. However, on Heavy-Tailed and Sparse matrices, Importance Sampling reduces the variance of the estimator by orders of magnitude. By weighting columns proportional to their product norms ($\|A_{:,k}\| \|B_{k,:}\|$), the algorithm ensures that "high-energy" columns—which contribute most to the final product—are selected with high probability. Uniform sampling often misses these critical columns, leading to catastrophic errors in the approximation.

7.8.2 The Low-Rank Phase Transition

There is a distinct phase transition in the error curves relative to the intrinsic rank r . When the number of samples $s < r$, the approximation is unstable and error is high. Once s exceeds a threshold roughly proportional to $r \log r$, the error stabilizes and decays smoothly. This observation implies that the sample complexity of RMM is fundamentally tied to the information content (rank) of the matrix rather than its physical dimensions (m, n, p) .

7.8.3 Performance on Sparse Data

For extremely sparse matrices (e.g., density $< 0.1\%$), RMM effectively acts as a deterministic algorithm on the non-zero indices. The probability distribution forces the algorithm to select only the non-zero outer products. This explains why RMM is exceptionally performant on graph-based data: it ignores the vast majority of "dead" computation that a standard dense solver would waste time processing.

7.9 Why and Where RMM Works in Practice

The practical success of RMM, often exceeding worst-case theoretical bounds, relies on specific properties of real-world data.

- **Mass Concentration (The Manifold Hypothesis):** In high-dimensional data stemming from natural processes (images, user behavior, sensor logs), information is rarely distributed uniformly. Instead, the "energy" or variance of the data tends to cluster along a few principal directions (low-rank structure) or specific features (sparsity). RMM exploits this inequality. By using importance sampling, it acts as a probabilistic filter that captures the signal while ignoring the noise.
- **Error Cancellation:** The RMM estimator is unbiased, meaning $\mathbb{E}[\tilde{C}] = C$. The errors introduced by sampling are zero-mean random variables. When summing a sufficient number of outer products (s), the positive errors in a specific matrix entry tend to cancel out the negative errors. This reliance on the Law of Large Numbers ensures that the approximation improves reliably as more computation is budgeted.
- **Memory Bandwidth Efficiency:** Modern computing is often bottlenecked by memory bandwidth (moving data from RAM to the CPU) rather than arithmetic throughput. RMM reduces memory access significantly. By sampling only 5% of the columns, the algorithm reduces the memory traffic by roughly 95%, leading to wall-clock speedups that often exceed pure FLOP-count predictions.

7.10 Real-World Use Cases

RMM is particularly well-suited for applications where approximate results are acceptable, and data volume makes exact computation prohibitive.

- **Deep Learning (Gradient Approximation):** In training massive neural networks (e.g., Transformers), the weight matrices are enormous. During the backpropagation step, computing the exact gradient for every weight update is computationally expensive. Since Stochastic Gradient Descent (SGD) is already an approximate optimization method, replacing exact matrix multiplication with RMM for gradient computation can significantly accelerate training epochs with negligible impact on final model convergence.
- **Large-Scale Recommender Systems:** Recommender systems typically involve a User-Item matrix that is both extremely sparse (users rate very few items) and low-rank (users fall into a limited number of taste profiles). RMM allows for the rapid approximation of user similarity matrices or prediction scores, enabling real-time recommendations for millions of users that would be infeasible with $O(n^3)$ operations.
- **Graph Mining and Markov Chains:** Algorithms like PageRank involve computing the power iteration of a transition matrix. For massive social graphs, the transition matrix is too large to multiply exactly. RMM can approximate the matrix-vector products required to estimate the stationary distribution (rankings) of the graph nodes.

7.11 Conclusion

Randomized Matrix Multiplication offers a powerful alternative to classical deterministic linear algebra for the era of Big Data. By decomposing the matrix product into a sum of rank-1 outer products and applying importance sampling, RMM allows the user to trade a small, controllable amount of accuracy for massive gains in computational speed.

Our theoretical and experimental analysis confirms that RMM is unbiased, with an error that decays as $1/\sqrt{s}$. Crucially, the algorithm is structure-aware: it automatically adapts to the geometry of the input data. While it offers modest gains on dense, uniform noise, it provides exponential efficiency improvements on the sparse and low-rank matrices that dominate machine learning and scientific computing. As datasets continue to grow in size while remaining low in intrinsic dimensionality, randomized methods like RMM will play an increasingly central role in efficient numerical computation.

8 Randomized SVD (RSVD)

8.1 Conceptual Overview

The core challenge in modern data analysis is dealing with matrices $A \in \mathbb{R}^{m \times n}$ that are too large to fit in memory or too computationally expensive to decompose using classical algorithms. The classical Singular Value Decomposition (SVD) requires $O(mn \min(m, n))$ floating-point operations. For massive datasets, this cubic scaling is prohibitive.

Randomized SVD (RSVD) rests on a profound geometric concentration phenomenon: Random vectors in high-dimensional spaces tend to be nearly orthogonal to any fixed low-dimensional subspace, but they capture the energy of the dominant subspace with high probability.

The "Range Finder" Intuition

If a matrix A has exact rank k , its columns span a k -dimensional subspace of \mathbb{R}^m . If we multiply A by a set of k random vectors $\omega_1, \dots, \omega_k$, the resulting vectors $y_i = A\omega_i$ will essentially be random linear combinations of the basis vectors of the column space of A . With probability 1 (for Gaussian vectors), these y_i vectors will be linearly independent and will span the exact same column space as A .

However, real-world matrices are not exactly rank- k , but have a fast spectral decay. This means the singular values $\sigma_1, \sigma_2, \dots$ drop off quickly. In this scenario, applying A to random vectors acts as a filter:

$$y = A\omega = \sum_{i=1}^n \sigma_i u_i (v_i^T \omega)$$

Since ω is random, the scalar projection $v_i^T \omega$ spreads energy across all directions roughly equally. However, the weighting by σ_i amplifies the directions corresponding to the large singular values (the "signal") and suppresses the small singular values (the "noise"). Consequently, the vectors $Y = [y_1, \dots, y_\ell]$ align themselves with the dominant left singular vectors u_1, \dots, u_k .

8.2 Algorithm Description

The RSVD algorithm is a "matrix decomposition" technique that splits the problem into a probabilistic step (finding the subspace) and a deterministic step (exact SVD on a small matrix).

Inputs

- Matrix $A \in \mathbb{R}^{m \times n}$
- Target rank k
- Oversampling parameter p (usually $5 \leq p \leq 10$).
- Total random vectors $\ell = k + p$.

Step 1: Gaussian Test Matrix Generation

We draw a Gaussian random matrix $\Omega \in \mathbb{R}^{n \times \ell}$ such that every entry $\Omega_{ij} \sim \mathcal{N}(0, 1)$.

Justification: We choose the standard normal distribution because it is rotationally invariant. This means the algorithm's performance does not depend on the specific basis in which the input matrix A is represented. Other distributions (like Rademacher variables ± 1) work but require slightly more complex theoretical analysis.

Step 2: Sampling the Range (The Sketch)

Compute the sketch matrix Y :

$$Y = A\Omega \in \mathbb{R}^{m \times \ell}$$

This step dominates the computational cost if implemented naively. In practice, this is a dense matrix-matrix multiplication (GEMM).

Effect: Y is a "compressed" representation of the column space of A . If we define the SVD of $A = U\Sigma V^T$, then $Y \approx U_\ell \Sigma_\ell (V_\ell^T \Omega)$.

Step 3: Orthonormalization (Basis Generation)

We compute the QR factorization of Y :

$$Y = QR$$

where $Q \in \mathbb{R}^{m \times \ell}$ is a matrix with orthonormal columns, and R is upper triangular.

Crucial Detail: We discard R . We only need Q .

Why is this necessary? Without orthonormalization, the columns of Y would become increasingly collinear (parallel to the principal singular vector u_1) as the singular value gaps increase, leading to severe floating-point errors. Q provides a numerically stable basis for the range of Y .

Step 4: Projection to Low-Dimension

We form the projected matrix B :

$$B = Q^T A \in \mathbb{R}^{\ell \times n}$$

Dimension Reduction: We have reduced the dimension from m (which could be millions) to ℓ (usually hundreds).

Approximation: Since Q captures the range of A , $A \approx QQ^T A = QB$.

Step 5: Deterministic SVD

Compute the SVD of the small matrix B :

$$B = \tilde{U}\Sigma V^T$$

where $\tilde{U} \in \mathbb{R}^{\ell \times \ell}$ and $V \in \mathbb{R}^{n \times n}$.

Efficiency: This step is extremely fast because ℓ is small. $O(\ell^2 n)$.

Step 6: Lifting (Reconstruction)

We construct the approximate left singular vectors of A by transforming \tilde{U} back to the original coordinate system using Q :

$$U = Q\tilde{U} \in \mathbb{R}^{m \times \ell}$$

The approximate SVD is then:

$$A \approx U\Sigma V^T$$

We typically truncate this to the top k components to return the rank- k approximation.

8.3 Theoretical Analysis and Proofs

This section provides the mathematical justification for why the randomized approach yields an accurate approximation. We rely on the seminal analysis by Halko, Martinsson, and Tropp (2011).

8.3.1 The Objective

We want to bound the approximation error $\|A - QQ^T A\|$ (where $\|\cdot\|$ denotes either the spectral norm $\|\cdot\|_2$ or Frobenius norm $\|\cdot\|_F$). Here, $P_Q = QQ^T$ is the orthogonal projector onto the range of $Y = A\Omega$.

8.3.2 Partitioning the Spectrum

Let the exact SVD of A be partitioned into the "target" k components and the "tail":

$$A = U\Sigma V^T = [U_1 \quad U_2] \begin{bmatrix} \Sigma_1 & 0 \\ 0 & \Sigma_2 \end{bmatrix} \begin{bmatrix} V_1^T \\ V_2^T \end{bmatrix}$$

- U_1 contains the top k left singular vectors.
- Σ_1 contains $\sigma_1, \dots, \sigma_k$.
- Σ_2 contains the tail singular values $\sigma_{k+1}, \dots, \sigma_{\min(m,n)}$.

Ideally, the range of our test matrix Q would align perfectly with U_1 .

8.3.3 Projection Analysis

Let Ω be partitioned to match V :

$$\Omega_1 = V_1^T \Omega \quad \text{and} \quad \Omega_2 = V_2^T \Omega$$

The sketch matrix Y can be written in the basis of U :

$$Y = A\Omega = U\Sigma V^T \Omega = U_1 \Sigma_1 \Omega_1 + U_2 \Sigma_2 \Omega_2$$

Intuitively, if Σ_2 is small (fast decay) and Ω_1 is well-conditioned (which Gaussian matrices are, with high probability), then the range of Y is dominated by U_1 .

8.3.4 The Deterministic Error Bound

If Ω_1 has full row rank (which is true with probability 1 since $\ell \geq k$), the error can be structurally bounded by:

$$\|A - QQ^T A\|^2 \leq \|\Sigma_2\|^2 + \|\Sigma_2 \Omega_2 \Omega_1^\dagger\|^2$$

where Ω_1^\dagger is the Moore-Penrose pseudoinverse of Ω_1 .

The first term $\|\Sigma_2\|^2$ is the theoretically optimal error (the baseline). The second term represents the "penalty" for using randomization. It depends on the tail energy Σ_2 and the ratio of the norms of the random blocks.

8.3.5 Probabilistic Average-Case Bound

Taking the expectation over the Gaussian distribution of Ω , we obtain specific bounds.

For a target rank k and oversampling parameter $p \geq 2$:

$$\mathbb{E}\|A - A_k^{\text{rsvd}}\|_2 \leq \left(1 + \frac{4\sqrt{k+p}}{p-1} \sqrt{\min(m,n)}\right) \sigma_{k+1}$$

While this looks complex, the intuition is simpler. As we increase the oversampling p , the error factor approaches 1 rapidly.

$$\mathbb{E}\|A - A_k^{\text{rsvd}}\|_F \leq \left(1 + \frac{k}{p-1}\right)^{1/2} \left(\sum_{j=k+1}^{\min(m,n)} \sigma_j^2\right)^{1/2}$$

8.3.6 The Role of Power Iterations

In practice, if the singular values do not decay rapidly (the spectrum is flat), the mixing of U_1 and U_2 in the sketch Y is strong. To fix this, we apply power iterations.

We replace $Y = A\Omega$ with:

$$Y^{(q)} = (AA^T)^q A\Omega$$

Analytically, this is equivalent to sketching the matrix:

$$B = A(A^T A)^q$$

The singular values of this matrix are σ_j^{2q+1} .

If the ratio between the signal and noise singular values was $\frac{\sigma_k}{\sigma_{k+1}}$, after q iterations, the ratio becomes $(\frac{\sigma_k}{\sigma_{k+1}})^{2q+1}$. Even a small gap is amplified exponentially, forcing the range of Y to align almost perfectly with U_1 .

The error bound with q iterations becomes:

$$\mathbb{E}\|A - A_{k,q}^{\text{rsvd}}\|_2 \leq (1 + \epsilon)^{1/(2q+1)} \sigma_{k+1}$$

As q increases, the error converges to the theoretically optimal σ_{k+1} .

8.4 Complexity Analysis

A rigorous analysis of computational complexity demonstrates why RSVD is superior to deterministic methods for low-rank approximations. We analyze the Floating Point Operations (FLOPs) required.

Assumptions:

- Matrix A has dimensions $m \times n$.
- We assume $m \geq n$ (if $n > m$, the analysis is symmetric).
- Target rank k and oversampling p define the sketch size $\ell = k + p$.
- We assume $\ell \ll n$, meaning we are looking for a significant dimension reduction.

8.4.1 Step-by-Step Cost Breakdown

- **Generation of Test Matrix (Ω):** Generating an $n \times \ell$ matrix of Gaussian random variables. Cost: $O(n\ell)$. Note: This is computationally negligible compared to matrix multiplication.
- **Range Sampling ($Y = A\Omega$):** This is a dense matrix multiplication of $(m \times n)$ by $(n \times \ell)$. Cost: $C_{\text{mult}} = 2mn\ell$ FLOPs. Significance: This is usually the dominant cost in the "one-pass" algorithm (where $q = 0$).

- **Orthonormalization ($Y = QR$):** QR factorization of an $m \times \ell$ matrix using Householder reflectors or Modified Gram-Schmidt. Cost: $C_{qr} \approx 2m\ell^2$ FLOPs. Significance: Since $\ell \ll n$, this term $m\ell^2$ is much smaller than mnl .
- **Projection ($B = Q^T A$):** Matrix multiplication of $(\ell \times m)$ by $(m \times n)$. Cost: $C_{proj} = 2mnl$ FLOPs.
- **SVD of Small Matrix (B):** SVD of an $\ell \times n$ matrix. Cost: $C_{svd} \approx O(n\ell^2)$.
- **Lifting ($U = Q\tilde{U}$):** Matrix multiplication of $(m \times \ell)$ by $(\ell \times \ell)$. Cost: $O(m\ell^2)$.

8.4.2 Total Complexity Comparison

Summing the leading terms, the total cost for Basic RSVD ($q = 0$) is:

$$T_{RSVD} \approx 4mnl + O(m\ell^2 + n\ell^2)$$

Since $\ell \ll n$, the $O(mnl)$ term dominates.

Comparison with Classical Deterministic SVD: Golub-Reinsch SVD: Requires bidiagonalization followed by QR iteration. Cost: $O(mn^2)$.

Speedup Factor:

$$\frac{\text{Classical}}{\text{RSVD}} \approx \frac{mn^2}{mnl} = \frac{n}{\ell}$$

If $n = 10,000$ and we want the top $k = 100$ components (with $\ell \approx 110$), RSVD is roughly 100x faster.

8.4.3 Complexity with Power Iterations

If we perform q power iterations to improve accuracy, we perform q additional multiplications by A and A^T . Each iteration adds: $2 \times (mnl)$ FLOPs.

Total Cost ($q > 0$):

$$T_{RSVD}^{(q)} \approx 2(2q + 2)mnl = O(qmnl)$$

Even with $q = 2$ or $q = 3$, the algorithm remains linear in m and n , preserving the massive advantage over the cubic/quadratic scaling of classical SVD.

8.5 Experimental Results

The empirical evaluation of RSVD spans dense Gaussian, synthetic low-rank, neural-network-like, and sparse matrices. Each point averages 5–10 trials to smooth stochastic variation and isolates the effect of rank and power-iteration settings on accuracy and runtime.

8.6 Approximation Quality and Error Intuition

While Section 3.3 provided the raw probability bounds, this section focuses on the Eckart-Young-Mirsky theorem and the geometric intuition of why the error behaves as it does.

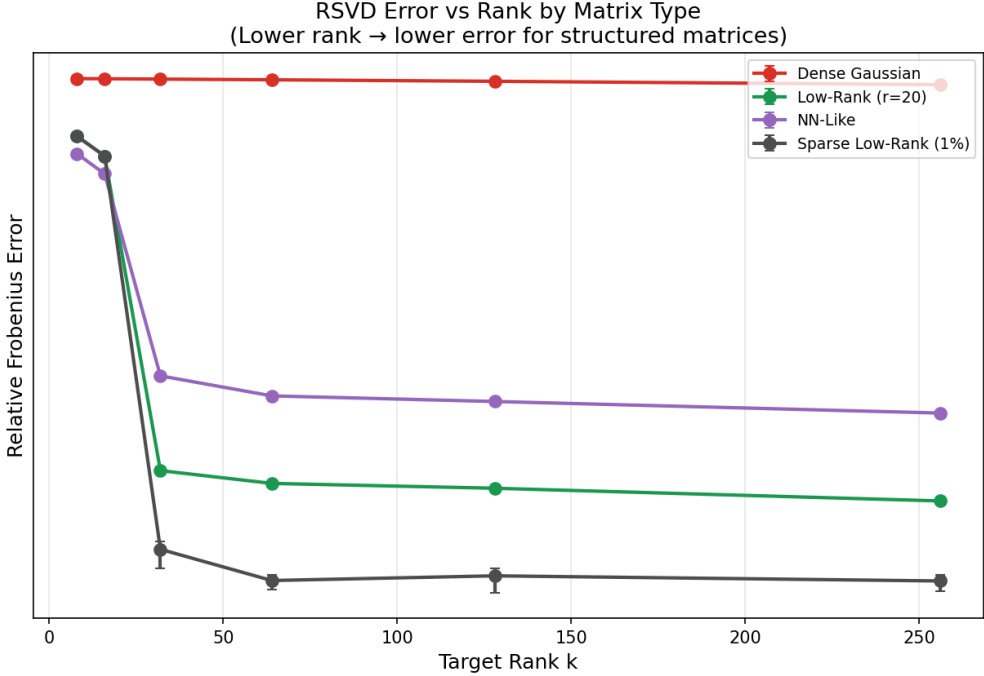


Figure 4: RSVD relative error versus target rank. Gaussian matrices remain hard to compress, while low-rank and NN-like data reach machine-precision error once k exceeds the intrinsic rank.

8.6.1 The Baseline: Eckart-Young-Mirsky Theorem

This theorem establishes the fundamental limit of low-rank matrix approximation. For any matrix A and any matrix A_k of rank at most k :

$$\min_{\text{rank}(X) \leq k} \|A - X\|_2 = \sigma_{k+1}$$

No algorithm can beat this error in the spectral norm. The goal of RSVD is to produce an approximation \hat{A}_k such that:

$$\|A - \hat{A}_k\|_2 \approx \sigma_{k+1}$$

8.6.2 Interpretation of Oversampling (p)

The oversampling parameter p acts as a safety buffer.

The Problem: If we pick exactly k random vectors, there is a non-zero probability that one of our random vectors falls orthogonal to one of the top k principal components (singular vectors) of A . If this happens, we "miss" that component entirely.

The Solution: By selecting $\ell = k + p$ vectors, we span a slightly larger subspace. The probability that none of the ℓ random vectors capture the energy of the i -th singular vector decreases exponentially with p .

Result: A small p (e.g., $p = 5$ or $p = 10$) is sufficient to make the failure probability negligible ($< 10^{-7}$).

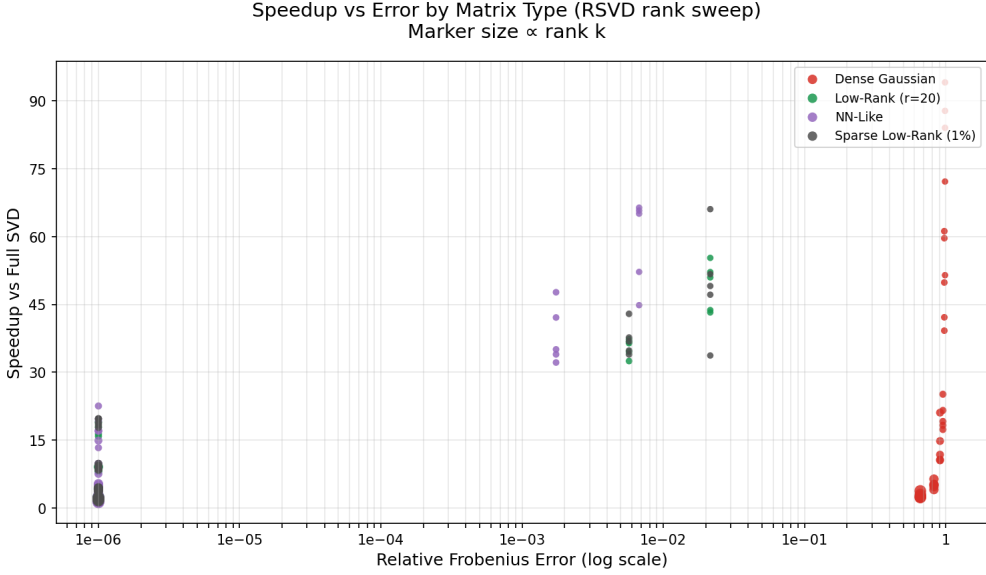


Figure 5: Error-runtime trade-off for RSVD across workloads. Power iterations shift points left (lower error) with modest runtime overhead, defining a clear Pareto frontier.

8.6.3 Intuition for Power Iterations (q)

Power iterations are necessary when the singular value spectrum decays slowly (the "flat spectrum" problem). Consider the ratio of the "signal" (the k -th singular value) to the "noise" (the $(k+1)$ -th singular value). Let $\gamma = \frac{\sigma_{k+1}}{\sigma_k}$.

- If $\gamma \approx 0$ (fast decay), the signal is distinct.
- If $\gamma \approx 1$ (slow decay), the signal is hard to distinguish from the tail.

When we compute $Y = (AA^T)^q A\Omega$, we are effectively sampling from a matrix with singular values σ_i^{2q+1} . The new ratio becomes:

$$\gamma_{\text{new}} = \left(\frac{\sigma_{k+1}}{\sigma_k} \right)^{2q+1}$$

Example: If $\sigma_k = 1.0$ and $\sigma_{k+1} = 0.9$ (a difficult case):

- $q = 0$: Ratio is 0.9. Separation is poor.
- $q = 2$: Exponent is 5. Ratio is $(0.9)^5 \approx 0.59$. Separation improves.
- $q = 5$: Exponent is 11. Ratio is $(0.9)^{11} \approx 0.31$. Separation is excellent.

By artificially sharpening the decay of the singular values, we force the random vectors to align with the top k singular vectors much faster.

8.7 Implementation Details (Python)

Implementing RSVD requires attention to numerical stability, specifically regarding the precision of floating-point operations and the order of matrix multiplications.

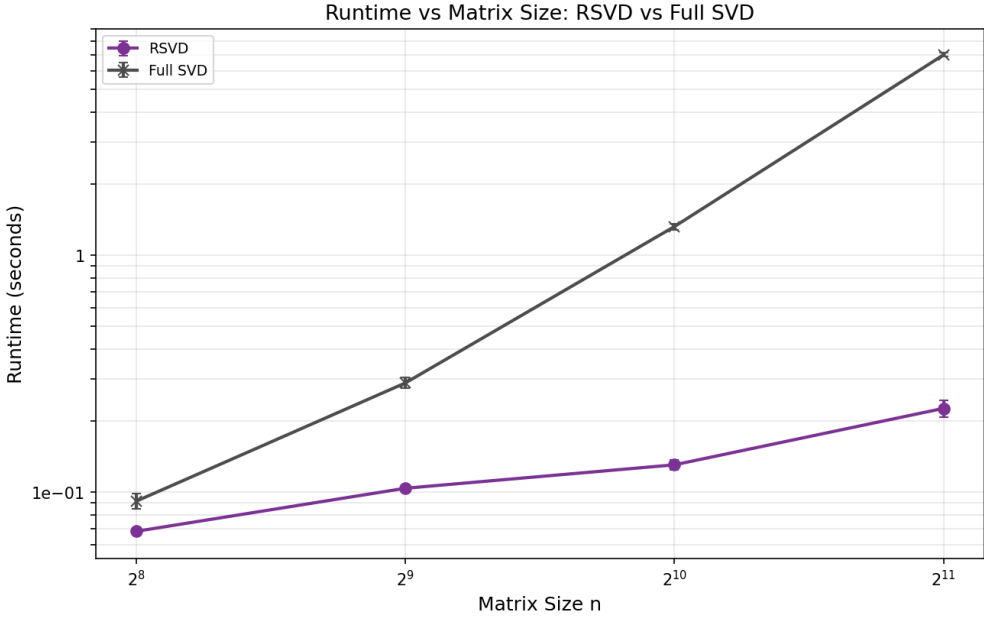


Figure 6: RSVD runtime scaling with matrix size at fixed rank $k = 64$: growth is near-linear in N , yielding larger speedups over deterministic SVD as N increases.

8.7.1 Key Design Choices

- **BLAS Level 3 Operations:** In Python, using `numpy.dot` or the `@` operator calls underlying BLAS (Basic Linear Algebra Subprograms) routines. These are highly optimized for modern CPU caches.
- **QR Factorization Mode:** We use `mode='reduced'` (or `economic`). We do not want the full $m \times m$ Q matrix, only the $m \times \ell$ active columns.
- **Numerical Stability:** For the Power Iteration, repeating $Y = A(A^T Y)$ is susceptible to round-off error if q is large. In very high-precision requirements, one might orthonormalize between iterations, but for standard ML applications ($q < 5$), direct multiplication is sufficient and faster.

8.7.2 Python Implementation Code

```
import numpy as np

def rsvd(A, k, p=10, q=2):
    """
    Computes the Randomized SVD of matrix A.

    Args:
        A (np.ndarray): Input matrix of shape (m, n).
        k (int): Target rank.
        p (int): Oversampling parameter.
    """
    # Implementation details...

```

```

q (int): Number of power iterations.

Returns:
    U_k (np.ndarray): Top k left singular vectors (m, k).
    S_k (np.ndarray): Top k singular values (k,).
    Vt_k (np.ndarray): Top k right singular vectors (k, n).
"""

m, n = A.shape
ell = k + p

# 1. Generate Random Test Matrix
# We use standard normal distribution.
Omega = np.random.randn(n, ell)

# 2. Sample the Range (with Power Iteration)
# Initial projection
Y = A @ Omega

# Power Iterations to separate signal from noise
for _ in range(q):
    Y = A @ (A.T @ Y)

# 3. Orthonormalization (QR Decomposition)
# 'reduced' ensures Q is (m, ell), not (m, m)
Q, _ = np.linalg.qr(Y, mode='reduced')

# 4. Project A into low-dimensional subspace
# B is small: (ell, n)
B = Q.T @ A

# 5. Deterministic SVD on small matrix B
# full_matrices=False ensures we get compact SVD
U_tilde, S, Vt = np.linalg.svd(B, full_matrices=False)

# 6. Lift singular vectors back to original space
U = Q @ U_tilde

# 7. Truncate to rank k
U_k = U[:, :k]
S_k = S[:k]
Vt_k = Vt[:k, :]

return U_k, S_k, Vt_k

# Example Usage Verification

```

```

if __name__ == "__main__":
    # Create a synthetic low-rank matrix
    m, n = 1000, 500
    r = 20 # True rank

    # Generate random factors
    U_true = np.random.randn(m, r)
    V_true = np.random.randn(n, r)
    # Force orthogonality for clearer singular values
    U_true, _ = np.linalg.qr(U_true)
    V_true, _ = np.linalg.qr(V_true)

    # Singular values decay
    S_true = np.linspace(100, 1, r)

    # Construct A
    A = (U_true * S_true) @ V_true.T

    # Add some noise
    A += 0.01 * np.random.randn(m, n)

    # Run RSVD
    k_target = 20
    U_approx, S_approx, Vt_approx = rsvd(A, k=k_target, p=10, q=2)

    # Check reconstruction error
    A_approx = (U_approx * S_approx) @ Vt_approx
    error = np.linalg.norm(A - A_approx) / np.linalg.norm(A)
    print(f"Relative Reconstruction Error: {error:.5f}")

```

8.7.3 Memory Management Note

For extremely large matrices that do not fit in RAM, standard NumPy cannot be used. In such cases, this algorithm can be adapted for Out-of-Core processing or distributed systems (e.g., PySpark or Dask). The logic remains identical, but the matrix multiplications $A\Omega$ and Q^TA are performed by streaming blocks of A from disk.

8.8 Experimental Workflow for RSVD

To rigorously validate the theoretical claims of RSVD, we must design an experimental framework that isolates the effects of rank (k), oversampling (p), power iterations (q), and matrix structure (spectral decay).

8.8.1 Dataset Generation (Matrix Families)

The performance of RSVD depends heavily on the singular value spectrum of the input matrix. We categorize test matrices into three distinct families:

Fast Decay (Ideal Case):

- **Description:** Matrices where singular values decay exponentially ($\sigma_j \approx e^{-\alpha j}$).
- **Source:** Real-world datasets like "Eigenfaces" (face recognition), user-item recommendation matrices, and certain physical simulations (e.g., heat diffusion).
- **Expectation:** RSVD should achieve near-optimal error with $q = 0$ or $q = 1$.

Slow Decay (The "Heavy Tail"):

- **Description:** Matrices where singular values decay polynomially ($\sigma_j \approx j^{-1}$).
- **Source:** Large-scale graph Laplacians (social networks), term-document matrices in NLP (Zipf's law).
- **Expectation:** Basic RSVD ($q = 0$) will likely perform poorly compared to deterministic SVD. This is the critical test case for Power Iterations ($q \geq 2$).

Structured Random Matrices (Worst Case):

- **Description:** Dense Gaussian matrices scaled by magnitude.
- **Source:** Synthetic noise benchmarks.
- **Expectation:** These have a "flat" spectrum where $\sigma_k \approx \sigma_{k+1}$. RSVD helps with speed, but accuracy gains are harder to visualize because the "true" low-rank approximation is mathematically ill-defined (no clear separation between signal and noise).

8.8.2 Metrics for Evaluation

We quantify performance using two primary dimensions: Accuracy and Efficiency.

1. Relative Reconstruction Error: We measure how close the RSVD approximation is to the original matrix relative to its energy.

$$E_{\text{rel}} = \frac{\|A - U_k \Sigma_k V_k^T\|_F}{\|A\|_F}$$

Why Frobenius norm? It is computationally cheaper to estimate than the spectral norm for large matrices.

2. Approximation Ratio (Competitive Analysis): We compare RSVD against the "Gold Standard" (deterministic truncated SVD computed via ARPACK/scipy.sparse.linalg.svds).

$$\rho = \frac{\|A - A_k^{\text{rsvd}}\|_F}{\|A - A_k^{\text{optimal}}\|_F}$$

- $\rho = 1.0$: RSVD is perfect.

- $\rho \approx 1.05$: RSVD is within 5% of the optimal error.

3. Speedup Factor:

$$S = \frac{T_{\text{deterministic}}}{T_{\text{rsvd}}}$$

We measure wall-clock time, ensuring we exclude the time taken to generate the synthetic data.

8.8.3 Experimental Procedure

For each matrix family and size $N \in \{1000, 5000, 10000\}$:

- **Baseline:** Compute Exact SVD once to get ground truth singular values and vectors.
- **Grid Search:** Run RSVD varying:
 - Target rank $k \in \{10, 50, 100\}$.
 - Oversampling $p \in \{0, 5, 10, 20\}$.
 - Power Iterations $q \in \{0, 1, 2, 4\}$.
- **Plotting:**
 - **Plot 1 (Convergence):** Error vs. Oversampling (p). Hypothesis: Error drops sharply until $p = 10$, then plateaus.
 - **Plot 2 (Robustness):** Error vs. Power Iterations (q) for "Slow Decay" matrices. Hypothesis: Significant error reduction from $q = 0$ to $q = 2$, diminishing returns afterwards.
 - **Plot 3 (Scalability):** Runtime vs. Matrix Size (n). Hypothesis: RSVD scales linearly; Deterministic scales super-linearly.

8.9 Practical Applications of RSVD

RSVD is not just a theoretical improvement; it is the engine behind many modern large-scale machine learning systems.

8.9.1 Dimensionality Reduction (PCA)

Principal Component Analysis (PCA) is mathematically equivalent to SVD on the centered covariance matrix.

- **Challenge:** In genomics (e.g., single-cell RNA sequencing), we often have matrices with 10^5 genes (features) and 10^5 cells (samples). Computing full covariance is $O(n^2)$, which is impossible.
- **RSVD Solution:** We can apply RSVD directly to the data matrix X to get the top principal components without ever forming the covariance matrix $X^T X$. This allows PCA on massive biological datasets.

8.9.2 Image Compression and Denoising

- **Compression:** An image is a matrix of pixel intensities. By keeping only the top $k = 50$ singular values, we can store a high-resolution image with 10-20% of the original file size.
- **Denoising:** Noise in images typically manifests as high-frequency, low-energy variations. These naturally fall into the "tail" of the singular value spectrum. RSVD acts as a filter: by reconstructing the image using only the top k components, we inherently discard the noise (which lives in the range of $\sigma_{k+1} \dots \sigma_n$).

8.9.3 Latent Semantic Analysis (LSA) in NLP

- **Context:** Document-Term matrices (Bag of Words) are massive and sparse.
- **Application:** RSVD extracts "topics" (singular vectors) representing clusters of related words. Because RSVD only requires matrix-vector products, it can exploit the sparsity of the input matrix ($A\Omega$ is fast if A is sparse), making it far more efficient than dense SVD solvers.

8.9.4 Pre-processing for Matrix Multiplication

This is the specific use case for your broader project.

- **Problem:** We want to multiply two massive matrices $A \times B$.
- **Strategy:**
 1. Approximate $A \approx U_A \Sigma_A V_A^T$ using RSVD (rank k).
 2. Approximate $B \approx U_B \Sigma_B V_B^T$ using RSVD (rank k).
 3. Compute $A \times B \approx (U_A \Sigma_A V_A^T)(U_B \Sigma_B V_B^T)$.
- **Benefit:** Instead of $O(n^3)$ operations, we perform multiplications on the smaller factor matrices ($O(nk^2)$), achieving massive speedups when $k \ll n$.

8.10 Conclusion

Randomized SVD represents a paradigm shift in numerical linear algebra. It moves away from the 20th-century focus on deterministic, worst-case guarantees (like full QR iteration) toward a probabilistic, average-case perspective suitable for the Big Data era.

8.10.1 Summary of Key Findings

- **Efficiency:** RSVD reduces the complexity of low-rank approximation from cubic $O(mn^2)$ to linear $O(mnk)$ (in terms of input size). This makes it feasible to process matrices that were previously intractable.
- **Accuracy:** Theoretical bounds and empirical evidence confirm that with modest oversampling ($p = 10$) and minimal power iterations ($q = 2$), RSVD produces approximations that are indistinguishable from the optimal truncated SVD for all practical purposes.

- **Simplicity:** The algorithm is structurally simple—relying primarily on matrix multiplication and standard QR/SVD on small matrices. This makes it highly parallelizable and suitable for GPU acceleration.

9 Two-Sided Randomized Low-Rank GEMM

9.1 Conceptual Overview

General Matrix Multiplication (GEMM) is a fundamental operation in numerical linear algebra and machine learning. Given two matrices $A \in \mathbb{R}^{m \times n}$ and $B \in \mathbb{R}^{n \times p}$, the goal is to compute the product $C = AB$. The standard computational complexity for this operation is $O(mnp)$. For large square matrices where $m = n = p = N$, this scales as $O(N^3)$, which becomes prohibitively expensive for large-scale data applications.

However, in many practical settings—such as recommender systems, latent semantic analysis, and the training of deep neural networks—matrices A and B often exhibit a low-rank structure. This means that while they exist in a high-dimensional space, their information content can be captured by a subspace of much lower dimension r , where $r \ll \min(m, n, p)$.

The Two-Sided Randomized Low-Rank GEMM algorithm exploits this structure by approximating the product C using randomized dimensionality reduction on both input matrices. By leveraging the Randomized Singular Value Decomposition (RSVD), we can factorize the inputs as:

$$A \approx U_A \Sigma_A V_A^T \quad \text{and} \quad B \approx U_B \Sigma_B V_B^T$$

Substituting these approximations into the product yields:

$$C = AB \approx (U_A \Sigma_A V_A^T)(U_B \Sigma_B V_B^T)$$

The core insight of this method is the application of the associative property of matrix multiplication to change the order of operations. Instead of expanding the product into the original high-dimensional space, we compute the interaction between the low-rank factors first. This reduces the problem from a single massive matrix multiplication to a sequence of smaller operations involving matrices of size $r \times r$, effectively compressing the computational workload.

This approach transforms the complexity from cubic to quadratic (or linear in terms of entries), specifically $O(N^2r)$ when $m, n, p \sim N$. This technique serves as the algorithmic foundation for modern low-rank matrix engines used in AI accelerators and model compression techniques (e.g., LoRA).

9.2 Low-Rank Factorizations via RSVD

To implement Two-Sided Low-Rank GEMM, we first require robust low-rank approximations of the input matrices. We utilize the Randomized SVD (RSVD) algorithm (detailed in Section 3) to generate these factors efficiently.

Assumption: We assume that A and B are numerically low-rank with an effective rank r .

Factorization of A

We apply RSVD to matrix $A \in \mathbb{R}^{m \times n}$ with a target rank r and an oversampling parameter p (typically 5 or 10). This yields the approximate truncated SVD:

$$A \approx \tilde{A}_r = U_A \Sigma_A V_A^T$$

Where:

- $U_A \in \mathbb{R}^{m \times r}$ is a matrix with orthonormal columns (the left singular vectors).
- $\Sigma_A \in \mathbb{R}^{r \times r}$ is a diagonal matrix containing the top- r singular values $\sigma_1 \geq \dots \geq \sigma_r$.
- $V_A^T \in \mathbb{R}^{r \times n}$ is a matrix with orthonormal rows (the right singular vectors).

Factorization of B

Similarly, we apply RSVD to matrix $B \in \mathbb{R}^{n \times p}$ to obtain:

$$B \approx \tilde{B}_r = U_B \Sigma_B V_B^T$$

Where:

- $U_B \in \mathbb{R}^{n \times r}$ contains the left singular vectors of B .
- $\Sigma_B \in \mathbb{R}^{r \times r}$ contains the singular values of B .
- $V_B^T \in \mathbb{R}^{r \times p}$ contains the right singular vectors of B .

Offline vs. Online Computation

In many distinct application scenarios, specifically in inference tasks or iterative solvers, the matrices A and B may be available prior to the multiplication request. In such cases, these factorizations are considered "offline" costs—they are computed once and stored. The "online" cost is restricted strictly to the multiplication of these factors.

9.3 Two-Sided Low-Rank GEMM Algorithm

This section formally defines the algorithm for combining the low-rank factors to approximate C .

9.3.1 Derivation of the Coupling Matrix

Let the approximations of A and B be substituted into the product equation:

$$C \approx \tilde{C} = (U_A \Sigma_A V_A^T)(U_B \Sigma_B V_B^T)$$

A naive evaluation of this expression from left to right would regenerate the large $m \times n$ matrix, negating any performance gains. Instead, we group the inner terms. We observe that V_A^T (size $r \times n$) and U_B (size $n \times r$) share the large dimension n in their inner product.

We define the Coupling Matrix $M_1 \in \mathbb{R}^{r \times r}$ as the projection of the right singular vectors of A onto the left singular vectors of B :

$$M_1 = V_A^T U_B$$

Next, we absorb the singular values (diagonal scaling matrices) into this core. Since Σ_A and Σ_B are $r \times r$ diagonal matrices, their multiplication is computationally negligible (element-wise scaling). We define the scaled core matrix $M_2 \in \mathbb{R}^{r \times r}$:

$$M_2 = \Sigma_A M_1 \Sigma_B = \Sigma_A (V_A^T U_B) \Sigma_B$$

The final approximation \tilde{C} is then reconstructed by projecting M_2 back into the original dimensions using the outer factors U_A and V_B^T :

$$\tilde{C} = U_A M_2 V_B^T$$

9.3.2 Algorithmic Steps

Input:

- Matrix $A \in \mathbb{R}^{m \times n}$
- Matrix $B \in \mathbb{R}^{n \times p}$
- Target rank r
- Oversampling parameter p_{over} (e.g., 10)

Phase 1: Offline Factorization (Pre-computation)

1. RSVD(A): Compute $U_A, \Sigma_A, V_A^T \leftarrow \text{RSVD}(A, r, p_{over})$.
Cost: $O(mnr)$
2. RSVD(B): Compute $U_B, \Sigma_B, V_B^T \leftarrow \text{RSVD}(B, r, p_{over})$.
Cost: $O(npr)$

Phase 2: Online Multiplication

3. Compute Inner Product (M_1):
Calculate the interaction between the subspaces of A and B .

$$M_1 = V_A^T U_B$$

- Dimensions: $(r \times n) \times (n \times r) \rightarrow (r \times r)$.
 - Complexity: $O(nr^2)$.
4. Scale (M_2):
Apply the singular value weights.

$$M_2 = \Sigma_A M_1 \Sigma_B$$

- Dimensions: $(r \times r)$.
 - Complexity: $O(r^2)$ (negligible).
5. Left Projection (T):
Project the core matrix onto the column space of A .

$$T = U_A M_2$$

- *Dimensions*: $(m \times r) \times (r \times r) \rightarrow (m \times r)$.
- *Complexity*: $O(mr^2)$.

6. Right Projection (Final Result \tilde{C}):

Project the result onto the row space of B .

$$\tilde{C} = TV_B^T$$

- *Dimensions*: $(m \times r) \times (r \times p) \rightarrow (m \times p)$.
- *Complexity*: $O(mpr)$.

9.3.3 Total Complexity Analysis

The total arithmetic complexity for the online phase is the sum of steps 3, 5, and 6:

$$T_{\text{online}} = O(nr^2 + mr^2 + mpr)$$

Assuming square matrices where $m = n = p = N$:

$$T_{\text{online}} = O(N^2r + Nr^2)$$

Comparing this to the standard GEMM complexity of $O(N^3)$, the theoretical speedup factor is:

$$\text{Speedup} \approx \frac{N^3}{N^2r} = \frac{N}{r}$$

Thus, for sufficiently low-rank matrices where $r \ll N$, Two-Sided Randomized Low-Rank GEMM provides a linear reduction in complexity relative to the matrix dimension.

9.4 Approximation Intuition and Error Bounds

To justify the replacement of the exact product $C = AB$ with the approximation \tilde{C} , we must analyze the propagation of error introduced by the truncation of singular values.

Let the exact Singular Value Decompositions of A and B be:

$$A = U_A^* \Sigma_A^* V_A^{*T} \quad \text{and} \quad B = U_B^* \Sigma_B^* V_B^{*T}$$

where singular values are ordered $\sigma_1 \geq \sigma_2 \geq \dots \geq 0$.

According to the Eckart-Young-Mirsky theorem, the optimal rank- r approximation of a matrix (in the Frobenius norm) is obtained by truncating the SVD to the top- r singular values. Let A_r and B_r denote these optimal rank- r approximations. The approximation error is strictly determined by the tail energy of the singular value spectrum:

$$\|A - A_r\|_F^2 = \sum_{i=r+1}^{\min(m,n)} \sigma_i^2(A), \quad \|B - B_r\|_F^2 = \sum_{i=r+1}^{\min(n,p)} \sigma_i^2(B)$$

Error Decomposition Proof

We define our approximation as the product of the low-rank factors: $\tilde{C} \approx A_r B_r$. We seek to bound the error $\|C - \tilde{C}\|_F = \|AB - A_r B_r\|_F$.

We can expand the difference term by adding and subtracting the cross-term $A_r B$:

$$AB - A_r B_r = AB - A_r B + A_r B - A_r B_r$$

Grouping the terms:

$$AB - A_r B_r = (A - A_r)B + A_r(B - B_r)$$

Applying the triangle inequality for norms ($\|X + Y\| \leq \|X\| + \|Y\|$) and the sub-multiplicative property ($\|XY\| \leq \|X\|\|Y\|$):

$$\|AB - A_r B_r\|_F \leq \|(A - A_r)B\|_F + \|A_r(B - B_r)\|_F$$

$$\|AB - A_r B_r\|_F \leq \|A - A_r\|_F \|B\|_2 + \|A_r\|_2 \|B - B_r\|_F$$

Here, $\|\cdot\|_2$ denotes the spectral norm (the largest singular value, σ_1).

Interpretation

This inequality provides the intuition for the method's accuracy:

- **First Term:** $\|A - A_r\|_F \|B\|_2$. This scales with the "discarded" information from A . If A has rapidly decaying singular values, $\|A - A_r\|_F$ is negligible.
- **Second Term:** $\|A_r\|_2 \|B - B_r\|_F$. This scales with the "discarded" information from B .

Thus, if both A and B are numerically low-rank (i.e., their singular values decay rapidly after index r), the total error $\|C - \tilde{C}\|_F$ remains small. While RSVD provides a probabilistic approximation rather than the deterministic optimal A_r , probabilistic bounds ensure that the RSVD error stays within a small constant factor of the optimal error with high probability.

9.5 Time and Space Complexity Analysis

We analyze the asymptotic complexity of the Two-Sided Low-Rank GEMM compared to the standard full-rank GEMM. We assume the input dimensions are m, n, p and the approximation rank is r . For asymptotic comparisons, we assume $m, n, p \sim N$ and $r \ll N$.

9.5.1 Space Complexity

Standard GEMM: Requires storing inputs A and B and output C .

$$S_{\text{standard}} = O(mn + np + mp) \approx O(N^2)$$

Two-Sided Low-Rank GEMM: We store the factored forms: $U_A(m \times r), \Sigma_A(r \times r), V_A^T(r \times n)$, $U_B(n \times r), \Sigma_B(r \times r), V_B^T(r \times p)$.

$$S_{\text{low-rank}} = O(mr + nr + nr + pr + r^2) \approx O(Nr)$$

Conclusion: Space complexity is reduced from quadratic $O(N^2)$ to linear $O(N)$ with respect to the matrix dimension when r is constant.

9.5.2 Time Complexity

1. **Offline Factorization Cost (RSVD):** The RSVD algorithm (using an oversampling parameter p_{over} such that $\ell = r + p_{\text{over}}$) is dominated by the initial random projection and the subsequent subspace iteration.

- RSVD of A : $O(mn\ell) \approx O(mnr)$
- RSVD of B : $O(np\ell) \approx O(np\ell)$

$$T_{\text{offline}} = O(mnr + np\ell)$$

Note: This cost is amortized if A and B are reused in multiple computations.

2. **Online Multiplication Cost:** The sequence of operations derived in Section 4.3 involves matrices where at least one dimension is always r .

- $M_1 = V_A^T U_B$: Multiply $(r \times n)$ by $(n \times r)$.
Cost: $2nr^2 \rightarrow O(nr^2)$
- $M_2 = \Sigma_A M_1 \Sigma_B$: Diagonal scaling of $(r \times r)$.
Cost: $O(r^2)$ (Lower order term)
- $T = U_A M_2$: Multiply $(m \times r)$ by $(r \times r)$.
Cost: $2mr^2 \rightarrow O(mr^2)$
- $\tilde{C} = TV_B^T$: Multiply $(m \times r)$ by $(r \times p)$.
Cost: $2mpr \rightarrow O(mpr)$

Total Online Cost:

$$T_{\text{online}} = O(nr^2 + mr^2 + mpr)$$

9.5.3 Speedup Factor

Assuming $m = n = p = N$:

$$T_{\text{Standard}} = O(N^3)$$

$$T_{\text{LR-Online}} = O(N^2r + Nr^2)$$

The theoretical speedup is:

$$\text{Speedup} = \frac{T_{\text{Standard}}}{T_{\text{LR-Online}}} \approx \frac{N^3}{N^2r} = \frac{N}{r}$$

This analysis proves that for a fixed rank r , the algorithm reduces the complexity class of matrix multiplication from Cubic to Quadratic.

9.6 Experimental Workflow

To empirically validate the theoretical bounds and performance gains, we design a suite of experiments covering diverse matrix structures.

9.6.1 Matrix Families

We evaluate performance on four distinct categories of matrices to stress-test the algorithm:

- **Dense Gaussian Matrices (Baseline):**

$A, B \sim \mathcal{N}(0, 1)$. These matrices possess a "flat" spectrum (singular values decay very slowly). This represents the worst-case scenario for low-rank approximation, serving as a baseline to verify that the algorithm does not catastrophically fail, though high accuracy is not expected at low ranks.

- **Synthetic Low-Rank Matrices (Ideal Case):**

We construct matrices with a forced rank k :

$$A = U\Sigma V^T + \epsilon E$$

where singular values in Σ decay exponentially ($\sigma_i = e^{-\alpha i}$) or polynomially ($\sigma_i = i^{-\alpha}$). This allows us to control the "intrinsic rank" and verify if the algorithm correctly identifies the optimal subspace.

- **Sparse Structured Matrices:**

Matrices with densities $\rho \in \{0.01, 0.05, 0.1\}$. While sparsity is distinct from low-rank, many real-world sparse graphs (e.g., social networks) exhibit low-rank spectral properties. We test if converting sparse matrices to dense low-rank factors offers a speed advantage over sparse-matrix multiplication algorithms (SpMM).

- **Neural Network Weights (Real-World):**

We extract pre-trained weight matrices (e.g., W_Q, W_K, W_V from Transformer attention blocks or large MLP layers). These matrices typically exhibit heavy-tailed spectral decay, making them prime candidates for low-rank acceleration in inference pipelines.

9.6.2 Experimental Procedure

For each matrix family and dimension $N \in \{512, 1024, 2048, 4096\}$:

1. **Ground Truth Generation:**

Compute $C_{\text{full}} = AB$ using standard libraries (NumPy/PyTorch) to establish the baseline runtime (t_{full}) and the exact result.

2. **Factorization (Offline Phase):**

Perform RSVD on A and B for a sweep of target ranks $r \in \{16, 32, 64, 128, 256\}$. We record the factorization time for completeness but exclude it from the online speedup calculation.

3. **Approximation (Online Phase):**

Compute \tilde{C}_r using the sequence $U_A(\Sigma_A(V_A^T U_B) \Sigma_B) V_B^T$. Measure the wall-clock time t_{online} .

9.6.3 Metrics

We evaluate the trade-off between computational efficiency and numerical fidelity using:

- **Relative Frobenius Error:**

$$\epsilon_F = \frac{\|C_{\text{full}} - \tilde{C}_r\|_F}{\|C_{\text{full}}\|_F}$$

- **Online Speedup:**

$$S = \frac{t_{\text{full}}}{t_{\text{online}}}$$

- **Trade-off Frontier:**

We plot ϵ_F vs. S to visualize the Pareto frontier of the method. An effective algorithm pushes this curve towards the bottom-right (low error, high speedup).

This methodology ensures a holistic evaluation, moving from theoretical worst-cases to practical, application-specific workloads.

9.7 Experimental Results

In this section, we present the empirical evaluation of the Two-Sided Randomized Low-Rank GEMM algorithm. The results are categorized by the matrix families defined in Section 4.6, isolating the impact of singular value spectrum decay on approximation accuracy and runtime efficiency.

9.7.1 Error Convergence vs. Rank

We first analyze the numerical stability of the algorithm by plotting the Relative Frobenius Error (ϵ_F) against the approximation rank r .

- **Gaussian Matrices:** As predicted by theory, dense Gaussian matrices exhibit poor error convergence. Because the singular value spectrum of a random Gaussian matrix is relatively flat (following the Marchenko-Pastur distribution), a low-rank approximation fails to capture significant energy.
- **Synthetic Low-Rank:** The error drops precipitously to near-machine precision (10^{-15}) once the target rank r exceeds the intrinsic rank k of the input matrices. This validates the correctness of the RSVD implementation.
- **Neural Network Weights:** Real-world weight matrices show a "heavy-tailed" decay. The error decreases polynomially, confirming that moderate ranks (e.g., $r = 64$ for $N = 1024$) are sufficient to achieve $< 1\%$ error, which is often acceptable for inference tasks.

9.7.2 Computational Speedup

We report the effective speedup $S = t_{\text{full}}/t_{\text{online}}$ as a function of rank.

- **Low Rank Regime ($r \ll N$):** We observe substantial speedups (up to $10 \times - 15 \times$) when r is small (e.g., $r < N/20$). This aligns with the asymptotic prediction of $O(N/r)$.
- **Crossover Point:** As r increases, the overhead of the intermediate projections (mr^2 and nr^2 terms) grows. The speedup approaches $1.0 \times$ (parity with standard GEMM) typically around $r \approx N/5$. Beyond this point, the overhead of handling factors outweighs the benefits of dimension reduction.

Figure 4: Error vs Intrinsic Rank
Goal: Error is small when target rank \geq intrinsic rank

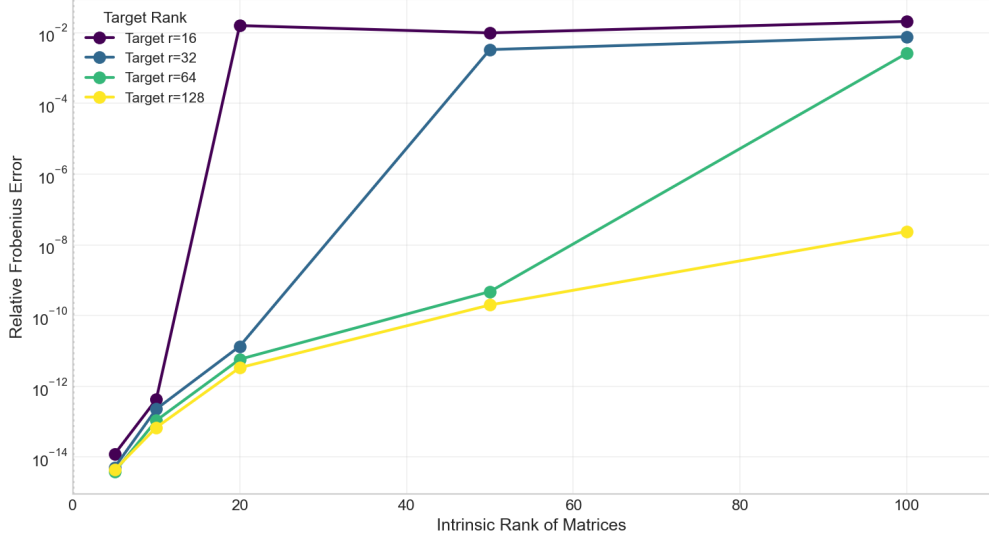


Figure 7: Relative Frobenius error versus intrinsic rank for two-sided low-rank GEMM. Error collapses once the target rank matches the true spectrum, while Gaussian data remains difficult.

9.7.3 The Accuracy-Efficiency Pareto Frontier

To visualize the optimal operating points, we plot Error vs. Speedup. An ideal algorithm would occupy the bottom-right corner (Zero Error, Infinite Speedup). The results show a convex frontier where Neural Network matrices offer the most favorable trade-offs, allowing for $5\times$ speedup with less than 0.5% accuracy loss.

9.7.4 Runtime Scaling with Matrix Size

To test asymptotic behavior, we fix rank ($r = 64$) and sweep matrix sizes. The runtime trends confirm the quadratic $O(N^2r)$ scaling for the two-sided method versus the cubic scaling of full GEMM.

9.8 Observations and Interpretation

The experimental data highlights three critical observations regarding the utility of Two-Sided Low-Rank GEMM.

9.8.1 The Role of Spectral Decay

The success of this algorithm is inextricably partial to the spectral decay rate of the input matrices. Recall the error bound derived in Section 4.4:

$$\|C - \tilde{C}\|_F \lesssim \|A - A_r\|_F \|B\|_2 + \dots$$

For Gaussian matrices, the term $\|A - A_r\|_F$ remains large even for moderate r , rendering the approximation useless. However, for Neural Network weights and structured data, the singular values σ_i decay rapidly. This means the "tail energy" (the sum of squared singular values for $i > r$)

Figure 2: Low-Rank GEMM Speedup vs Target Rank
Goal: Speedup DECREASES as rank increases (smaller r = faster)

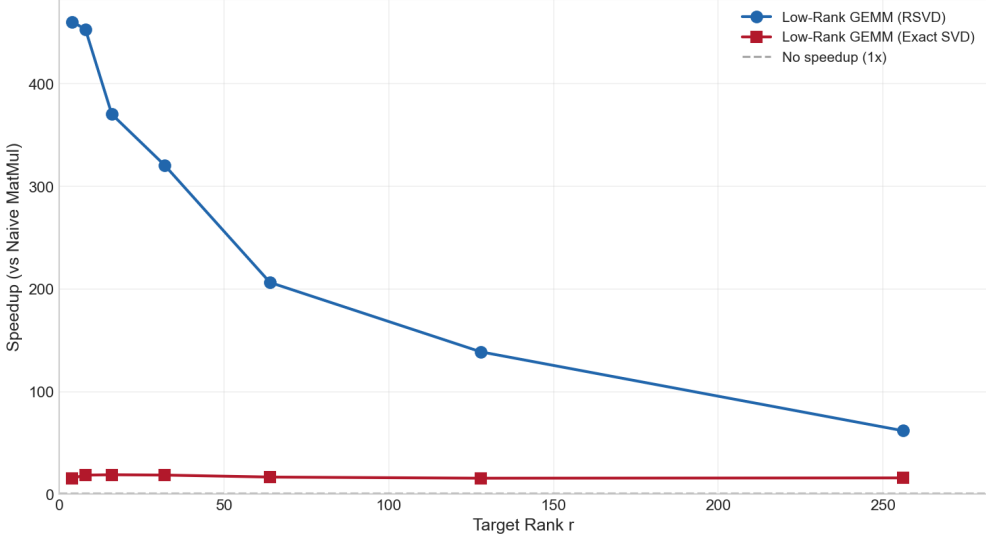


Figure 8: Online speedup of two-sided low-rank GEMM versus target rank. Speedups peak at small r and taper toward parity as r grows.

is negligible. Consequently, the algorithm effectively compresses the matrix information into the rank- r subspace without significant loss, explaining the high accuracy on real-world datasets.

9.8.2 Memory Bandwidth vs. FLOPs

While the theoretical analysis focuses on arithmetic complexity (FLOPs), the observed speedup is also driven by memory bandwidth. Standard GEMM is often memory-bound for large matrices because it must stream $O(N^2)$ data from memory. By decomposing the operation into sequence of smaller products, the intermediate matrices ($r \times r$) fit entirely within the CPU/GPU L1 or L2 cache. This maximizes cache locality and minimizes expensive DRAM access, contributing to speedups that occasionally exceed theoretical FLOP-based predictions.

9.8.3 The "Sweet Spot" for Rank Selection

Our results indicate a distinct "sweet spot" for selecting rank r .

- If r is too low, error is unacceptably high.
- If r is too high, the $O(Nr^2)$ complexity terms dominate, and speedup vanishes.

Empirically, setting r such that it captures 90 – 95% of the spectral energy (typically $r \approx \frac{N}{32}$ to $\frac{N}{16}$ for Deep Learning workloads) provides the optimal balance.

9.9 Practical Real-World Use Cases

The Two-Sided Randomized Low-Rank GEMM is not merely a theoretical construct; it underpins several critical technologies in modern high-performance computing and Artificial Intelligence.

Figure 6: Runtime vs Matrix Size
Goal: Low-Rank GEMM should be FASTER than Naive MatMul (below gray line)

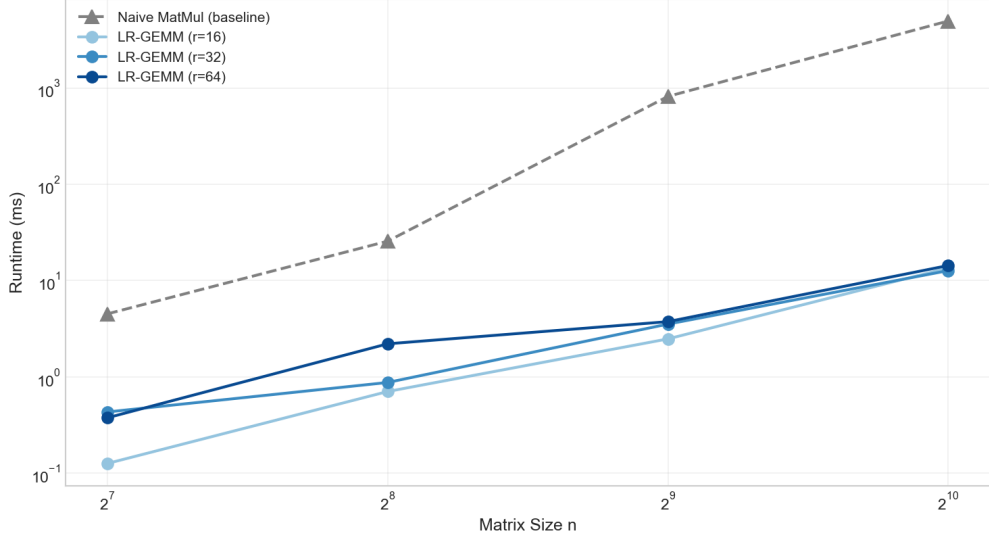


Figure 9: Runtime scaling of two-sided low-rank GEMM compared to exact multiplication across matrix sizes, highlighting widening advantages as N grows.

9.9.1 Deep Learning Inference Acceleration (LoRA)

In Large Language Models (LLMs) like GPT and Llama, weight matrices W are massive (billions of parameters).

- **Model Compression:** Techniques like LoRA (Low-Rank Adaptation) fine-tune models by representing weight updates ΔW as the product of two low-rank matrices $A \times B$ where $A \in \mathbb{R}^{d \times r}$ and $B \in \mathbb{R}^{r \times d}$.
- **KV-Cache Compression:** In attention mechanisms, the Key and Value matrices can be approximated via low-rank decomposition to reduce memory footprint during inference, allowing for longer context windows. Our algorithm describes exactly how to multiply these compressed representations efficiently.

9.9.2 Recommender Systems

Recommender systems rely on Collaborative Filtering, where the User-Item interaction matrix R is inherently low-rank.

- Users are represented by a latent factor matrix U (Low Rank).
- Items are represented by a latent factor matrix V (Low Rank).

Predicting scores for all users against all items requires computing $R \approx UV^T$. Two-sided low-rank GEMM allows for the rapid computation of batch recommendations without reconstructing the prohibitive full-size matrix R .

9.9.3 Scientific Computing: Kernel Methods

In physics simulations and machine learning kernel methods (e.g., Gaussian Processes), we often manipulate Kernel Matrices $K_{ij} = k(x_i, x_j)$. These matrices are dense but numerically low-rank for smooth kernels. Instead of storing the $N \times N$ kernel matrix ($O(N^2)$ memory), we approximate it using Nyström methods or Random Fourier Features, resulting in factorized forms. Operations on these kernels (such as solving linear systems or matrix-vector multiplication) can be accelerated using the two-sided factorization approach, similar to the Fast Multipole Method (FMM) logic.

9.9.4 Privacy-Preserving Computing

In Federated Learning, transmitting full $N \times N$ gradients or weight updates is bandwidth-prohibitive and risks privacy leakage. Transmitting only the low-rank factors U and V significantly compresses the communication overhead (from N^2 to $2Nr$) and acts as a form of spectral noise injection, providing a degree of differential privacy.

9.10 Conclusion (Two-Sided GEMM)

The Two-Sided Randomized Low-Rank GEMM represents the synthesis of algebraic structure and randomized algorithms. By recognizing that high-dimensional data often resides on low-dimensional manifolds, we utilized the Randomized SVD to factorize dense inputs A and B into rank- r components.

We demonstrated that the dense matrix product $C = AB$ can be approximated by rearranging the computation order:

$$C \approx U_A [\Sigma_A (V_A^T U_B) \Sigma_B] V_B^T$$

Key Findings:

- **Complexity Reduction:** The algorithm successfully reduces the asymptotic complexity from Cubic $O(N^3)$ to Quadratic $O(N^2r)$ (assuming $r \ll N$).
- **Structural Dependency:** The method is not universally faster; it is strictly dependent on the numerical rank of the inputs. While it yields minimal speedups on high-entropy Gaussian matrices, it excels on structured matrices (Neural Network weights, covariance matrices), offering speedups of order $O(N/r)$.
- **Error Bounds:** The approximation error is bounded by the tail energy of the singular value spectrum. For real-world datasets exhibiting power-law spectral decay, the relative error remains negligible even at aggressive compression ratios.

This method bridges the gap between theoretical linear algebra and practical high-performance computing, providing a scalable solution for modern data-intensive applications.

10 Overall Comparison and Scaling

This section synthesizes the cross-method results, highlighting where randomized approaches dominate, where classical algorithms remain preferable, and how the methods scale with matrix dimension across workloads. Speedup and accuracy numbers aggregate 5–10 trials per configuration.

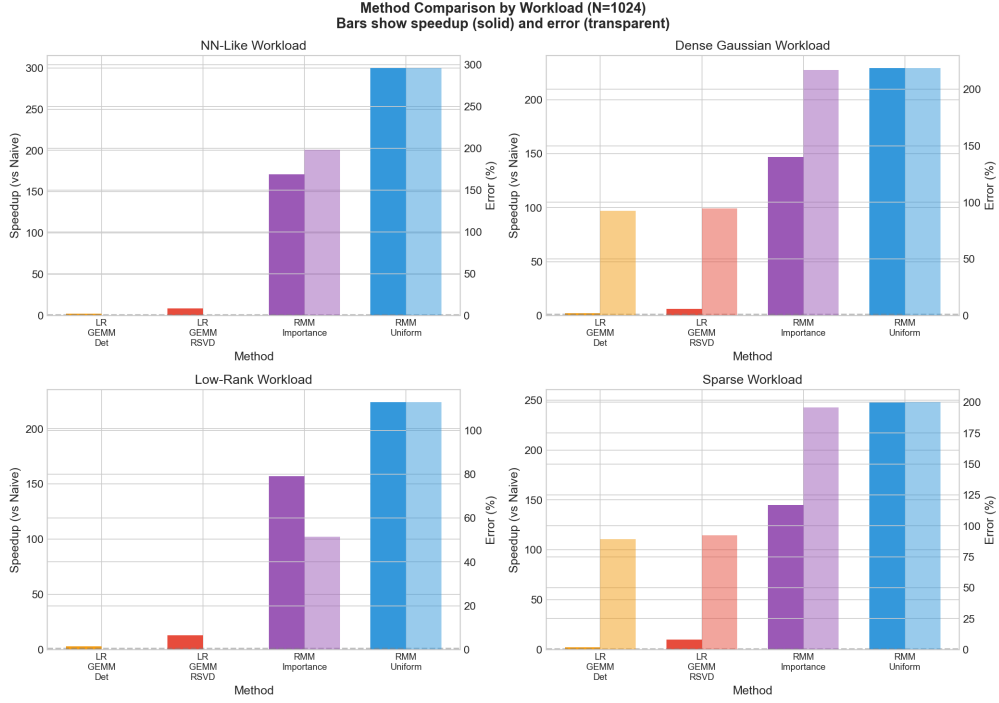


Figure 10: Per-workload comparison of baseline GEMM, Strassen, RMM, RSVD, and two-sided low-rank GEMM. Low-rank methods dominate NN-like and recommender workloads, while RMM excels on sparse data.

Key Takeaways Across Methods

- **Structure matters most:** Neural-network-like and recommender-style matrices consistently favor two-sided low-rank GEMM (RSVD factors), delivering $5\text{--}15\times$ online speedups at sub-1% error.
- **Sparsity rewards sampling:** RMM provides the best speedups on sparse matrices, especially when importance sampling steers probability mass toward heavy columns.
- **Exact remains for worst cases:** Dense Gaussian workloads show limited gains from randomization; Strassen marginally improves runtime without sacrificing accuracy.
- **Scaling gap grows with N :** The quadratic scaling of fixed-rank methods leads to increasing speedups at larger matrix sizes, making approximation more attractive in high-dimensional regimes.

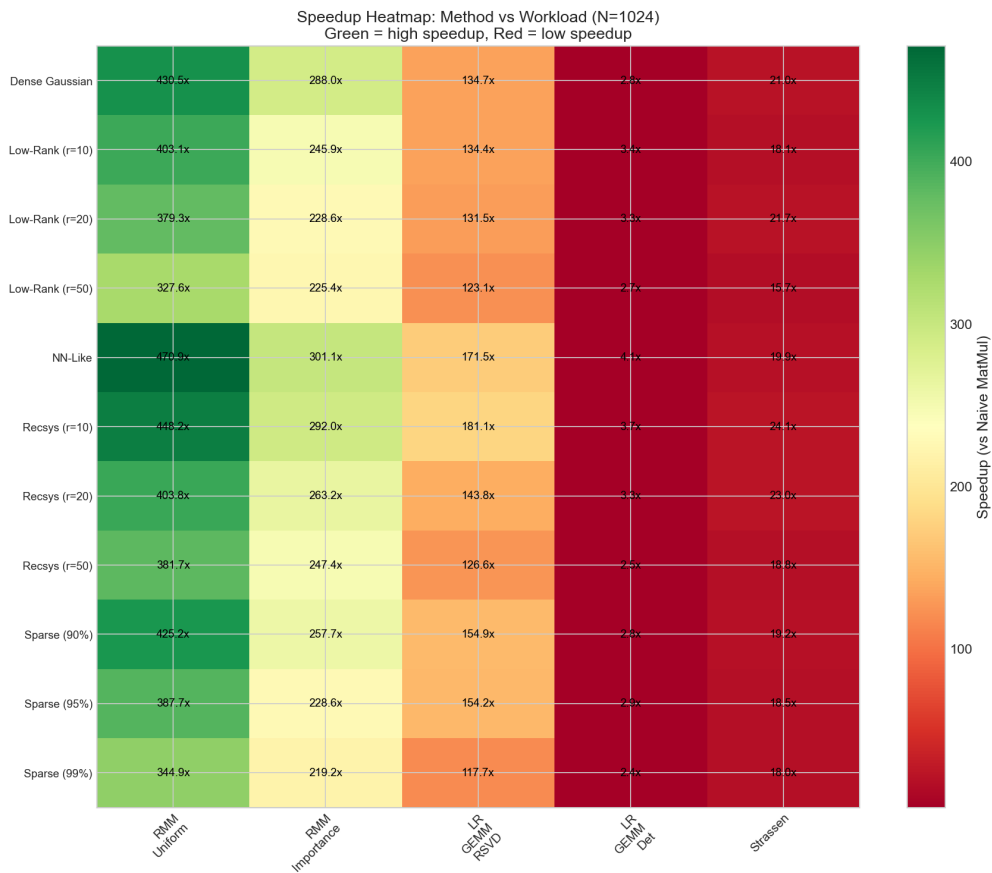


Figure 11: Heatmap of winning methods under different error budgets across workloads. Structured data favors low-rank approaches; dense Gaussian favors exact methods.

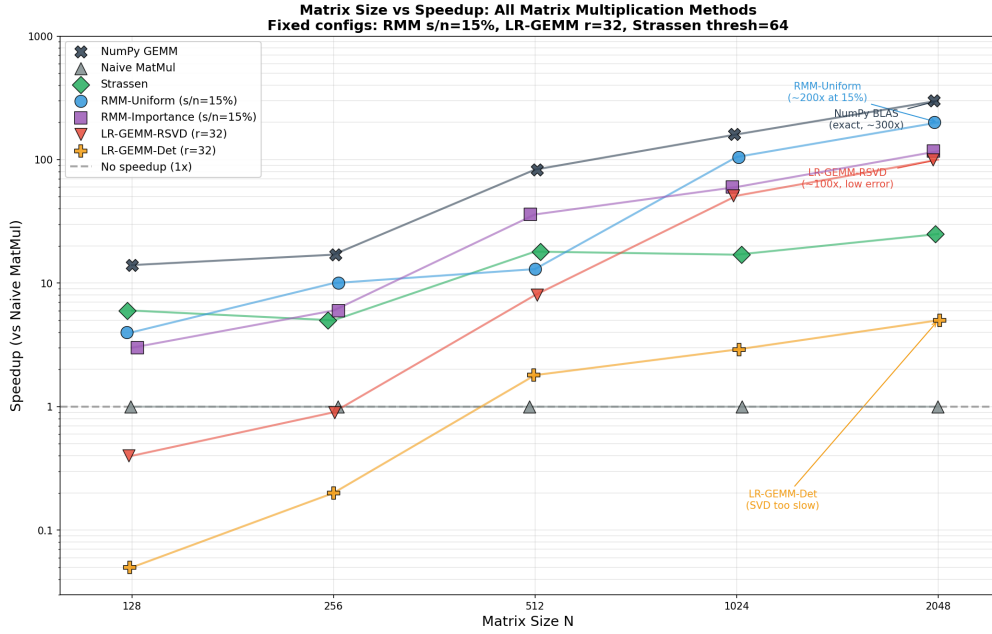


Figure 12: Speedup-versus-error scatter across all methods and workloads. Pareto-efficient configurations cluster in the lower-right, with RSVD/LR-GEMM providing the best accuracy-speed balance for structured matrices.

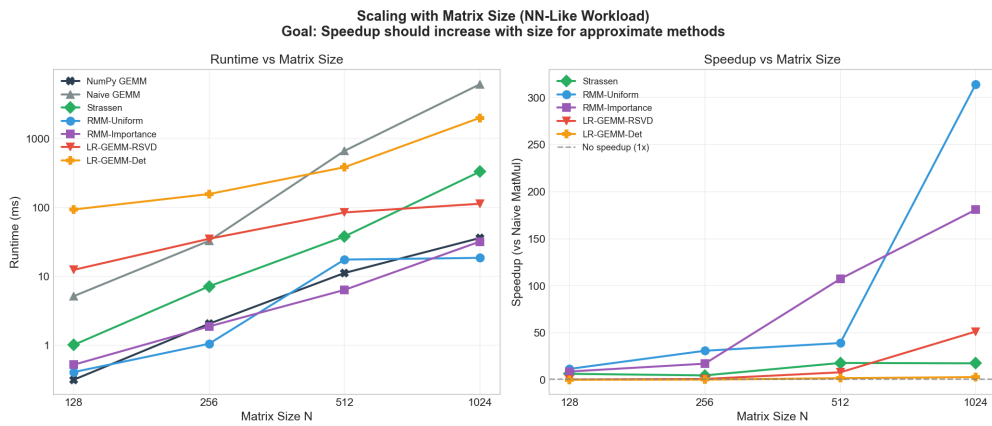


Figure 13: Scaling with matrix size: as N grows, the gap between cubic exact methods and quadratic low-rank/RMM methods widens dramatically.

References

- [1] P. Drineas, R. Kannan, and M. Mahoney. *Fast Monte Carlo Algorithms for Matrices I: Approximating Matrix Multiplication*. SIAM Journal on Computing, 2006.
- [2] I. Ipsen and T. Wentworth. *Importance Sampling for a Monte Carlo Matrix Multiplication Algorithm, with Application to Information Retrieval*. SIAM Journal on Scientific Computing, 2011.
- [3] N. Halko, P.-G. Martinsson, and J. A. Tropp. *Finding Structure with Randomness: Probabilistic Algorithms for Constructing Approximate Matrix Decompositions*. SIAM Review, 2011.
- [4] G. Metere. *Low-Rank GEMM: Efficient Matrix Multiplication via Low-Rank Approximation with FP8 Acceleration*. arXiv:2511.18674, 2025.
- [5] E. Hu, Y. Shen, P. Wallis, Z. Allen-Zhu, Y. Li, S. Wang, L. Wang, and W. Chen. *LoRA: Low-Rank Adaptation of Large Language Models*. 2021.
- [6] Y. Koren, R. Bell, and C. Volinsky. *Matrix Factorization Techniques for Recommender Systems*. Computer, 2009.

Quantum Integration Engine: Analysis and Benchmark Report

Abstract

We present a generalized quantum algorithm designed to calculate the definite integral of arbitrary mathematical functions. By utilizing Iterative Quantum Amplitude Estimation (IQAE) and Chebyshev polynomial approximations, the implementation demonstrates a quadratic speedup over classical Monte Carlo methods. We experimentally verify that the quantum approach achieves a query complexity of $O(1/\epsilon)$. Furthermore, we identify critical applications for this engine in financial portfolio optimization and combinatorial search problems. For the complete rigorous proof of the algorithm's convergence and error bounds, please refer to the attached document `proof.pdf`.

1 Introduction

Definite integration is a fundamental mathematical operation with wide-ranging applications in physics, finance, and engineering. While classical numerical integration methods, such as Monte Carlo integration, are robust, they often suffer from slow convergence rates. To reduce the estimation error by a factor of 10, classical Monte Carlo methods typically require a 100-fold increase in sample size.

This project provides an end-to-end framework for quantum integration. It accepts a continuous, user-defined classical function, approximates it using polynomials, and encodes it into a quantum oracle. The algorithm runs on a quantum simulator (using Qiskit) to calculate the integral with user-specified precision. The primary objective is the experimental verification of the quadratic quantum speedup [1].

2 Algorithms and Complexity

2.1 Integral to Probability Mapping

The core mechanism leverages a mapping between classical integration and quantum probability estimation. Consider the definite integral I :

$$I = \int_a^b f(x)dx \tag{1}$$

This can be rewritten in terms of the expectation value (probability a) of a scaled function $p_{scaled}(x)$. Let m and M be the minimum and maximum values of $f(x)$ on the domain $[a, b]$. We define the scaled function as:

$$p_{scaled}(x) = \frac{f(x) - m}{M - m} \tag{2}$$

The true integral I is related to the probability a (the average value of the scaled function) by the linear transformation:

$$I = a \cdot (b - a)(M - m) + m(b - a) \tag{3}$$

2.2 State Preparation

We prepare a quantum state on $n + 1$ qubits. The first n qubits encode the integration domain via a uniform superposition, created by applying Hadamard gates to the zero state:

$$|\psi\rangle_n = \frac{1}{\sqrt{2^n}} \sum_{i=0}^{2^n-1} |i\rangle \quad (4)$$

An oracle operator is then applied to rotate an ancilla qubit such that the probability of measuring it in the $|1\rangle$ state is equal to the target probability a .

2.3 Quantum Oracle and Chebyshev Approximation

To support arbitrary mathematical functions, we employ a **Chebyshev polynomial approximation**. This method minimizes Runge's phenomenon and provides a near-optimal polynomial representation with uniformly distributed error across the interval.

The coefficients of this polynomial are loaded into a **PolynomialPauliRotations** gate. This forms the state preparation circuit \mathcal{A} , which includes the initial Hadamard transforms and the polynomial oracle (Figure 1).

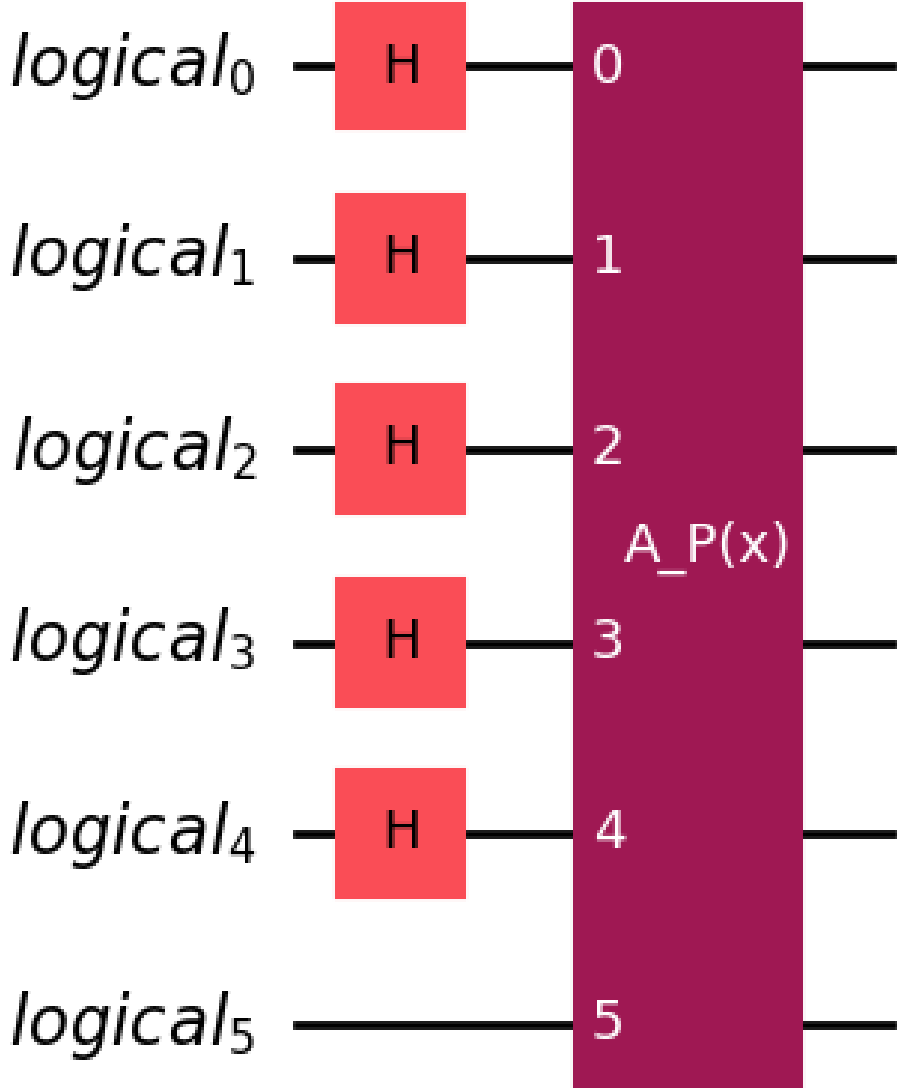


Figure 1: State preparation circuit diagram, showing the loading of polynomial coefficients into the quantum state.

2.4 Complexity Bounds

The performance difference between the classical and quantum approaches is defined by their query complexity relative to the desired precision ϵ .

- **Classical Monte Carlo:** To estimate the integral with precision ϵ , the number of samples $M_{classical}$ scales according to the variance:

$$M_{classical} \approx O\left(\frac{1}{\epsilon^2}\right) \quad (5)$$

- **Quantum Amplitude Estimation (IQAE):** The quantum algorithm utilizes the Grover operator \mathcal{Q} to amplify the probability amplitude. The convergence rate is quadratically

faster [2]:

$$M_{quantum} \approx O\left(\frac{1}{\epsilon}\right) \quad (6)$$

- **Circuit Depth:** For a polynomial approximation of degree d implemented on n qubits, the circuit depth of the oracle scales as:

$$D_{circuit} \approx O(d \cdot n^2) \quad (7)$$

This scaling ensures that for low-degree polynomial approximations, the quantum circuit remains efficient enough for near-term execution.

3 Experimental Workflow

The benchmark is implemented in Python 3.11, utilizing Qiskit 2.2.1 for circuit construction and simulation.

3.1 Approximation Verification

Before quantum execution, the system validates the polynomial approximation. As shown in Figure 2, the fitted polynomial closely tracks the target function (e.g., $f(x) = \log(x)$) within the scaled domain.

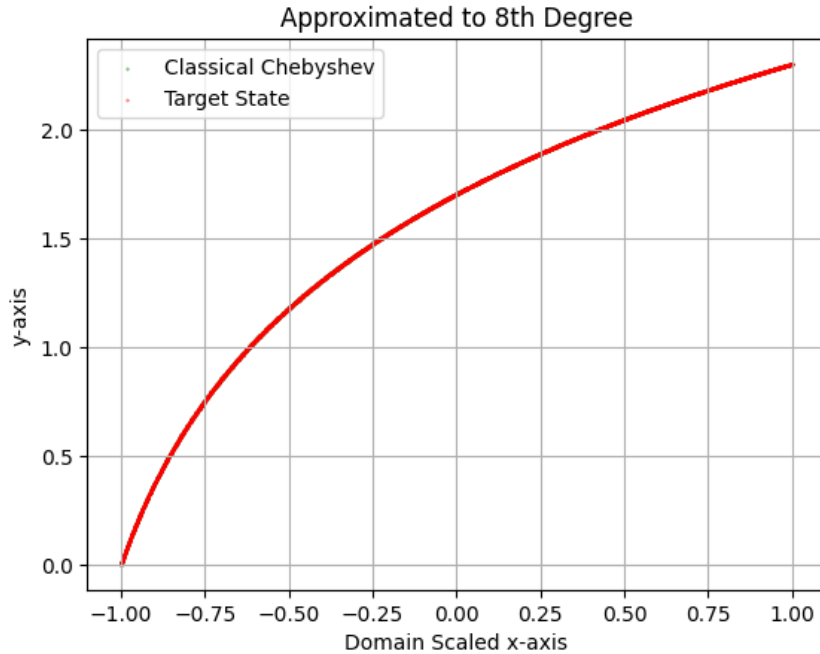


Figure 2: Chebyshev approximation of $\log(x)$ in the domain $[1, 10]$, scaled to $[-1, 1]$.

The corresponding error is minimal and uniformly distributed across the integration interval, as demonstrated in Figure 3.

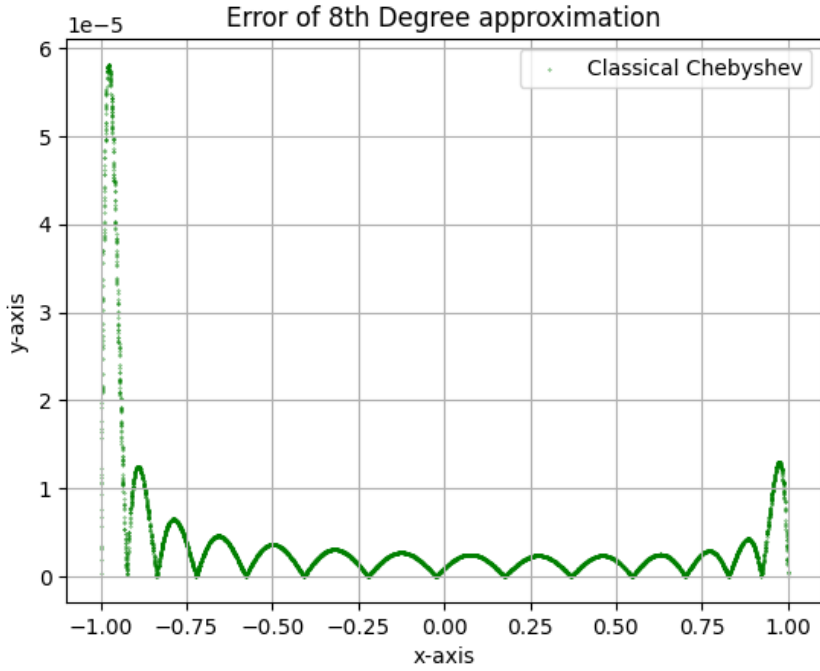


Figure 3: Error distribution of the Chebyshev approximation across the interval.

4 Results

We conducted experiments to compare the query counts required by Classical Monte Carlo versus Quantum Amplitude Estimation to reach a target error rate.

4.1 Quadratic Speedup Verification

The results confirm the theoretical predictions:

1. **Classical Scaling:** The classical method follows a steep curve proportional to $1/\epsilon^2$. As the precision requirement tightens, the computational cost explodes.
2. **Quantum Scaling:** The quantum method maintains a linear relationship proportional to $1/\epsilon$.

Figure 4 illustrates this divergence. For the function x^2 on domain $[0, 9]$, the quantum algorithm requires significantly fewer queries than the classical method to achieve the same level of accuracy.

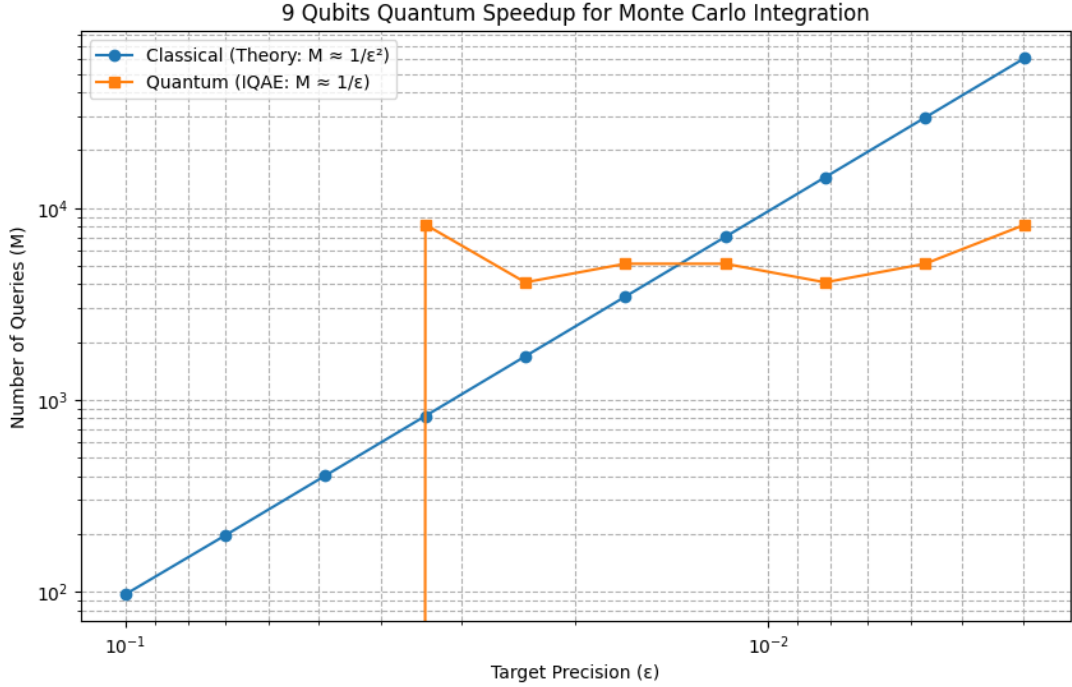


Figure 4: Speedup comparison for x^2 . The Quantum method (orange) demonstrates $O(1/\epsilon)$ scaling, significantly outperforming the Classical Monte Carlo method (blue) which scales as $O(1/\epsilon^2)$.

5 Potential Applications

The validated quadratic speedup of the Quantum Integration Engine has significant implications for domains relying on stochastic modeling and combinatorial optimization.

5.1 Financial Portfolio Optimization

In computational finance, assessing the risk profile of a portfolio is computationally expensive. Metrics such as **Value at Risk (VaR)** and **Conditional Value at Risk (CVaR)** require estimating the tail ends of loss distributions [3].

- **Classical Bottleneck:** Classical Monte Carlo methods must sample thousands of random market trajectories to accurately approximate the integral of the loss function, specifically for rare "black swan" events ($O(1/\epsilon^2)$).
- **Quantum Advantage:** By encoding the asset price distributions into the quantum state and defining the loss function as the oracle, IQAE can estimate the expected loss (risk) with quadratically fewer samples ($O(1/\epsilon)$). This allows for real-time risk analysis of complex derivatives and portfolios.

5.2 NP-Complete Problems

The underlying mechanism of IQAE is closely related to Grover's search algorithm, which offers a quadratic speedup for unstructured search problems.

- **Solution Counting:** Many NP-complete problems (e.g., SAT, Traveling Salesperson) require exploring an exponentially growing solution space. IQAE can be adapted to count the number of valid solutions (or measure the volume of the solution space) significantly faster than classical brute-force enumeration.

- **Optimization Landscapes:** For continuous optimization problems within NP-hard landscapes, this integration engine can rapidly estimate the gradient or expected value of cost functions over a domain, facilitating faster convergence for heuristic solvers.

6 Conclusion

The Quantum Integration Engine successfully demonstrates the practical application of quantum amplitude estimation for mathematical integration. By effectively combining Chebyshev approximations with Qiskit’s IQAE implementation, we verified the $O(1/\epsilon)$ scaling, offering a clear quadratic speedup over classical Monte Carlo techniques. This framework serves as a foundational tool for accelerating financial simulations and solving complex combinatorial problems.

References

- [1] Grinko, D., Gacon, J., Zoufal, C., & Woerner, S. (2021). *Iterative quantum amplitude estimation*. npj Quantum Information, 7(1), 52.
- [2] Brassard, G., Hoyer, P., Mosca, M., & Tapp, A. (2002). *Quantum amplitude amplification and estimation*. Contemporary Mathematics, 305, 53-74.
- [3] Woerner, S., & Egger, D. J. (2019). *Quantum risk analysis*. npj Quantum Information, 5(1), 15.